UNIVERSITY OF OKLAHOMA

GRADUATE COLLEGE

STUDIES ON THE VIRULENCE MECHANISMS OF *CLOSTRIDIUM SORDELLII*

A Dissertation

SUBMITTED TO THE GRADUATE FACULTY

in partial fulfillment of the requirements for the

degree of

Doctor of Philosophy

By

DANIEL EZRA VOTH
Norman, Oklahoma

2006

Downloaded from SHAREOK. Persistent Handle URL: https://hdl.handle.net/11244/985

UMI Number: 3207057



UMI Microform 3207057

Copyright 2006 by ProQuest Information and Learning Company.
All rights reserved. This microform edition is protected against
unauthorized copying under Title 17, United States Code.

ProQuest Information and Learning Company
300 North Zeeb Road
P.O. Box 1346
Ann Arbor, MI 48106-1346

STUDIES ON THE VIRULENCE MECHANISMS OF *CLOSTRIDIUM SORDELLII*

A Dissertation APPROVED FOR THE

DEPARTMENT OF BOTANY AND MICROBIOLOGY

BY

_____

Jimmy D. Ballard, Ph.D.
Co-chairman

_____

Lee R. Krumholz, Ph.D.
Co-chairman

_____

Rodney K. Tweten, Ph.D.

_____

William Ortiz-Leduc, Ph.D.

_____

Tyrrell Conway, Ph.D.

© Copyright by DANIEL EZRA VOTH 2006
All Rights Reserved.

DEDICATION

This dissertation is dedicated to my loving wife, Chrissy, and my two daughters, Clara and Anna, who have lived the graduate school experience with me these past few years. Chrissy has been a constant source of love and support throughout graduate school and is always encouraging and ready to listen when I get home from the lab. Her unselfish devotion to my life and career has been a driving force behind the completion of my dissertation research and will continue to be a strength in the years to come. I have told Chrissy many times that she deserves an honorary degree for putting up with me while I have worked to attain my own. Clara and Anna have been the best cure for any difficult times that I've gone through the past five years. I know that at the end of the day I can go home to the two most loving little girls for which a dad could ever ask. I cannot imagine having gone through the past five years without any of these three most important people in my life.

This dissertation is also dedicated to my parents, Dan and Rhonda. My Dad and Mom are the two strongest and bravest people I have ever, or will ever, know. They have shown unlimited support for, and interest in, my career through very tough times, and they are the model of how I strive to live my own life as a husband, father, and friend.

ACKNOWLEDGEMENTS

Many people deserve acknowledgement for in some way helping me through the last five years of graduate school. First, and foremost, is my advisor, mentor, and friend, Jimmy Ballard. Jimmy took me into his lab as an unexperienced small college Oklahoma boy and gave me the chance to pursue a scientific career. I am indebted to him for the values he has displayed as a scientist throughout my time in his lab. Jimmy's commitment to research and learning is an excellent example that I will strive to follow throughout my own career. I would also like to acknowledge the members of my doctoral committee, Dr. Rodney Tweten, Dr. William Ortiz-Leduc, Dr. Lee Krumholz, and Dr. Tyrrell Conway, who have been very supportive during my graduate career.

In addition to the family members above, I would also like to acknowledge my brother, Joe, who has been very supportive of my career and is always available to help me clear my mind by taking me out to play a round of golf or hunt down some poor defenseless animal (there is nothing like sitting in the dark at 4:30 am freezing to death, trying to locate deer, to clear your mind!). I would also like to acknowledge my father-in-law and mother-in-law, Laverne and Darlene, who have always been there to help me out whenever a need arises or just to take us out four-wheeling or boating for a break from the norm.

There are also many individuals that I have spent many hours with in the Ballard lab over the past five years. When I joined the Ballard lab, I quickly

became friends with Maen Qa'dan and Amy Tucker. I learned early on that these two senior graduate students were very intelligent and, so, I followed them both around the lab for the first few months trying to learn everything I could. I greatly appreciate their willingness to help the new guy learn the ropes and not laugh too much when I really messed something up. I would like to acknowledge Elaine Hamm (for letting me tell her how stellar my research is every day!), Kevin Deguisti (for golfing, music, and just generally listening to me ramble on about anything), Lan Nguyen, Isabelle Salles, Matt McKevitt, and Jason Larabee who have all spent a lot of time with me in the lab the past few years. I will miss working with these people and greatly appreciate their friendship. I would also like to acknowledge Dr. Marvin Whiteley, who has become a good friend and colleague, and the members of his lab who have put up with being in the room next to me for quite a while now.

I would like to acknowledge Dr. Venkata Moorthy, who was my Microbiology professor at Northwestern Oklahoma State University. Dr. Moorthy took an interest in my life at an early stage of my career and introduced me to the field of microbiology. His guidance and influence early in my education is one of the biggest reasons I am in research today and I greatly appreciate his continued support and interest in my life and career.

Finally, I thank God for giving me the strength and guidance to make it through the many experiences I have had during my time in graduate school.

TABLE OF CONTENTS

Page

LIST OF FIGURES……..viii

LIST OF TABLES……..xi

Chapter

I. INTRODUCTION AND LITERATURE REVIEW…….1

II. RATIONALE……...33

III. STRAIN CHARACTERIZATION AND ASSESSMENT OF THE VIRULENCE FACTOR PROFILE OF *CLOSTRIDIUM SORDELLII*……..35

IV. *CLOSTRIDIUM SORDELLII* LETHAL TOXIN IS MAINTAINED IN A MULTIMERIC PROTEIN COMPLEX…….69

V. MODULATION OF HOST CELL PHYSIOLOGY VIA INDUCTION OF APOPTOSIS BY *CLOSTRIDIUM SORDELLII* LETHAL TOXIN……...94

VI. SUMMARY……...117

LIST OF REFERENCES…….122

APPENDIX……..141

LIST OF FIGURES

Figures **Page**

1. Overview of intracellular modifications by TcdA and TcdB……15

2. Crystal structure of GDP-bound RhoA……..24

3. Proposed protein domain structure of the LCTs……26

4. PCR ribotyping of *C. sordellii* isolates……..40

5. TEM analysis of *C. sordellii* isolates…….41

6. Supernatant cytotoxicity of *C. sordellii* isolates……45

7. Analysis of *tcsl* and TcsL in *C. sordellii* isolates……..47

8. Analysis of *pfo* and SDL in *C. sordellii* isolates……...49

9. Cellular specificity of *C. sordellii* virulence factors…….51

10. Time course of CPE in TcsL and LFnTcsL$^{1\text{-}556}$ treated cells……74

11. Acid pH-induced dissociation of TcsL…….76

12. Impact of pH shifts and cross-linking on TcsL stability……..77

13. Toxicity, cell binding, and enzymatic activity of cross-linked TcsL……..78

14. Protease treatment of TcsL…….…..80

15. SDS-AGE analysis of TcsL, TcdB, and Tcnα and TEM analysis of TcsL…….82

16. Electroelution of TcsL and TcsL complex proteins…….83

17. Late stage apoptotic events occurring in TcsL-treated HeLa cells……..99

LIST OF FIGURES CONTINUED

Figure **Page**

18. Levels of phosphorylated Akt in TcsL-treated cells……...101

19. Effects of TcsL glucosyltransferase activity on Akt activation……..103

20. Downstream effects of Akt inactivation by TcsL……..105

21. Levels of phosphorylated Akt and phosphorylated GSK-3β in Wortmannin-treated HeLa cells……106

22. Effects of TcsL intoxication on mitochondrial apoptotic effector proteins……..108

23. Model of TcsL-induced apoptosis involving early glucosylation-specific events and amplification/feedback response……109

A-1. Impact of ET on cAMP levels and cell survival in zebrafish Pac2 embryonic fibroblasts……..146

A-2. Impact of ET on developing zebrafish embryos……147

A-3. Marked tissue necrosis following ET treatment of zebrafish embryos……149

A-4. Levels of cAMP and cell survival in cells treated with ET……151

A-5. Effect of ET on apoptosis in RAW 264.7 macrophages……153

LIST OF FIGURES CONTINUED

Figure **Page**

A-6. Cytopathic effects and cell death caused by $LFnTcsL^{1-556}$ in both IC-21 and NIH/3T3 cells……155

A-7. Morphological changes, cAMP accumulation, and cell viability following induction of NIH/3T3 fibroblasts, transfected with the *cya* gene (NIH/3T3-*cya*), with mifepristone……..157

A-8. cAMP accumulation and cell viability in ET-treated CHO cells…….158

A-9. ET effects on CHO cell sensitivity to staurosporine……...160

A-10. Analysis of PA oligomers in RAW 264.7^{ANTXR1} cells……..176

A-11. Cytotoxic effects of PA on RAW 264.7^{ANTXR1} cells……179

A-12. Influence of ANTXR1 derivatives and PA mutants on PA-induced cytotoxicity…….181

A-13. The role of acid pH during PA-mediated cytotoxicity in RAW 264.7^{ANTXR1} cells……...183

A-14. Induction of apoptosis in PA-treated RAW 264.7^{ANTXR1} macrophages……185

LIST OF TABLES

Table **Page**

1. Virulence Factor Profiles of *C. sordellii* Isolates…….38

2. Antimicrobial Resistance of *C. sordellii* Isolates…….43

3. Phenotypic and Genotypic Characterization of *C. sordellii* Isolates……...55

A-1. Relative PA heptamer levels and rates of degradation in RAW 264.7 and RAW 264.7^{ANTXR1} cells……177

STUDIES ON THE VIRULENCE MECHANISMS OF *CLOSTRIDIUM SORDELLII*

CHAPTER I

INTRODUCTION AND LITERATURE REVIEW

Clostridium

The genus *Clostridium* is comprised of over 60 species of Gram-positive, anaerobic, spore-forming bacilli that normally reside in the soil. This genus has been studied in a variety of microbiological arenas, some of which have resulted in the development of these organisms as beneficial industrial and medical tools. Both *Clostridium acetobutylicum* and *Clostridium beijerinckii* have been utilized for many years as an efficient means of producing solvents, such as acetone and butanol, through fermentation processes (103, 123). *Clostridium hydroxybenzoicum* and *Clostridium bifermentans* have been utilized as promising bioremediation agents in the degradation of certain chlorinated hydrocarbons (85, 126). In addition to these industrial applications, the clostridia have recently been used as reagents in specific areas of medicine. In particular, *Clostridium novyi* has been studied as a therapy for certain tumors. This initial research has shown that non-toxigenic forms of *C. novyi*, injected into mice, colonize the low-oxygen

regions of tumors, suggesting this organism could be used as a potential therapeutic reagent in cancer research (47, 48). Apart from these examples of beneficial clostridial uses, the members of the *Clostridium* genus have become most infamous for the ability of some species to cause a variety of life-threatening diseases.

Clostridial Disease in Humans

In order to cause disease in the host, the pathogenic clostridia produce and utilize an impressive array of virulence factors, including hemolysins, phospholipases, glycosyltransferases, neurotoxins, and neuraminidases that aid the bacterium in establishing infection and causing disease. To date, *Clostridium*, as a genus, produce the largest number of toxins among bacterial pathogens (72). While many of these virulence determinants have been functionally and structurally characterized, their contribution to disease is not fully understood. However, due to this versatility in virulence factor production, the clostridia have become one of the most clinically significant groups of pathogenic bacteria.

Clostridial diseases have been studied for many years, with gas gangrene being one of the most serious, traumatic wound infections observed in the clinical setting (135). However, disease caused by the clostridia is not restricted to traumatic gas gangrene. Several additional disease syndromes have been attributed to members of the clostridia including spastic paralysis (*Clostridium*

tetani) (51), flaccid paralysis (*Clostridium botulinum*) (150), atraumatic gangrene (*Clostridium septicum*) (72), antibiotic-associated diarrhea and pseudomembranous colitis (*Clostridium difficile*) (17), and toxic shock-like disease (*Clostridium sordellii*) (113). The clostridia also often cause disease in livestock. As residents of the soil, these organisms gain access to grazing hosts such as cattle, horses, and sheep. Once in the host, the clostridia are able to establish an infection and cause diseases such as blackleg (*Clostridium chauvei*) (168), gangrene (*Clostridium novyi*) (72), and malignant edema (*C. sordellii*) (116).

Clostridium sordellii

C. sordellii was originally discovered, in 1923, by Alfred Sordelli in Argentina (156), who cultured the organism from a wound sustained by a war injury. Sordelli initially named this newly identified organism *Bacillus oedematis sporogenes*, due to the edema observed at the site of infection. Following further characterization of the organism, Hall and Scott renamed the bacterium *Bacillus sordellii* in honor of the man who had discovered this pathogenic microbe (70). Eventually, the organism was renamed *C. sordellii* following classification as a member of the *Clostridium* genus. For many years following its discovery, *C. sordellii* was considered to be the pathogenic form of *Clostridium bifermentans*, due to the extensive similarities between these two soil-dwelling microorganisms.

Through numerous studies, however, it was determined that these two bacteria were not the same organism based largely on the ability of *C. sordellii* to produce a urease, its inability to ferment specific sugars, such as mannose and sorbitol (28, 124, 142) and, more recently, the observed differences in the 16S rRNA-encoding gene sequences of these two species (177). These distinctions have permanently classified *C. sordellii* as its own species, separate from its closest neighbors.

Like the other members of the clostridia, *C. sordellii* resides in the soil as a spore, which is considered the infectious form of the pathogen. The organism is a Gram-positive bacillus that measures ~ 3 - 4.5 μM in length and ~ 1 – 1.5 μM in width (141). *C. sordellii* spores are normally terminal to sub-terminal in position, with some strains producing spore appendages (141). Following germination, the organism releases virulence factors that aid in causing disease.

From the time of its discovery until the late 1970s, *C. sordellii* was widely regarded as the most probable cause of pseudomembranous colitis (PMC) (98, 140), a severe form of intestinal disease now known to be caused by *C. difficile*. This misidentification occurred because early studies utilized *C. sordellii* antitoxin to neutralize the toxic activity in animals with PMC (8, 17, 18, 19). In 1978, Bartlett et al. reported the seminal finding that the causative agent of PMC in clindamycin-treated hamsters was *C. difficile*, with the *C. sordellii* antitoxin protective effect due to the homology shared between the toxins produced by the two organisms (20). After excluding this organism as the cause of PMC, over the

next two decades, *C. sordellii* was rarely reported as a human pathogen. Indeed, there were only 14 reported cases of *C. sordellii* illness in humans from 1978 to 2000 (1, 2, 15, 26, 30, 46, 68, 83, 102, 110, 143, 155, 157, 162). More recently, however, *C. sordellii* has been emerging as a pathogen associated with toxic shock-like illnesses in humans (34, 95, 113, 151).

C. sordellii is still widely regarded as an important veterinary pathogen. As mentioned above, the organism resides in the soil, as a spore, which gains access to a variety of livestock hosts. In many cases, early definitive symptoms are not observed due to the rapid onset of disease and sudden death of the animal (100, 101). However, there have been a number of reports documenting specific diseases caused by *C. sordellii* that suggest the organism predominantly causes intestinal disease in animals. In sheep, *C. sordellii* causes abomasal bloat, hemorrhaging, ulcers, enteritis, and sudden death (5, 42, 100, 116, 139, 170), and in cattle, it has been reported to cause diarrhea and enteric lesions (6). A vaccine composed of products from seven different clostridial species, including *C. sordellii*, is the current immunization regimen used to prevent clostridial disease in the agricultural setting (163). However, this crude vaccine is only partially effective and *C. sordellii* remains a problem in areas of livestock overcrowding, such as stockyards.

***C. sordellii*-Associated Disease in Humans**

Since its discovery, in 1923, *C. sordellii* has been commonly grouped with the myonecrotic clostridia, which cause traumatic gangrene in animals and humans. As mentioned above, this organism was initially cultured from a war wound (156), and wound infection has historically been the primary presentation assumed for this pathogenic bacterium. However, an extensive investigation of the literature suggests that *C. sordellii* has been erroneously grouped with the myonecrotic clostridia. In a limited number of cases, necrosis is reported in the pathology findings; however, these studies are in the minority. In the more than 35 reports of *C. sordellii* disease since 1950, only four cases were reported that described the tissue necrosis that is typical of gangrene (14, 83, 95, 155). Additionally, many of these studies that reported this organism as a cause of gangrene also routinely observed the presence of additional myonecrotic clostridial species, such as *C. perfringens*, at the site of infection, suggesting a mixed infection contributed to the gangrenous conditions observed (14, 95, 155).

The most commonly reported form of *C. sordellii*-associated disease, and one increasing in number, presents as a toxic shock-like death (24, 34, 110, 113, 143, 151). In these reports, bacteremia is often reported, with septicemia and shock resulting within 2 – 4 days following observation of the first symptoms. The initial symptoms of the disease are normally non-descript and are

characterized by absence of fever. A concerning increase in this toxic shock-like death has been recently reported among postpartum and post-abortion patients (24, 34, 110, 143, 151). The first report of this type of postpartum toxic shock-like death attributable to *C. sordellii* was in 1989 and described a patient who was released from the hospital following a successful delivery and then succumbed to the disease with little warning (110). Since this report, three more cases of postpartum toxic shock-like death have been reported (24, 143, 151), indicating a potential risk for *C. sordellii* infection in these patients. While the origin of these infections was unknown, it was suggested that these patients were already colonized with a pathogenic strain of the organism, or that contamination occurred during delivery.

A second area of increasing *C. sordellii* infections is in post-abortion patients, particularly following medically induced abortions using RU-486, or Mifepristone, and Misoprostol. Since 2002, five cases of this type of *C. sordellii* infection have been reported, with each resulting in death of the patient following a rapid onset of disease (34, 151). Due to this rise in *C. sordellii* infections, in a very specific area of medicine, the Food and Drug Administration has recently issued a warning regarding the potential for infection with this organism following administration of the abortion pill, RU-486 (34). Again, as with the postpartum disease reports, the mode of infection in these patients is unknown,

and the effect of the abortion-inducing drugs on *C. sordellii* growth and virulence factor production has not been studied.

A third area of increased concern regarding *C. sordellii*, and the subject of Chapter III of this dissertation, is the transmission of the pathogen via musculoskeletal tissue allografts. In 2001, the Centers for Disease Control and Prevention (CDC) reported on the death of a patient, due to bacterial infection, following a routine knee transplant (35). The ensuing investigation found that transplant material had been taken from a cadaver donor that was contaminated by *C. sordellii*, the same organism cultured from the patient postmortem. Following this investigation, two studies in 2003 showed that *C. sordellii* is a common contaminant of cadavers that are commonly used for tissue samples in transplantation procedures (104, 106). In these studies, *Clostridium* spp. accounted for ~ 8% of the total bacterial species cultured from the cadavers, and *C. sordellii* made up ~ 40% of the *Clostridium*. As noted by Martinez et al. (106), *C. sordellii* contamination may occur when resident bacteria disseminate into tissue as the integrity of the bowel is compromised during the perimortem period or at death.

As described in Chapter IV of this dissertation, the exceptional stability of the lethal toxin (TcsL) produced by *C. sordellii* could pose a serious problem in this new presentation of the disease due to the fact that many types of tissue used in transplantation cannot be subjected to rigorous sterilization without damaging

the tissue. As a result, non-sterilized tissue could harbor *C. sordellii*, TcsL, or both, resulting in a potentially dangerous condition for the transplant recipient. These new areas of *C. sordellii* pathogenesis demonstrate how a rarely encountered pathogen in humans can present itself as an emerging threat given an appropriate set of conditions.

Treatment of *C. sordellii*-Associated Disease in Humans

A successful treatment for *C. sordellii*-associated disease has not been developed. *C. sordellii* infections are normally fatal, despite patients receiving intense antibiotic treatment. Common antibiotics, such as penicillin, vancomycin, clindamycin, and metronidazole, have been employed in reported cases of the disease (14, 26, 29, 30, 151). In a 1986 study, Nakamura et al. reported that several strains of *C. sordellii* were susceptible to most antibiotics, including penicillin, clindamycin, vancomycin, and metronidazole (122). In most cases, a combination of antibiotics is used; yet, the patient succumbs to the disease in a very short period of time after initial symptoms are observed. Difficulties in the early diagnosis of *C. sordellii* infections also contribute to its mortality rate in humans.

C. sordellii Virulence Factors

C. sordellii, like many of the pathogenic clostridia, produces a variety of virulence factors that can potentially contribute to disease. Unlike other pathogenic clostridia, these virulence determinants have not been well characterized, and, furthermore, their role in *C. sordellii*-associated disease is even less clear. However, the ability of this pathogen to produce an array of soluble, proteinaceous virulence determinants likely provides an advantage to the organism in establishing infection and causing disease. Among the virulence factors reportedly produced by this pathogen are lethal toxin (TcsL), hemorrhagic toxin (TcsH), hemolysin, phospholipase C, and neuraminidase (11, 93). Of this panel of proteins, TcsL and TcsH have been studied most extensively, but their contribution to disease remains unclear. The hemolysin, phospholipase C, and neuraminidase have been infrequently reported and their function during infection is not understood; however, other pathogenic clostridia produce and utilize similar proteins in order to cause disease, suggesting these proteins could also provide an advantage for *C. sordellii* in the host setting.

While their role in disease is not understood, toxoids of TcsL and TcsH protect against subsequent challenge with *C. sordellii* spores in the guinea pig model of infection (10). Due to these initial studies, and corresponding work regarding *C. difficile* TcdB and TcdA, these two toxins are considered the primary virulence determinants in *C. sordellii* disease. These two virulence factors also

belong to a five-member family of toxins collectively referred to as the large clostridial toxins (LCTs), and TcsL will be a major focus of this dissertation.

Large Clostridial Toxins

Clostridium difficile Toxins: Mechanism of Action and Role in Disease. (Daniel E. Voth and Jimmy D. Ballard. 2003. *Clinical Microbiology Reviews*. 18:247-263)

C. sordellii produces two toxic proteins, TcsL (131) and TcsH (108), that belong to the LCT family of bacterial toxins. This family of virulence determinants is comprised of five members that are grouped together due to their similar high molecular weight sizes and enzymatic activities. The LCT family is made up of five of the largest toxins discovered to date, ranging from 250 – 308 kDa in size. As mentioned, *C. sordellii* produces TcsL (270 kDa) and TcsH (300 kDa), *C. difficile* produces TcdB (280 kDa) and TcdA (308 kDa), and *C. novyi* produces Tcnα (250 kDa). Each of these proteins consists of a single polypeptide chain that does not possess a known signal sequence for secretion from its respective organism. In addition to their related unique size, each of these toxins modulate host cell physiology via the glycosyltransferase activity contained in the N-terminal region of the protein. Most of the LCT studies regarding genetics and mechanism of action have been performed using TcdA and TcdB.

Genetics of the LCTs

The gene encoding TcsL has been sequenced and is comprised of 7095 bp, in a single open reading frame, which encodes for a 2364 residue protein (69). The gene sequence of TcsH has not yet been reported. It is thought that these two LCTs are encoded on a pathogenicity locus as are the LCTs produced by *C. difficile* (71). This proposed genetic arrangement includes positive and negative regulators of toxin production (43, 86) and a region encoding a putative holin-like protein involved in toxin release from the organism (160). Like TcdA and TcdB from *C. difficile*, *tcsl* is a low G + C content gene. As with TcdB, the enzymatic activity of TcsL resides in the first 556 residues at the N-terminal end of the protein, as discussed in Chapter III. The C-terminus of the proteins contains repeat regions that, in the case of TcdA and TcdB, have been termed CROPs (Combined Repetitive OligoPeptides), which are involved in binding specific cell surface receptors (172, 173). These regions are comprised of 21 – 50 residues repeated throughout the C-terminal region of the toxins. While TcsL contains these repeat regions of homology (69), no receptor for the toxin has yet been identified.

The LCTs produced by *C. sordellii* demonstrate a high degree of homology to the other members of the LCT family. TcsL is most homologous to TcdB, which explains early observations on the cross-reactivity of antiserum

raised against crude supernatants of *C. sordellii* with TcdB (36). Subsequent purification of TcsL demonstrated cross-reactivity between TcsL-specific antiserum and TcdB (131). The major contrasting regions in these two proteins are found at the N-termini and are responsible for the difference in intracellular substrate specificity, with TcdB modifying Rho, Rac, and Cdc42 (25, 91) and TcsL glucosylating Ras, Rac, Rap, Ral, and Cdc42 (79). Interestingly, while TcdB is more cytotoxic to cultured cell *in vitro*, TcsL possesses an ~ 10-fold lower LD_{50} as compared to TcdB (107). As with TcsL and TcdB, TcdA antiserum cross-reacts with TcsH and vice versa (108), further demonstrating the close homology shared between these two proteins, which are considered the enterotoxins produced by their respective organisms. The remaining member of the LCT family, Tcnα, produced by *C. novyi*, shares the least amount of homology with the other LCTs, and this may be due to significant phylogenetic differences between the organisms (81).

Mechanism of Action of the LCTs

As mentioned above, most LCT studies have utilized TcdB from *C. difficile* as a representative member of this toxin family, and, thus, TcsL's mechanism of action will be discussed, in large part, in the context of TcdB. The LCTs utilize a well-defined mechanism of action in order to modulate cell physiology and, consequently, alter the host environment. As mentioned above,

these toxins target the Ras superfamily of small GTPases for modification via glycosylation. This irreversible modification inactivates these small regulatory proteins, leading to disruption of vital signaling pathways in the cell (Fig. 1). However, in addition to enzymatic modification of targets, there are several steps in receptor binding and cell entry, which are important for intoxication.

Cell surface receptors for the LCTs

In order to elicit cytotoxic effects, the LCTs must be internalized into the host cell, via endocytosis, and require an acidic endosome for access to the cytosol (54, 75, 114, 137). Receptor binding is the first essential step in the process of cell entry. The receptors for the LCTs are thought to be non-proteinaceous and, as shown for TcdA, share the disaccharide Galβ1-4GlcNac. This disaccharide is found on I, X, and Y blood antigens present on a variety of cells, and these antigens have been shown to act as receptors for TcdA (166). Various animal species susceptible to TcdA may not necessarily share identical receptors. For example, TcdA is reported to bind to Galα1-3Galβ1-4GlcNAc (96); yet, this receptor does not appear to be present on human cells.

In line with these studies, pretreatment of cells or tissue with galactosidase reduces binding by TcdA (41, 44, 96, 154). A possible protein receptor, sucrase-isomaltase, was found on cells in the ileum of rabbits, but, again, this protein is not found on cells targeted within the human colon (134). The receptor for the

Figure 1. Overview of intracellular modifications by the LCTs. The LCTs act intracellularly as glycosyltransferases. Each toxin modifies and inactivates small GTPases via transfer of a sugar moiety, using UDP-glucose as a co-substrate. The effects of these modifications include actin condensation, transcriptional activation, and apoptosis.

Figure 1.

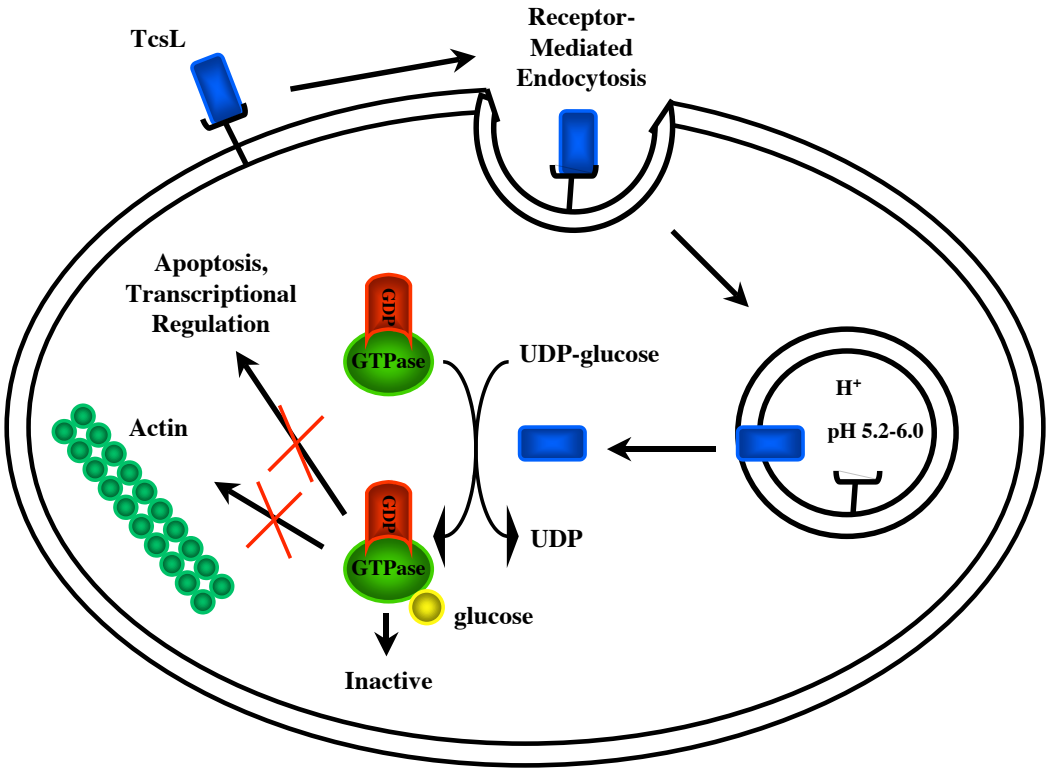
TcsL
Receptor-
Mediated
Endocytosis
Apoptosis,
Transcriptional
Regulation
GDP
GTPase
UDP-glucose
H+
pH 5.2-6.0
Actin
GDP
GTPase
UDP
glucose
Inactive

remaining LCTs has been more elusive than that for TcdA; however, due to C-terminal sequence homology, it is thought that the LCTs utilize similar cell surface proteins for cell entry. In our experiments, and those of others, TcdB and TcsL have been shown to intoxicate a broad range of cell types, indicating the receptor for these toxins, while undefined, is ubiquitous.

Receptor-mediated endocytosis and membrane translocation

The LCTs enter the cell through receptor-mediated endocytosis and require an acidified endosome for translocation. Cytotoxic effects of these toxins can be directly inhibited by a variety of lysosomotropic inhibitors, such as bafilomycin A and ammonium chloride (54). Furthermore, conditions that prevent lysosome fusion with the endosome attenuate TcdB activity (55).

The requirement for low pH appears to be due to important structural changes which occur in the toxins, leading to exposure of hydrophobic domains prior to insertion into the target membrane (137, 138). Indeed, Barth and colleagues have observed the formation of channels in lipid bilayers by TcdB through an acid pH-dependent process (16).

Until recently, it was not known as to whether the full toxin translocated to the cytoplasm or only the enzymatic domain. However, recent work by Pfeifer and colleagues showed that, following proteolytic cleavage, only the N-terminal domain of TcdB exits the endosome and gains access to substrates (130). While a

putative membrane insertion/translocation domain, located within the middle of the protein, has been proposed for the LCTs, this region of the proteins has not been definitively shown to promote translocation of the N-terminal enzymatic fragment.

Following translocation into the cytosol of the cell, little is known regarding trafficking of the LCTs in order for substrate modification to occur. In the case of TcsL, however, two recent studies show TcsL localization to cell membranes (112, 129). Petit et al. originally showed that TcsL localizes to the mitochondrial membrane within five minutes of exposure of cells to the toxin (129). In contrast, Mesmin et al. demonstrated a phosphatidylserine binding site in the N-terminal region of TcsL, suggesting the toxin localizes to the inner leaflet of the plasma membrane following cell entry (112). The latter finding appears to be the most likely event to occur for the toxin to access membrane-bound GTPases for modification. However, these two findings have yet to be reconciled and will be discussed further in the context of the results in Chapter V.

Modification of intracellular targets

Following receptor binding and internalization into the target cell cytosol, the LCTs elicit specific effects that modulate host cell physiology. Discoveries from initial studies indicated that cells exposed to TcdB exhibited marked changes in the organization of their actin cytoskeleton (114, 161, 175). Following

these studies on TcdB, TcsL was also found to adversely impact the actin cytoskeleton in a variety of cell lines (120, 121). However, TcsL intoxication of mammalian cells results in completely rounded cells, in contrast to the elongation observed during a routine TcdB treatment (13, 23). These adverse effects on the actin cytoskeleton have since become a hallmark in the intoxication of cells by the LCTs and are thought to be a prelude to cell death in a variety of cell types.

In line with these early observations, Just and colleagues discovered Rho from TcdB-treated cell lysates was no longer subject to ADP-ribosylation by *C. botulinum* C3 exoenzyme (88). C3 ADP-ribosylates Asn-41 in Rho (149), yet TcdB was not found to have a similar activity. These observations did suggest, however, that TcdB was somehow altering Rho within the cell. Other experiments found that over-expression of Rho protected cells from TcdB-induced rounding, further implicating this protein as a target for TcdB. TcdA was subsequently found to exert a similar effect on Rho (90). Additionally, expression of RhoA, -B, and -C in HeLa cells was found to provide protection against TcdB; however, these same conditions did not afford protection against TcsL, suggesting that TcsL targeted different GTPases than its closest neighbor toxin (67).

These initial studies allowed investigators to focus on the Rho family of GTPases as a putative target of the LCTs. In a seminal report, Just and colleagues demonstrated the ability of TcdB to glucosylate RhoA via transfer of a sugar moiety to Thr-37 of the GTPase using UDP-glucose as a co-substrate (91). In the

same study, two other GTPases, Rac and Cdc42, were also found to be glucosylated by TcdB. Additionally, this group observed the ability of TcdA to modify RhoA using the same UDP-glucose-dependent mechanism as TcdB (92). In line with these observations, cells with reduced levels of UDP-glucose are less sensitive to cytopathic effects (CPE) induced by the LCTs (38). Following these initial studies on TcdB, TcsL was likewise found to act as a glucosyltransferase (25, 82, 89, 132). In contrast to TcdB, however, TcsL was not capable of modifying Rho. Instead, this LCT glucosylates Ras, Rac, Rap, and Ral. Cdc42 is additionally glucosylated by TcsL produced by certain strains of *C. sordellii*. Further characterization of TcsH also identified the toxin to be a glucosyltransferase, modifying Rho, Rac, and Cdc42, as in the case of the *C. difficile* toxins (63). Collectively, these studies defined the LCTs as glucosyltransferases, capable of inactivating small GTPases within the cell.

Small GTPase proteins as targets of the LCTs

The studies highlighted in the previous section clearly defined LCTs as glucosyltransferases that inactivate small GTPases. Thus, to appreciate the role of these proteins in cellular intoxication, it is important to understand GTPase proteins and their activities. Small GTPases, such as Rho and Ras, bind and hydrolyze GTP to GDP, and it is the alternation between the GTP-bound (active) and GDP-bound (inactive) states that regulates activity. The exchange of GDP

for GTP is regulated by guanine exchange factors (GEFs) within the cell (181). Activated GTPases intrinsically hydrolyze GTP, removing the γ-phosphate group and returning to the "off" GDP-bound state through a process enhanced by GTPase activating proteins (GAPs) (61, 62). Further regulation comes from GDP dissociation inhibitors (GDIs), which block nucleotide exchange and maintain GTPases in the GDP-bound form within the cytoplasm, preventing association of the GTPase with the membrane and interactions with GEFs (60, 77, 115).

Activation of small GTPase signaling is initiated by factors that promote the dissociation of GDIs from GDP-bound GTPase and release the protein for localization to the cell membrane. Thus, in a model of GTPase activation, GDIs maintain the inactive protein in the cytosol, and, following dissociation from these inhibitors, the GTPase localizes to the membrane where GEFs enhance dissociation of GDP. As GTP is in excess compared to GDP in the cell, GTPases subsequently bind GTP and become activated, promoting downstream signaling events. Due to inherent GTPase activity and the action of GAPs, the protein subsequently returns to the "off" state, returning to the GDP-bound form. Each of the GTPases of importance to these studies, Ras, Rac, Rap, Cdc42, and Ral, share similar mechanisms of regulation, as described above.

Inactivation of these GTPases can exert a variety of adverse effects on the intoxicated cell due to the loss of normal GTPase functions. In the case of TcsL, Ras, Rap, Ral, and Cdc42 inactivation could potentially inhibit multiple cell

signaling pathways that are vital components of cell viability. In the case of Ras, this versatile GTPase is largely involved in cell proliferation and survival. The best-characterized downstream effector of Ras is Raf, and this protein is responsible for activation of the mitogen-activated protein kinase kinase cascade that ultimately results in phosphorylation and activation of ERK1 and 2, which are involved in transcriptional regulation (105). Ral is involved in cell transformation processes, likely through its influence on proteins such as Fos (119), and Ral is also regulated upstream by the Ras signaling pathway. As with Ral, Rap is involved in cell transformation and DNA synthesis (9, 180). In addition to these signaling GTPases, Rac and Cdc42 are more specifically involved with lamellipodium and filopodium formation (125). Lamellipodia and filopodia are important structural extensions at the leading edge of migrating cells and are essential to movement and sensing the environment during cell migration. These results suggest that Rac and Cdc42 could play a major role in TcsL-induced CPE in intoxicated cells.

Predictably, the inactivation of GTPase proteins by the LCTs could occur at various steps, including blocking membrane localization, GEF interaction, or contact with downstream effectors. The elucidation of the crystal structures of RhoA/GDP (176) and RhoA/GTPγS (87) have provided the information necessary for making predictions regarding the effects of glucosylation on these small GTPases. The RhoA/GDP structure has been determined to 2.1 Å while the

RhoA/GTPγS structure has been determined to 2.4 Å. Upon examination of the RhoA crystal structure, the impact of glucosylation would appear to prevent Thr-37 (Thr-35 in Ras, Rac, and Cdc42) from forming a complex at the γ phosphate of the bound GTP molecule. In the GTP-bound form of Rho, Thr-37 (Thr-35 in Ras, Rac, and Cdc42) contributes to Mg^{2+} interactions through the reactive hydroxyl group (87), which is also subject to glucosylation. Examination of the Rho three-dimensional structure in the GTP-bound form indicates this hydroxyl group is not readily accessible as it is complexed with Mg^{2+} and is directed away from the solvent. However, in the GDP-bound form, the hydroxyl group of Thr-37 (Thr-35 in Ras, Rac, and Cdc42) aids in the stabilization of a water molecule that coordinates the Mg^{2+} ion, but is susceptible to glucosylation. In fact, the ability of the LCTs to more easily modify GDP-bound GTPases, as opposed to the GTP-bound form, has been shown quite convincingly in previous studies (91). Interestingly, and as discussed further in Chapter IV, Herrmann et al. have shown that, while GTP blocks glucosylation of Ras by TcsL, glucosylation does not appear to reduce GTP binding (76). Based on the structure of GTP-bound Ras, it is difficult to appreciate how this protein is capable of stably binding GTP without the contributions from the hydroxyl group of Thr-35 (Thr-37 in Rho). This may suggest other, more subtle, yet poorly understood mechanisms are involved in the process of glucosylating GTPases. Additional studies suggest that glucosylation does, however, maintain the GTPase effector loop region in conformation that

inhibits downstream signaling (66, 171). While these reports demonstrate inhibition of downstream signaling, no information is available on the ability of glucosylated GTPases to maintain interactions with other proteins at the membrane, a condition that could adversely effect intracellular signaling. This possibility will be discussed further in the context of the results in Chapter V.

The Thr-37/Thr-35 residues are highly conserved among small GTPases; yet, only Rho, Rac, and Cdc42 are targeted by TcdA and TcdB and only Ras, Rap, and Ral are modified by TcsL. As shown in Fig. 2, the reason for this substrate specificity has been shown to be due to residues 24 – 29 in Rho (corresponding residues 22 – 27 in Ras, Rac, and Cdc42) that lie just outside the effector loop region and comprise part of the transition between the α1-helix and the switch I region (118). Through the use of Rho/Rac chimeric protein fusions and substitution mutagenesis, the importance of specific residues within this region has been defined, and the results indicate the lysine residue at position 27 (25 in Ras, Rac, and Cdc42) plays a major part in substrate distinction. Construction of the Rho mutant K27T allowed for glucosylation of Rho by TcsL, while native Rho is not targeted by TcsL. These mutagenesis results have provided a strong basis for the substrate specificity observed among the LCTs.

Figure 2. Crystal structure of GDP-bound RhoA. In the GDP-bound form of Rho, the Mg^{2+} ion is coordinated by the β phosphate group of GDP and a water molecule that interacts with T37 for stabilization. The OH group of T37 is glucosylated by the LCTs, consequently inactivating this regulatory protein. The region involved in substrate specificity is colored in purple and includes residues 24 – 29 (22 – 27 in Rac and Cdc42). This figure was generated and rendered using PyMOL.

Figure 2.

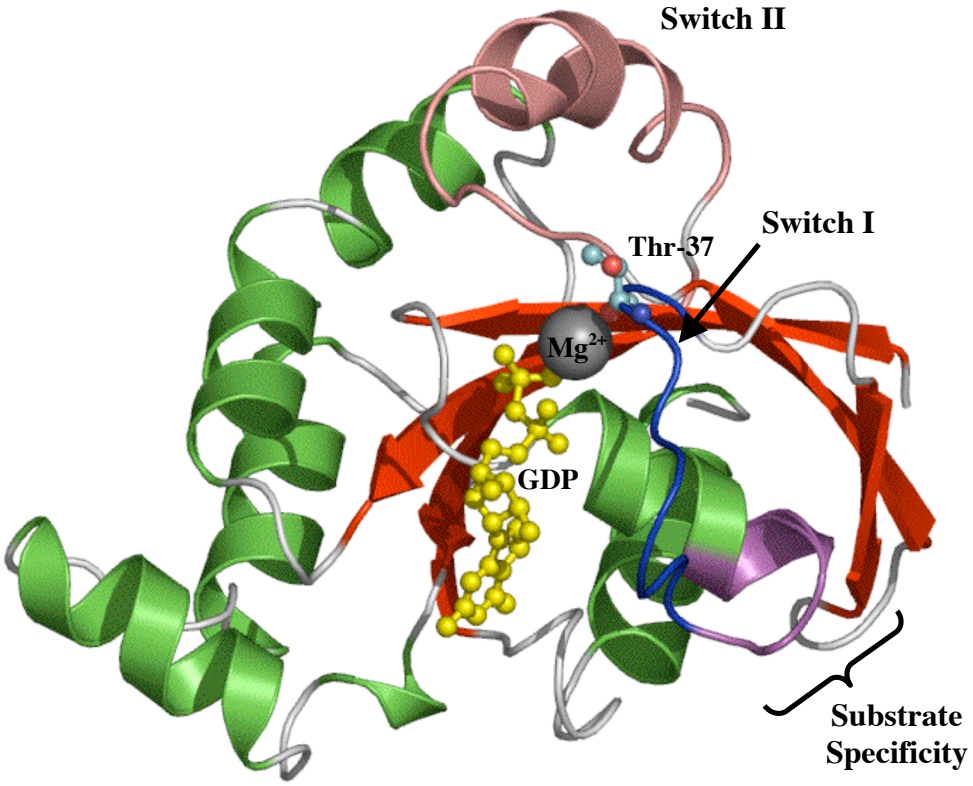

Functional Domains of the LCTs

Based on the known activities for the LCTs, the proteins were predicted to have enzymatic, translocation, and receptor-binding domains, each serving a specific function during cellular intoxication (see Fig. 3). The N-terminal enzymatic and C-terminal receptor-binding domains are the best-understood regions of these proteins, while the membrane-inserting, translocation domain remains undefined.

Organization of the enzymatic domain

The activities necessary for glucosylation are found within a 546 residue N-terminal region of TcdB (80) and the 556 residue N-terminal region of TcsL, as shown in Chapter III. This region can effectively complete glucosylation of substrates *in vitro* but lacks any detectable cytotoxic activity. Furthermore, delivery of this enzymatic domain, using surrogate cell entry systems, results in cytotoxic effects similar to that observed with full-length TcdB (159) and TcsL (Chapter III). It is worth noting 546 residues is still as large or larger than most full-length intracellular bacterial toxins, yet even minor deletions (e.g. 30 residues) from the C-terminal end of this fragment dramatically reduce activity. Conflicting with these studies, Wagenknecht-Wiesner et al. reduced the enzymatically active portion of TcdB to residues 1-467, a region that retained the

Figure 3. Proposed protein domain structure of the LCTs. Through deletion mutagenesis, research combined from multiple research groups has given rise to a three-domain structure of the LCTs. The glycosyltransferase activity is located at the N-terminus of the protein and the C-terminus is involved in receptor binding. Located in the middle domain of the protein is a putative transmembrane segment that is thought to be involved in membrane translocation.

Figure 3.

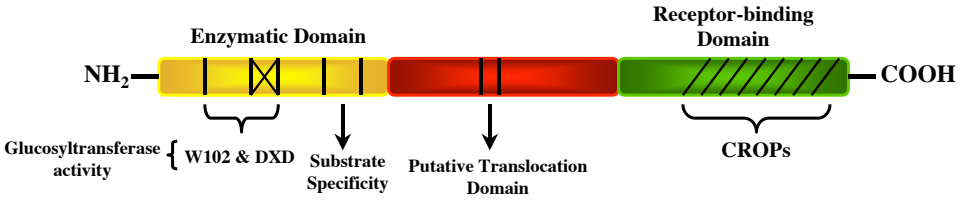
Enzymatic Domain
Receptor-binding Domain
NH2
COOH
Glucosyltransferase activity
W102 & DXD
Substrate Specificity
Putative Translocation Domain
CROPs

ability to glucosylate Rho, Rac, and Cdc42 *in vitro* (174). In contrast, deletions down to residues 1-500 were shown to be completely devoid of enzymatic activity (158).

The substrate recognition region of TcdB and TcsL has been narrowed to residues 364 to 516 by using chimeric hybrids between these two toxins, which target differing subsets of small GTPases (79). By swapping this region between the two toxins, it was possible to change the substrate specificity between TcsL and TcdB and identify the region important for substrate modification. In addition to delineating the region responsible for substrate specificity, Busch and colleagues found that the glucosyltransferase activity of these LCTs is dependent on the presence of a DXD motif in the enzymatic domain (32). Mutations in this vital motif rendered forms of the toxin deficient in the ability to modify small GTPases via glucosylation *in vitro*. The DXD motif is conserved amongst each of the LCTs, indicating its importance in this toxin family. Continuing the investigation of critical regions involved in LCT-induced glucosylation, Busch, et al. determined that Trp-102 is involved in UDP-glucose binding, and mutants lacking this residue were no longer cytotoxic to cells (31). The combined work of these groups has provided a strict basis for the regions of the LCTs involved in substrate specificity and enzymatic activity.

Receptor-Binding Domain

As mentioned above, LCT receptor-binding studies have been performed exclusively using TcdA as a representative member of this toxin family. The C-terminal, receptor-binding domain of TcdA makes up roughly one-third of the toxin, and contains up to 38 repeating CROP modules. However, as noted by Rupnik et al., the CROP region of TcdA has isolate-specific repeats and deletions, suggesting this region of the toxin may be derived from multiple duplication and recombination events within the gene (144). The CROP sequences vary in length, up to 50 amino acids in size, but contain a consensus triad (YYF) and an overall hydrophilic stretch of residues indicative of a solvent-exposed region of the protein (179). This high degree of repetition may explain the agglutinating activity of TcdA. Furthermore, the CROP regions are similar to other proteins including those from *Streptococcus downei* and *Streptococcus mutans*, which function as saccahride-binding proteins (178).

The experimental evidence for receptor binding by the C-terminus of TcdA comes from a series of studies showing the neutralizing capacity of monoclonal antibodies to this region of the protein (56) and the ability of recombinant fragments from this region to protect against the toxin. A fragment of the C-terminus containing the repeat moieties in TcdA was constructed by Sauerborn et al. and was shown to block TcdA-induced cytotoxicity in cell culture by competitive inhibition of receptor binding (145). The same protein fragment

was also found to immunize mice against TcdA. In recent studies, the entire C-terminal, receptor-binding domain has been shown to be necessary for both receptor binding and effective endocytosis of the holotoxin (57). While not yet experimentally shown, the C-terminal repeat regions of the remaining LCTs are thought to act similarly to TcdA.

Influence of LCTs on Cell Physiology

The LCTs have a dramatic influence on mammalian cell physiology, altering events ranging from cell signaling to ultrastructure maintenance. In many cases, cells do not survive intoxication by these toxins, even at relatively low doses in comparison with other cytotoxins. Thus, cell death is one of the most obvious impacts of these toxins on cell physiology. Early studies demonstrated the LCT's broad cell tropism and found TcsL and TcdB to be the more effective cytotoxins. In an initial study by Donta et al., the researchers indicated that TcdB could intoxicate mouse adrenal cells, hamster ovary cells, rat hepatic cells, and human cervical epithelial cells (50). Depending on the cell type, TcdB ranged from 4-fold to 200-fold more cytotoxic than TcdA in these studies. Subsequent studies found that mouse teratocarcinoma cells were more sensitive than CHO cells to TcdA, possibly due to increased levels of TcdA-specific carbohydrate receptors (165). Subsequent studies have shown TcsL to be a potent cytotoxin

similar to TcdB (13, 23), while TcsH has been labeled an enterotoxin that acts in a similar manner to TcdA (108).

Impact on cell morphology

The first, and most obvious, impact on cell physiology is the loss of structural integrity, which results from the decline in F-actin in cells exposed to the LCTs. Chang et al. were among the first investigators to examine ultrastructural changes in intoxicated cells and reported alterations in cell surface projections and rearranged microvilli (37). Upon closer examination, it was found that TcdA altered the ultrastructure of CHO cells, and distinct actinomorphic changes were identified by electron microscopy (53). TcdA-intoxicated cells also demonstrate a distinct cell retraction phenotype, and this is linked to changes in the microfilament system (53). In the same study, marginalization of the nucleus was observed, and, again, this was likely a reflection of changes in the cytoskeleton. Similar studies have been performed using TcdB, and the cytopathic effects observed are like those induced by TcdA. Mechanistically, the loss of structural integrity in TcdA- and TcdB-treated cells is expected since Rho, Rac, and Cdc42 each regulate structural processes dependent on actin polymerization. While the *C. difficile* toxins induce cell rounding with elongated filaments, TcsL induces a more complete cell rounding that makes its cellular effects distinct from those of the other LCTs (13, 23).

Recent studies indicate cell rounding and cell death are temporally distinct events (136). TcdB is capable of inducing cell rounding in less than 2 h, but cell death, as assayed by a variety of methods, does not occur until almost 24 h following treatment. As will be seen in Chapter IV, these observations are similar for TcsL, with cell rounding occurring 6 – 8 h and cell death occurring at 24 h post-treatment. Thus, as these events relate to disease, cytopathic effects may be more relevant than actual cell death, since cells with considerable loss of actin cytoskeleton integrity are unlikely to carry out their roles within the host.

Apoptosis accounts for the mechanism of death in cells exposed to the LCTs. Initial LCT apoptosis studies by Brito and colleagues showed that TcdA induced the apoptotic pathway in T84 intestinal cells via caspases-3, -6, -8, -9, and Bid activation and further demonstrated the disruption of mitochondrial membrane potential and release of cytochrome c (27). However, there are both temporal and spatial reasons to suggest TcdA can induce apoptosis outside of inactivating GTPases. Treatment of cells with TcdA results in accumulation of the toxin at the mitochondria within five minutes following exposure, and this localization event occurs before detectable glucosylation of Rho proteins (73). Thus, TcdA may induce apoptosis by disrupting mitochondria, which promotes pro-apoptotic events.

Following these TcdA studies, TcdB and TcsL were also found to induce apoptosis as a mechanism of death in intoxicated cells. HeLa cells intoxicated by

TcdB were shown to undergo caspase-3-dependent apoptosis with a concurrent loss in host cell vimentin (136). Results in the same study also found TcdB was able to not only induce caspase-dependent cell death, but was also able to induce caspase-independent apoptosis specifically due to substrate inactivation. The proteome of TcdB-treated cells contains fragments of intermediate filaments that result from cleavage by caspase-3. Since intermediate filaments, such as vimentin, are involved in maintaining the cell's structural integrity, the loss of these proteins may also account for changes in cell morphology.

Following this discovery, TcsL was also shown to employ a caspase-dependent form of cell death (129). Results from this study indicated TcsL also induces apoptosis via caspase-3; however, like TcdA, TcsL was shown to rapidly localize to the mitochondria following incubation with cells. These results initially suggest TcsL could also possess a mechanism of cell death separate from its known GTPase activity. Together, these results demonstrate some of the potential effects of GTPase inactivation on the host cell due to intoxication by the LCTs and implicate apoptosis as a major method by which the toxins induce cell death.

CHAPTER II

RATIONALE

While the number of *C. sordellii* cases appears to be on the rise in humans, and the organism continues to present itself as an important veterinary pathogen, little progress has been reported regarding the mechanisms by which this versatile microbe establishes human infection and causes disease. Some progress has been made in understanding biochemical aspects of the LCTs; however, this research has largely been performed alongside the *C. difficile* LCTs. As such, this information, while beneficial to understanding toxin enzymatic activities, lends little to understanding *C. sordellii*-specific pathogenesis.

Following initial reports of LCT production by *C. sordellii*, TcsL and TcsH have been considered to be the primary virulence factors of this pathogen. This, however, has only been experimentally supported in one report, which demonstrated protection from *C. sordellii* following administration of TcsL and TcsH toxoids to hamsters (10). Furthermore, the frequency at which strains of *C. sordellii* produce these LCTs is unknown. While the *C. sordellii* LCTs have been studied in some detail, the remaining virulence determinants, hemolysin, phospholipase C, and neuraminidase, have not been characterized, and, therefore, their contribution to disease is not understood.

In light of these gaps in the current understanding of *C. sordellii*-associated virulence and disease, the work in this dissertation has been performed in order to characterize virulence factor production in this anaerobic pathogen, and these results will be described in Chapter III of this dissertation. Following these initial determinations of *C. sordellii* virulence factor profiles, Chapters IV and V of this dissertation will describe biochemical studies of TcsL and its impact on mammalian cell physiology in order to better understand the mechanism by which this potent cytotoxin induces host cell death. In total, the work described herein, and future studies of *C. sordellii* virulence factors, should, in my opinion, contribute to this area of pathogenesis through a better understanding of the role played by the LCTs and accessory virulence factors.

CHAPTER III

STRAIN CHARACTERIZATION AND ASSESSMENT OF THE VIRULENCE FACTOR PROFILE OF *CLOSTRIDIUM SORDELLII*

TcsL and TcsH, which glucosylate small GTP-binding proteins in the cytosol of mammalian cells, are among the primary virulence factors produced by *C. sordellii* (25) and exhibit low a LD_{50} ranging from 5 – 50 ng/kg in mice (107). In addition, *C. sordellii* has been reported to produce a hemolysin, neuraminidase, and phospholipases (11). Furthermore, whether clinical *C. sordellii* isolates produce one, or combinations, of these virulence factors is currently unknown.

The overall virulence factor profiles of *C. sordellii* isolates have not been determined. Many of the pathogenic clostridia are known to produce a plethora of virulence factors, with some species (e.g. strains of *Clostridium perfringens*) releasing over a dozen different toxins (72). Yet, various types of *C. perfringens* can cause markedly different illnesses, ranging from food poisoning to gas gangrene, and the specific disease directly correlates with the particular toxins produced by the type infecting the host (153). In contrast, other pathogenic clostridia, such as *Clostridium difficile*, *Clostridium tetani*, and *Clostridium botulinum*, produce only one or two major exotoxins and are generally associated with only one disease (72). A survey of clinical descriptions of diseases caused

by *C. sordellii*, suggest this pathogen may be more like *C. perfringens*, as a variety of distinct illnesses have been attributed to this organism (14, 153, 155). In some cases, *C. sordellii* remains localized to the site of infection, with limited myonecrosis, and a shock-like death occurs (143, 151), while in other reports, *C. sordellii* bacteremia directly correlates with death of the patient (1, 46, 117). In cases of postpartum shock, bacteremia can occur, while in other descriptions *C. sordellii* could not be detected in the bloodstream (24, 143). Tissue necrosis also varies among patients with severe *C. sordellii* disease, despite similar modes of infection (14, 29, 155). Indeed, the different forms *C. sordellii* disease - shock-like, localized, systemic, and myonecrotic - do not correlate with the mode of infection, suggesting that different virotypes may largely contribute to the type of disease occurring in the infected patient. Unfortunately, a collective analysis of the virulence factor profiles of different *C. sordellii* isolates has not been performed.

For these reasons, in the current study, we sought to characterize 14 *C. sordellii* isolates collected from cadaver-derived tissue transplant material. The data described herein suggest strain differences are dictated by the presence, or absence, of TcsL and a previously undescribed hemolysin, sordellilysin (SDL). Interestingly, although TcsL has been touted as a major virulence factor, this exotoxin was found at a relatively low frequency, with only one strain producing detectable toxin; yet, this strain was substantially more virulent than other

cadaver-derived isolates. In contrast, SDL was detected at a higher frequency but demonstrated an ~ 10-fold higher LD_{50} compared to TcsL. Collectively, the current findings indicate cadaver-derived isolates of *C. sordellii* differ substantially in their virulence factor profiles and toxicity, raising the possibility of a range of clinical outcomes following transplant of tissue contaminated with this organism.

RESULTS

Characterization of cadaver-derived *C. sordellii* isolates. Candidate isolates of *C. sordellii* were collected from the ATCC, a laboratory stock collection, and during the routine screening of prospective donors of tissue for transplantation. The strains used in this study, and the source of each strain, are listed in Table 1. Although each strain was initially identified as *C. sordellii* by biochemical analysis, the close relationship of this organism to *Clostridium bifermentans* required further analysis of the genes encoding 16S rRNA in each of these isolates for definitive confirmation of genus and species. Each of the *C. sordellii* isolates in this study revealed between 98% and 100% homology with the 16S rRNA-encoding sequence of ATCC strain 9714, which also corresponded to the GenBank reported sequence (accession number M59105) for the 16S rRNA-encoding gene of *C. sordellii*.

Table 1. Virulence Factor Profiles of *C. sordellii* Isolates

Strain	Source	Supernatant Cytotoxicity	*tcsl*	TcsL	Neuraminidase	Hemolytic Activity	*cdc*	Phospholipase C Activity
ATCC9714	ATCC	+	+	+	+	-	+	+
UMTB1	Cadaver	+	-	-	+	+	+	+
UMTB2	Cadaver	+	-	-	+	+	+	+
UMC164	BMA[a]	+	+	+	+	-	+	+
UMC178	BL[b] & BMA	-	-	-	+	-	+	+
UMC193	hemipelvis	-	-	-	+	-	+	+
UMC212	BL & BMA	-	-	-	+	-	+	+
PS4401	BL & ilium	+	-	-	+	+	+	+
PS4404	BL & BMA	+	-	-	+	+	+	+
PS4422	hemipelvis	-	-	-	+	-	+	+
PS4423	BL, BMA, & ilium	-	-	-	+	-	+	-
PS4451	BL, BMA, ilium, & hemipelvis	-	-	-	+	-	+	+
PS4475	BL, ilium, femur, & patella	+	-	-	+	+	+	+
PS4477	BL, BMA, & ilium	-	-	-	+	-	+	+
PS4490	BMA, tibia, & femur	-	-	-	+	-	+	+

[a] BMA = Bone Marrow Aspirate
[b] BL = Blood Culture

Ribotype analysis of *C. sordellii* strains. PCR ribotyping was employed to determine the relative genotypic similarity between the cadaver-derived isolates of *C. sordellii*. The profile of PCR amplified products ranging in size from 400 to 800 bp was analyzed to make relative comparisons among the isolates of *C. sordellii*, since this size region demonstrated the most variation between strains. As shown in Fig. 4, this analysis led to the identification of five distinct ribotypes. For reasons that remain unclear, one strain (PS4401) yielded weaker amplification products than the remaining 14 isolates, despite the addition of excess primers and template DNA to the standard reaction. Collectively, these strains were categorized into the following ribotype groups: Ribotype I (ATCC9714), Ribotype II (UMTB2 and UMC178), Ribotype III (UMTB1), Ribotype IV (UMC164, UMC193, UMC212, PS4423, and PS4475), and Ribotype V (PS4401, PS4404, PS4422, PS4451, PS4477, and PS4490).

Phenotypic characterization of cadaver-derived isolates of *C. sordellii*. In light of the genotypic variation observed among the *C. sordellii* isolates, each of the strains was further examined for phenotypic differences including variations in morphology, antibiotic susceptibility, phospholipase activity, and presence of neuraminidase activity. As shown in Fig. 5, when observed using transmission electron microscopy, all strains used in this study exhibited a similar rod-shaped morphology. Each of the rods measured ~ 3 – 6 μM in length and

Figure 4. PCR ribotyping of *C. sordellii* isolates. Oligonucleotide primers designed to amplify the intergenic region between the 16S and 23S rRNA-encoding genes were included in PCR reactions for each isolate. Amplification products were separated via 2% agarose gel electrophoresis and visualized via ethidium bromide staining. Lanes are designated by the strain name of each isolate in the figure, and ribotype designations are indicated below the gel. The profile shown is representative of five experimental repeats of this analysis.

Figure. 4.

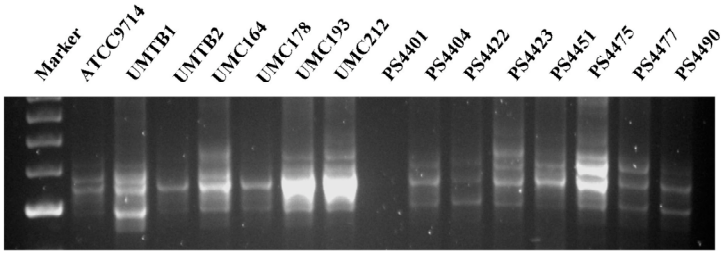
Marker
ATCC9714
UMTB1
UMTB2
UMC164
UMC178
UMC193
UMC212
PS4401
PS4404
PS4422
PS4423
PS4451
PS4475
PS4477
PS4490

Figure 5. TEM analysis of *C. sordellii* isolates. Mid-log phase cultures of each isolate were collected and placed on Formvar-coated electron microscopy grids. Following a 5 min incubation on the grids, each sample was stained with 2% phosphotungstic acid for 15 sec. After drying, grids were examined via TEM and the pictures shown are representative of the cells seen across the grid for each isolate. Samples were observed at 4000 – 6000 X magnification and strain designations are indicated in the figure.

Figure 5.

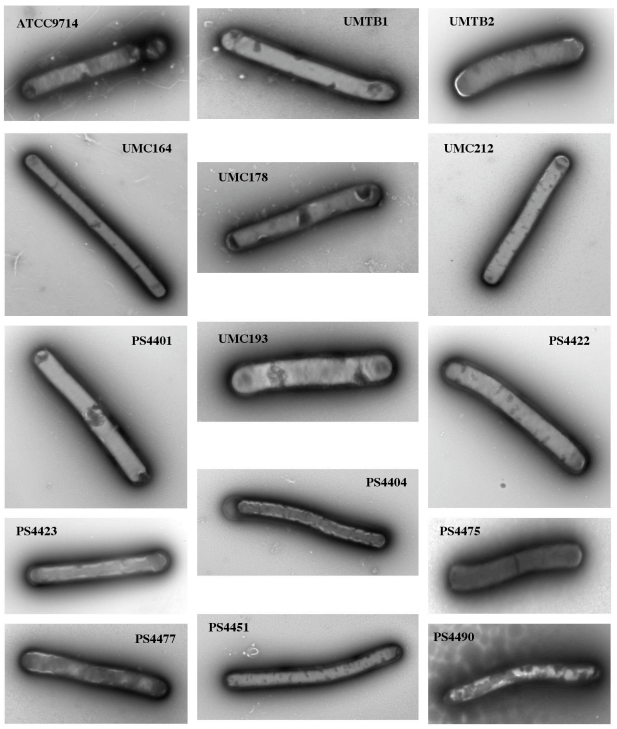
ATCC9714
UMTB1
UMTB2
UMC164
UMC178
UMC212
PS4401
UMC193
PS4422
PS4404
PS4423
PS4475
PS4477
PS4451
PS4490

contained sub-terminal endospores, all of which corresponded with the reported characteristics of *C. sordellii* (141).

Using the antibiotic disk method for relative comparisons among strains, each of the *C. sordellii* isolates were examined for sensitivity/resistance to cefoxitin, ceftriaxone, gentamicin, erythromycin, clindamycin, vancomycin, ampicillin, penicillin G, amoxicillin/clavulanic acid, ciprofloxacin, levofloxacin, and tetracycline. As shown in Table 2, 11 of the strains showed intermediate resistance to clindamycin. Nine of the isolates demonstrated intermediate resistance to ciprofloxacin and two of the 15 strains showed intermediate resistance to gentamicin. Additionally, one isolate, PS4490, demonstrated resistance to tetracycline relative to the other *C. sordellii* strains tested. Since clindamycin is used as a first line of treatment in anaerobic infections, strain susceptibility to this antibiotic was further confirmed using the E-test method for direct minimal inhibitory concentration (MIC) measurements. Using this method, the same 11 isolates showed resistance at 4 – 10 μg clindamycin/ml (data not shown), which is consistent with intermediate resistance when compared to the known clindamycin susceptibility standards for anaerobic organisms.

For further phenotypic characterization of the *C. sordellii* isolates, phospholipase and neuraminidase activities were examined, since these proteins have been previously described as putative virulence factors produced by *C. sordellii* (11). As shown in Table 1, each of the strains in this study produced

Table 2. Antimicrobial Resistance of *C. sordellii* Isolates (zones of clearing (mm))

Strain	GEN	CLI	TET	CIP
ATCC9714	**I**[a] (13)	**R**[b] (12)	S[c] (28)	**I** (16)
UMTB1	S (19)	**I** (18)	S (36)	S (21)
UMTB2	S (15)	**R** (13)	S (31)	**I** (20)
UMC164	**I** (12)	**R** (10)	S (29)	**I** (16)
UMC178	S (23)	**I** (15)	S (35)	**I** (17)
UMC193	S (18)	**R** (14)	S (40)	S (21)
UMC212	S (16)	S (20)	S (29)	**I** (19)
PS4401	S (16)	**R** (12)	S (32)	**I** (20)
PS4404	S (19)	**I** (16)	S (36)	**I** (20)
PS4422	S (20)	S (29)	S (35)	**I** (20)
PS4423	S (18)	S (19)	S (38)	S (21)
PS4451	S (17)	**R** (11)	S (33)	**I** (20)
PS4475	S (18)	S (23)	S (35)	S (22)
PS4477	S (19)	**I** (18)	S (36)	**I** (19)
PS4490	S (15)	**R** (13)	**I** (16)	**I** (19)

[a] I = Intermediate Resistance
[b] R = Resistant
[c] S = Sensitive

active neuraminidase, and 14 of the 15 strains demonstrated phospholipase activity. Collectively, these data, along with the ribotyping and antibiotic susceptibility results, suggested both genotypic and phenotypic variability among these isolates of *C. sordellii*.

Cytotoxicity of supernatants from *C. sordellii* isolates. As shown in Table 1, initial analysis of 24 h and 48 h culture supernatants from each of the isolates found 7 of the 15 strains to possess cytotoxic activity when incubated with cultured HeLa cells. Cell rounding, indicative of TcsL-like cytopathic effects (CPE), was only detected upon exposure to supernatants from *C. sordellii* ATCC9714 and UMC164, even when the supernatants from other strains were concentrated 10-100 fold and assayed for activity (Fig. 6C). The CPE observed following treatment with supernatant from strains UMTB1, UMTB2, PS4401, PS4404, and PS4475 were different from morphological changes observed in a routine TcsL treatment. Supernatants from these 5 strains caused rapid cell rounding, blebbing, and lysis within 2 h following treatment (Fig. 6B). This time-course of cytolysis contrasted with the effects observed following exposure of the cells to supernatants from ATCC9714 and UMC164, in which case, CPE were not observed until 24 h following treatment. Furthermore, cells treated with supernatants from ATCC9714 and UMC164 showed morphological changes similar to those observed in treatments with purified TcsL, wherein cells demonstrated marked cell rounding without blebbing or detectable lysis (Fig. 6C).

Figure 6. Supernatant cytotoxicity of *C. sordellii* isolates. Culture supernatant (48 h) from each of the *C. sordellii* strains was incubated with an ~ 75% confluent HeLa cell monolayer in a 96-well plate in a total of 100 μl/well and observed for 72 h for CPE. Pictures shown are representative of a routine cell treatment with the indicated supernatant, and cells were observed at a magnification of 140 X. All hemolytic strains induced similar effects as the PS4404 cell treatment shown here. (A) Control cells. (B) PS4404 treatment at 2 h. (C) UMC164 treatment at 24 h.

Figure 6.

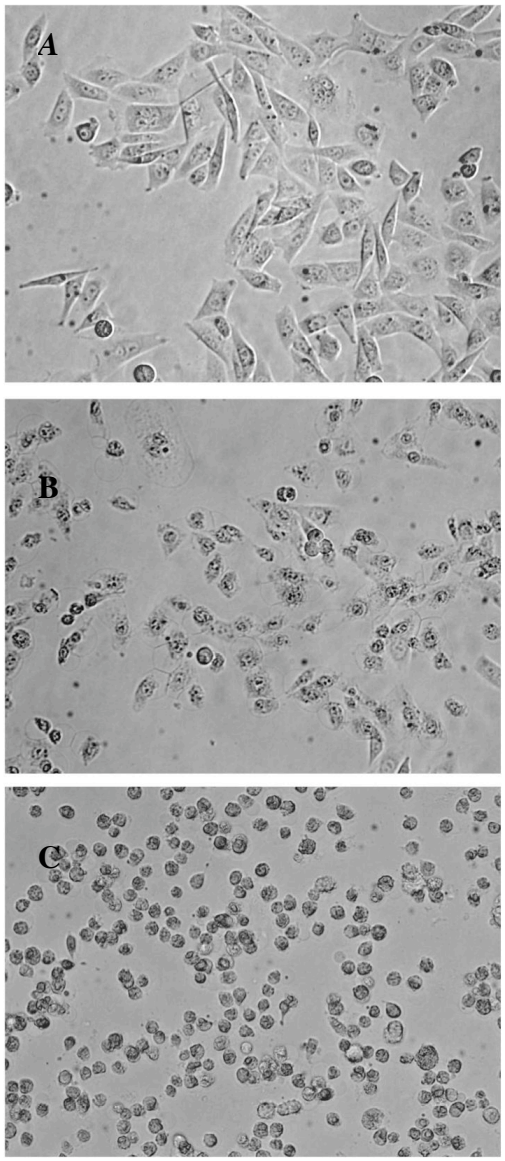

These observations indicated that cytolytic strains UMTB1, UMTB2, PS4401, PS4404, and PS4475 caused cell death through a non-TcsL mechanism, which differed from ATCC9714 and UMC164.

TcsL in isolates of *C. sordellii*. Based on these observations, each of the 15 isolates was examined for the presence of the gene encoding TcsL. In line with the absence of TcsL-like CPE in the strains described above, only strains ATCC9714 and UMC164 contained amplified DNA fragments corresponding to regions of *tcsl* (Fig. 7A). Furthermore, using Southern hybridization, *tcsl* was detected only in ATCC9714 and UMC164 (Fig. 7B).

Following PCR and Southern blot analysis, the presence of TcsL was confirmed by purifying and analyzing TcsL isolated from dialysis bag cultures of *C. sordellii* ATCC9714 and UMC164. As shown in Fig. 7C, TcsL produced by *C. sordellii* UMC164 migrated at the correct size (~ 270 kDa) as a protein doublet, as described in Chapter IV for TcsL produced by *C. sordellii* ATCC9714, when examined via SDS-PAGE. Additionally, both bands of the TcsL protein doublet produced by this strain reacted with TcsL-specific antiserum (Fig. 7D). Immunoblot analysis of supernatant from the remaining *C. sordellii* strains did not detect proteins corresponding to TcsL (data not shown). To further examine TcsL-UMC164, the protein was analyzed in a glucosylation assay for TcsL-specific activity. TcsL is known to modify Ras, Rac, and Cdc42, while it does not glucosylate Rho, a *C. difficile* Toxin B-specific substrate (25). As shown

Figure 7. Analysis of *tcsl* and TcsL in *C. sordellii* isolates. (A) Oligonucleotide primers designed to amplify defined regions of the *tcsl* gene were included in PCR reactions for each *C. sordellii* isolate. Amplification products were separated via 0.8% agarose gel electrophoresis and visualized via ethidium bromide staining. Shown are the reactions for ATCC9714 and UMC164. Lane 1 = $tcsl_{1\text{-}1668}$, Lane 2 = $tcsl_{1669\text{-}3468}$, Lane 3 = $tcsl_{3469\text{-}5271}$, and Lane 4 = $tcsl_{5272\text{-}7095}$. (B) Chromosomal DNA from *C. sordellii* ATCC9714 and UMC164 was probed for the presence of a ~ 1.7 kb region of *tcsl* via Southern blot analysis. Lanes are designated by the name of the respective *C. sordellii* strain. (C) Purified TcsL from *C. sordellii* UMC164 was visualized via 10% SDS-PAGE and Coomassie Blue staining. *C. sordellii* ATCC9714 was visualized for size comparison. (D) Purified TcsL from *C. sordellii* UMC164 was detected via Western blotting using TcsL-specific antiserum. Lanes are designated by the strain name of each *C. sordellii* isolate. (E) TcsL isolated from *C. sordellii* UMC164 was included in a standard glucosylation assay with Rho, Ras, Rac, and Cdc42. TcsL from *C. sordellii* ATCC9714 is included as a control and samples are designated above the gel.

Figure 7.

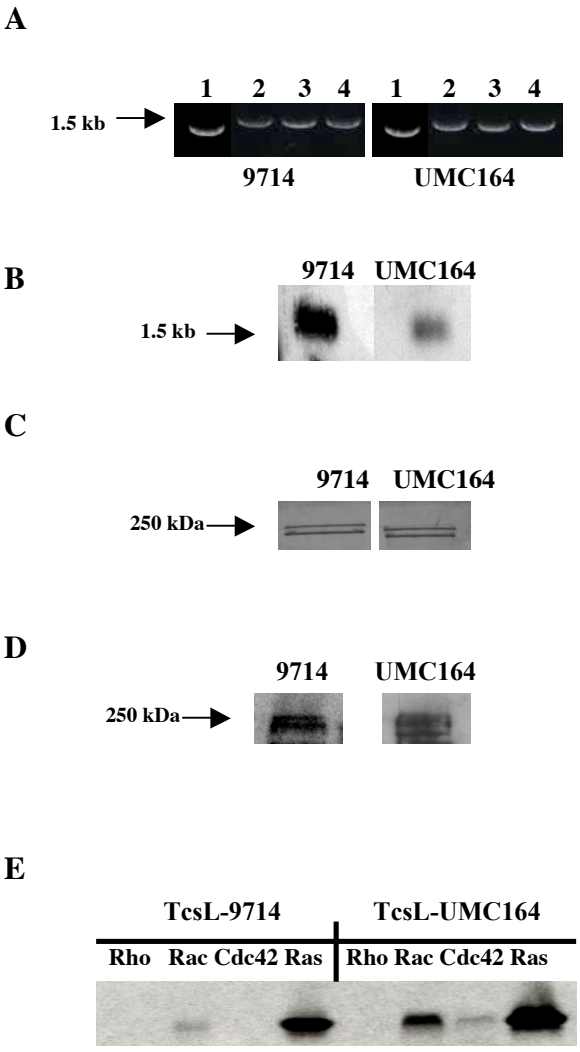
A
1 2 3 4 1 2 3 4
1.5 kb
9714
UMC164
B
9714 UMC164
1.5 kb
C
9714 UMC164
250 kDa
D
9714 UMC164
250 kDa
E
TcsL-9714
TcsL-UMC164
Rho Rac Cdc42 Ras
Rho Rac Cdc42 Ras

in Fig. 7E, TcsL-UMC164 glucosylated Ras, Rac, and Cdc42 similar to TcsL-9714, while no modification of Rho was observed in this assay.

Characterization of cytolytic activity in *C. sordellii* isolates. The cytolytic activity of TcsL$^-$, cytolytic supernatants was similar to that reported in studies of the cholesterol-dependent cytolysins (CDCs) (167). These bacterial toxins induce erythrocyte lysis and have been reported to cause tissue culture cell lysis (167). Thus, TcsL$^-$, cytolytic strains were examined using a standard hemolytic assay, which indicated that each of the TcsL$^-$, cytolytic strains lysed erythrocytes (data not shown). To investigate the nature of this hemolytic factor, these strains were further examined for the presence of a CDC by PCR analysis using primers homologous to *pfo*, the gene encoding *Clostridium perfringens* perfringolysin O (PFO). As shown in Fig. 8A, each of the 15 *C. sordellii* strains was found to contain an ~ 1 kbp region of *pfo*. Since each strain contained a homologous segment of DNA corresponding to *pfo*, each of the five hemolytic *C. sordellii* strain supernatants was analyzed via Western blot analysis, using a PFO-specific primary antibody, to determine protein homology with the CDC toxin family. As shown in Fig. 8B, each of the five hemolytic supernatants contained a protein that reacted with, and was similar in molecular weight, to PFO. These results correlated directly with the ability of these strains to induce cytolysis in tissue culture and erythrocyte lysis *in vitro*.

Figure 8. Analysis of *pfo* and SDL in *C. sordellii* isolates. (A) Oligonucleotide primers designed to amplify *cdc* based on the reported sequence of *pfo* were included in PCR reactions for each *C. sordellii* isolate. Amplification products were separated by 0.8% agarose gel electrophoresis and visualized via ethidium bromide staining. Lanes are designated by the strain names of each isolate in the figure. pRT20, a plasmid containing the *pfo*-encoding gene, was included as the positive control. (B) Ten μg of each supernatant was separated via 10% SDS-PAGE and proteins were transferred to a PVDF membrane. Following transfer, the membrane was incubated with a PFO-specific primary antibody for observation of reacting proteins. Reacting proteins were visualized via enhanced chemiluminescence and the lanes are designated above the blot.

Figure 8.

A

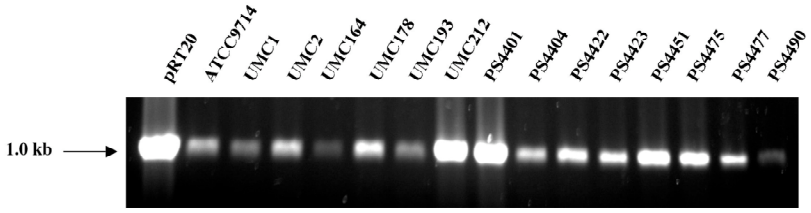
pRT20
ATCC9714
UMC1
UMC2
UMC164
UMC178
UMC193
UMC212
PS4401
PS4404
PS4422
PS4423
PS4451
PS4475
PS4477
PS4490
1.0 kb

B

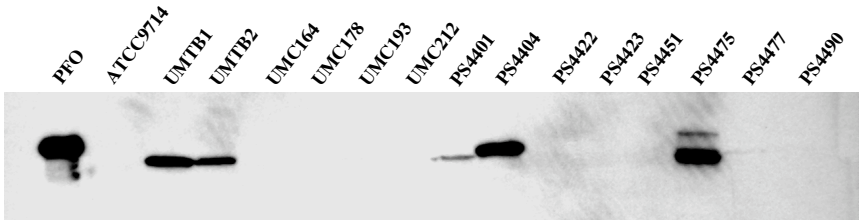
PFO
ATCC9714
UMTB1
UMTB2
UMC164
UMC178
UMC193
UMC212
PS4401
PS4404
PS4422
PS4423
PS4451
PS4475
PS4477
PS4490

Cell type specificity of TcsL and sordellilysin (SDL). Based on the initial characterization of the *C. sordellii* isolates, we reasoned that supernatants from these strains might demonstrate differences in cell tropism and cytotoxicity. To address this, a panel of cell lines was examined for sensitivity to supernatants from cytotoxic $TcsL^-$ and $TcsL^+$ strains. HeLa (human epithelial), CHO (hamster fibroblast), NIH/3T3 (mouse fibroblast), Raw 264.7 (mouse macrophage), and HUV-EC-C (human endothelial) cells were examined for sensitivity to strain supernatants. As shown in Fig. 9A, each cell type was sensitive to $TcsL^-$, SDL^+ supernatants (PS4404) when exposed to 1 and 10 μg of supernatant for 24 h. However, HUV-EC-C cells were substantially more resistant to cytolytic activity at these concentrations, with ~ 40 – 50% reduction in cell viability at 24 h.

As shown in Fig. 9B, each cell type was sensitive to supernatant from the $TcsL^+$, SDL^- *C. sordellii* isolate (UMC164). However, Raw 264.7 cells were only marginally sensitive to this supernatant, with an ~ 15 – 20% reduction in cell viability at 24 h. This resistance, however, did not correlate with CPE (Fig. 9C), as Raw 264.7 cells displayed CPE when exposed to 1 and 10 μg of supernatant protein. In contrast to supernatant from a $TcsL^-$, SDL^+ strain, HUV-EC-C cells showed increased sensitivity to supernatant from $TcsL^+$, SDL^- isolates, with 80-100% CPE occurring at each concentration tested. Additionally, the viability of HUV-EC-C cells, in response to $TcsL^+$, SDL^- supernatant, decreased at each concentration, with an ~ 25% decrease in survival when exposed to 0.01 μg of

Figure 9. Cellular specificity of *C. sordellii* virulence factors. Culture supernatants from *C. sordellii* UMC164 ($TcsL^+$, non-hemolytic) and *C. sordellii* PS4404 ($TcsL^-$, hemolytic) were incubated separately with HeLa, CHO, NIH/3T3, Raw 264.7, and HUV-EC-C cells at the indicated concentrations in a total volume of 100 µl/well. At 24 h post treatment, cells were examined for CPE by visualization and for viability via CCK-8 staining as described in Materials and Methods. Treatments were performed in triplicate and error bars indicate the standard deviation from the mean. (A) Viability of cells incubated with PS4404 supernatant. (B) Viability of cells incubated with UMC164 supernatant. (C) CPE of cells incubated with UMC164 supernatant. % CPE was determined by counting the number of rounded cells in a field of 100 cells in three separate wells for each condition. ◪ = HeLa, ■ = CHO, ⊡ =NIH/3T3, ■ =Raw 264.7, and □ =HUV-EC-C.

Figure 9.

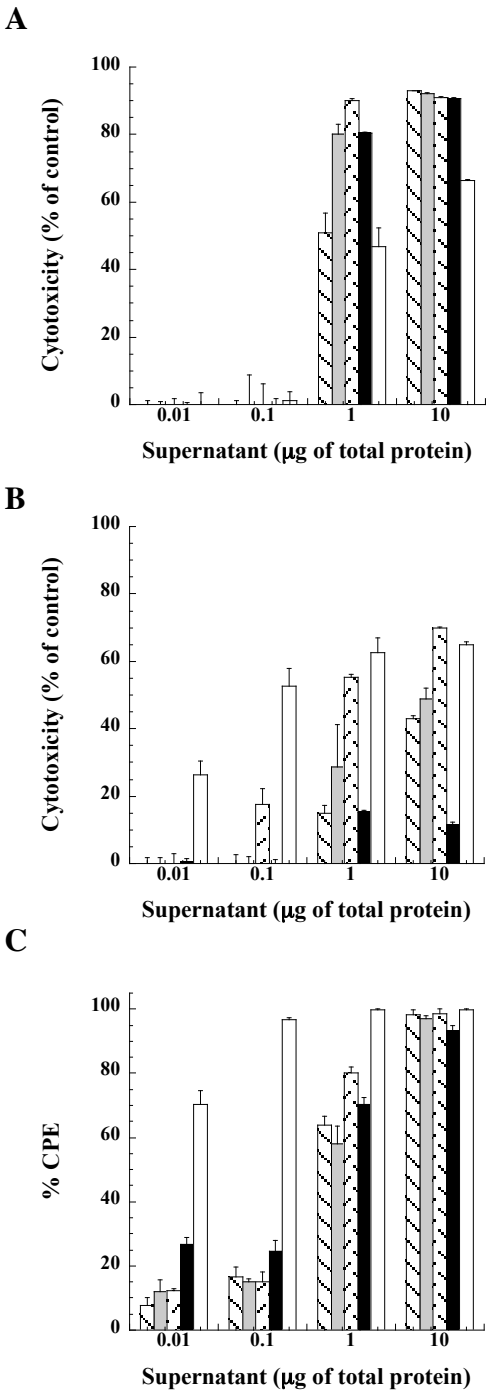
A
Cytotoxicity (% of control)
100
80
60
40
20
0
0.01
0.1
1
10
Supernatant (μg of total protein)
B
Cytotoxicity (% of control)
100
80
60
40
20
0
0.01
0.1
1
10
Supernatant (μg of total protein)
C
% CPE
100
80
60
40
20
0
0.01
0.1
1
10
Supernatant (μg of total protein)

supernatant protein and an ~ 65% decrease when exposed to 10 μg of supernatant protein.

LD_{50} analysis of $TcsL^+$ and SDL^+ supernatants in BALB/c mice. Findings from the tissue culture analyses indicated supernatants from the two *C. sordellii* strains might exhibit differing effects *in vivo*, since distinct differences exist in tissue tropism for these isolates. To examine the effect of TcsL and SDL on virulence *in vivo*, *C. sordellii* supernatant - $TcsL^+$, SDL^- or $TcsL^+$, SDL^- - was injected into the tail veins of female BALB/c mice and mice were observed for 24 h. Mice injected with 25 – 50 μg of $TcsL^+$, SDL^- supernatant showed lethargy leading to death by 24 h, while mice injected with a 10-fold excess (400 – 500 μg) of $TcsL^-$, SDL^+ supernatant demonstrated lethargy leading to death by 24 h (data not shown). Indeed, further analysis revealed an LD_{50} between 30-40 μg for $TcsL^+$ supernatant. These results indicate the importance of TcsL in *C. sordellii* infection, with $TcsL^+$ supernatant demonstrating much lower LD_{50} values than SDL^+ supernatants.

DISCUSSION

In the current study, virulence profiles were determined for 14 *C. sordellii* cadaver-derived isolates, which had been collected from candidate tissue transplant material. Prior to this work, *C. sordellii* has been recognized as a severe pathogen capable of causing disease in a variety of clinical settings; yet,

very little is known about the phenotypic and genotypic variability of this organism, especially in regard to virulence.

C. sordellii is a primary bacterial contaminant of tissue transplant material and is detected at a relatively high frequency (104, 106). Since the cadaver donors died from causes other than *C. sordellii*, and transplant material is harvested under sterile conditions, these isolates likely came from bowel flora that entered the bloodstream soon after death. *C. sordellii* residing in the normal bowel flora may also be responsible for post-partum infection, as intestinal contents come in contact with damaged tissue. Yet, such observations present a conundrum because isolates are identified more often than the actual frequency of disease. One possible explanation for this observation is that initiation of disease requires a combination of events before serious illness can occur. Alternatively, it is plausible that most isolates of *C. sordellii* are avirulent, and, despite their detection, these strains do not have the capacity to cause disease. Finally, a limited number of early reports suggest *C. sordellii* as a cause of myonecrotic disease (14, 155, 157), while many recent studies have associated this organism with a shock-like illness involving limited tissue damage (24, 143, 151). Again, these differences in *C. sordellii* disease could be due to the mechanism and site of infection or due to the fact that some strains possess virulence factors that mediate tissue destruction, while other strains produce toxins that induce shock.

To address this issue, in the current study, we were able to take advantage of the fact that *C. sordellii* is routinely isolated from cadaver-derived tissue transplant material. By using this single source of *C. sordellii* isolates, we were able to assess differences in virulence among strains that exist in similar host settings. Prior to analysis of the virulence factor profiles, the strains were characterized for basic genotypic and phenotypic differences. These preliminary analyses suggested a notable degree of diversity among the strains, with at least 10 unique strains based on ribotyping, antibiotic resistance profile, and virulence factor variation (summarized in Table 3). This is a relatively high level of diversity, even for a member of the genus *Clostridium*. For example, in a recent study of *C. difficile* toxinotypes, ~ 80% of the 153 strains examined belonged to the same toxinotype (65). Additionally, *C. perfringens* strains are grouped into one of five different toxinotypes, A – E, with no variation in the virulence factor profiles in each toxinotype (153).

Although *C. sordellii* is considered a highly virulent, toxigenic pathogen, only 6 of the 14 strains analyzed conferred cytotoxic effects in the panel of cell lines tested. While each of the strains produced neuraminidase, and all but one was positive for phospholipase C activity, only the isolates producing TcsL or SDL induced cytotoxic effects. Yet, even the $TcsL^+$ and SDL^+ strains demonstrated differences in cell type specificity. Most cell types were sensitive to the SDL^+ supernatants, and this was somewhat expected since CDCs are known

Table 3. Phenotypic and Genotypic Characterization of *C. sordellii* Isolates

Ribotype & Strain	Characterization
Ribotype I	
ATCC9714	*tcsl*$^{+}$, *cdc*$^{+}$, TcsL^{+}, Neu^{+}, CDC^{-}, Csp^{+}, GEN^{I}, CLI^{R}, CIP^{I}
Ribotype II	
UMTB2	*tcsl*$^{-}$, *cdc*$^{+}$, TcsL^{-}, Neu^{+}, CDC^{+}, Csp^{+}, CLI^{R}, CIP^{I}
UMC178	*tcsl*$^{-}$, *cdc*$^{+}$, TcsL^{-}, Neu^{+}, CDC^{-}, Csp^{+}, CLI^{I}, CIP^{I}
Ribotype III	
UMTB1	*tcsl*$^{-}$, *cdc*$^{+}$, TcsL^{-}, Neu^{+}, CDC^{+}, Csp^{+}, CLI^{I}
Ribotype IV	
UMC164	*tcsl*$^{+}$, *cdc*$^{+}$, TcsL^{+}, Neu^{+}, CDC^{-}, Csp^{+}, GEN^{I}, CLI^{R}, CIP^{I}, LVX^{I}
UMC193	*tcsl*$^{-}$, *cdc*$^{+}$, TcsL^{-}, Neu^{+}, CDC^{-}, Csp^{+}, CLI^{R}
UMC212	*tcsl*$^{-}$, *cdc*$^{+}$, TcsL^{-}, Neu^{+}, CDC^{-}, Csp^{+}, CIP^{I}
PS4423	*tcsl*$^{-}$, *cdc*$^{+}$, TcsL^{-}, Neu^{+}, CDC^{-}, Csp^{-}
PS4475	*tcsl*$^{-}$, *cdc*$^{+}$, TcsL^{-}, Neu^{+}, CDC^{+}, Csp^{+}
Ribotype V	
PS4401	*tcsl*$^{-}$, *cdc*$^{+}$, TcsL^{-}, Neu^{+}, CDC^{+}, Csp^{+}, CLI^{R}, CIP^{I}
PS4404	*tcsl*$^{-}$, *cdc*$^{+}$, TcsL^{-}, Neu^{+}, CDC^{+}, Csp^{+}, CLI^{I}, CIP^{I}
PS4422	*tcsl*$^{-}$, *cdc*$^{+}$, TcsL^{-}, Neu^{+}, CDC^{-}, Csp^{+}, CIP^{I}
PS4451	*tcsl*$^{-}$, *cdc*$^{+}$, TcsL^{-}, Neu^{+}, CDC^{-}, Csp^{+}, CLI^{R}, CIP^{I}
PS4477	*tcsl*$^{-}$, *cdc*$^{+}$, TcsL^{-}, Neu^{+}, CDC^{-}, Csp^{+}, CLI^{I}, CIP^{I}
PS4490	*tcsl*$^{-}$, *cdc*$^{+}$, TcsL^{-}, Neu^{+}, CDC^{-}, Csp^{+}, CLI^{R}, CIP^{I}, TET^{I}

to lyse a broad range of cell types (167). In contrast, the TcsL$^+$ supernatant was cytotoxic but more specific in cell tropism, and the TCD_{50} varied depending on the type of cell tested. This is likely due to either limitations in cell surface receptor number or the dependence of different cells on small GTPase-targeted signaling pathways. The extensive sensitivity of endothelial cells to TcsL$^+$ supernatants was of particular interest, since *C. sordellii* is known to cause severe shock-like illness in post-partum women and sudden death in livestock. In future studies, it will be of particular interest to characterize strains involved with shock from *C. sordellii* infections to determine if these are TcsL$^+$ isolates.

Based on our LD_{50} analyses, SDL demonstrated an ~ 10-fold higher LD_{50} in mice compared to TcsL. The absence of a pronounced *in vivo* effect of SDL is not unusual given what has been found in studies involving other CDCs. Indeed, in the case of PFO, mutants lacking this CDC show only minor alterations in virulence (12). Finally, it is worth noting that the SDL-encoding gene was detected in all of the *C. sordellii* strains examined in this study; however, the toxin was only expressed in five of the isolates. This suggests that many strains may have attenuated the expression of SDL as the organism resides as part of the normal bowel flora.

While the current study focused on characterizing the virulence profile of *C. sordellii* in the context of tissue transplant material, these findings can be extrapolated to other types of disease caused by this organism. With the

exception of intravenous drug users, *C. sordellii* disease is initiated from endogenous sources, likely through the relocalization of bowel flora to the site of tissue damage. Thus, the variations in strains, detected in tissue transplantation material, also represents the possible differences in isolates that could contribute to other types of *C. sordellii* disease. This may also explain why *C. sordellii* disease is sporadic, yet, invariably severe. One would predict that post-partum contamination of damaged tissue with bowel flora is not particularly uncommon; yet, *C. sordellii* causes disease infrequently in this clinical setting (24, 110, 143, 151). However, *Clostridium* species have been reported to be isolated from the vaginal flora of ~ 4% of non-pregnant women and ~ 29% of women following abortion, making this a favorable niche for anaerobic growth (21, 84). Furthermore, a shock-like disease caused by *C. sordellii* has been reported in 3 women taking RU486 (34). While still speculative, based on our findings, these cases may involve an unfortunate combination of post-partum or post-abortion tissue damage and women colonized with a virulent strain of *C. sordellii*.

MATERIALS AND METHODS

Mammalian cell culture, bacterial strains, and TcsL purification. Human epitheloid carcinoma (HeLa) cells, Chinese Hamster Ovary (CHO) cells, NIH/3T3 mouse fibroblasts, human umbilical vein endothelial cells (HUV-EC-C), and Raw 264.7 mouse macrophage-like cells were obtained from the American

Type Culture Collection (ATCC). HeLa, CHO, and NIH/3T3 cells were maintained in RPMI 1640 medium supplemented with 10% fetal bovine serum (Gibco) at 37°C in the presence of 6% CO_2. HUV-EC-C cells were maintained in CS-C medium (Sigma) containing 0.1 mg/ml heparin (Sigma) and 0.05 mg/ml endothelial cell growth supplement (Sigma). Raw 264.7 cells were maintained in Dulbecco's Modified Eagle's Medium (Gibco) containing 10% fetal bovine serum. All cells were used between passages 10 and 20. *C. sordellii* ATCC9714 was obtained from the ATCC, and all other *C. sordellii* strains were isolated in the microbiology laboratory of the University of Miami Tissue Bank during routine screening of cadaver-derived tissues from clinically non-septic donors. All *C. sordellii* strains were cultured anaerobically in Brain Heart Infusion (BHI) broth (Difco) at 37°C prior to analysis. For anaerobic growth, strains were cultured in 10 ml of BHI broth in anaerobic Balch tubes. TcsL was purified from *C. sordellii* strains ATCC9714 and UMC164 as previously described (137). Unless otherwise indicated, all chemical reagents used in this study were obtained from Sigma.

Isolation and initial characterization of cadaver-derived *C. sordellii* isolates. All isolates were recovered from anaerobic cultures of the blood, bone marrow aspirates, or excised bones of donors previously screened by medical history and physical examination to exclude the presence of clinically evident sepsis. All samples of blood, bone marrow, and tissues were collected under aseptic conditions in designated sterile facilities. The organisms isolated were

identified to the species level by means of biochemical tests using the Microscan Rapid Anaerobic ID Panel (Dade Behring). Organisms with a biochemical profile consistent with *C. sordellii* were further tested for confirmation of key reactions by conventional methods. These included tests for indole production by a spot indole test (Remel), tests for urease production in urea agar slants (BBL) and/or urea broth (Remel), and assays for phospholipase production. Phospholipase activity was determined by the presence of a visible precipitate around colonies of the organism after growth on egg yolk agar (McClung-Toabe Agar, Modified) (Remel).

PCR analysis of the 16S rRNA-encoding gene, *tcsl*, and *cdc* in *C. sordellii* isolates. Oligonucleotides (Integrated DNA Technologies, Inc.) were included in PCR reactions with bacterial cells from each *C. sordellii* isolate for amplification of the indicated genes. Amplifications were performed in a 50 µl reaction that included PCR reaction buffer containing 1.5 mM $MgCl_2$ (Roche Diagnostics), 300 nM of each primer indicated below, 200 µM dNTPs (Roche Diagnostics), 1 µl of bacterial culture, and 2.6 units of Expand High Fidelity polymerase (Roche Diagnostics). Products were amplified using the following temperature cycling conditions: 1 min at 95°C for initial denaturation followed by 35 cycles consisting of 1) 95°C 1 min, 2) indicated annealing temperature 1 min, 3) 72°C 90 sec, followed by a final extension at 72°C for 15 min. PCR

amplification products were subsequently visualized via 0.8% agarose gel electrophoresis and ethidium bromide staining.

i) Amplification of the 16S rRNA-encoding gene. Oligonucleotides were designed to amplify the gene encoding 16S rRNA based on conserved sequence among members of the domain *Bacteria* (97) and are designated 27F and 1492R. Primer sequences were as follows: 27F = 5'-AGAGTTTGATCMTGG-3' and 1492R = 5'-TACCTTGTTACGACTT-3'. An annealing temperature of 55°C was used in each reaction. PCR amplification products were subsequently purified using the Qiaquick PCR purification kit (Qiagen) and were cloned into the pGEM/T-Easy vector (Promega) according to the manufacturer's instructions. Plasmid from candidate clones was purified using the Qiaquick MiniPrep system (Qiagen) and subsequently analyzed by DNA sequencing for identification of the 16S rRNA species-specific sequences of each strain. Sequence alignments were performed and the entire 16S rRNA-encoding gene sequences were examined for homology. The resulting sequences were compared to each other and also compared against the GenBank database.

ii) Amplification of *tcsl*. Primers were designed to amplify four separate regions (nucleotides 1-1668, 1669-3468, 3469-5271, and 5272-7095) of the *tcsl* gene and were as follows: forward primer 1 = 5'-GACTGACATATGATGAACTTAGTTAACAAAGCCCAA-3', reverse primer 1 = 5'-GACTGAGGATCCTTATACTGTATTTTGAGCAAAATC-3', forward

primer 2 = 5'-GACTGACATATGCTTGATAAAGATTATGTTTCTAAA-3', reverse primer 2 = 5'-GACTGAGGATCCTTAGTCTATTTCTGATAATACCAA-3', forward primer 3 = 5'-GACTGACATATGTTTAATAATAATTCAATAACTTTA-3', reverse primer 3 = 5'-GACTGAGGATCCTTACTCACTATTTGCTATAAGAAT-3', forward primer 4 = 5'-GACTGACATATGGAAGATAATCAACGACAAGTTAAA-3', reverse primer 4 = 5'-GACTGAGGATCCTTATTCACTAACTACTAATTCAGC-3'. An annealing temperature of 52°C was used in each PCR amplification.

iii) Amplification of *cdc*. PCR analysis was performed using primers to a highly conserved genetic region of the gene known to encode for cholesterol-dependent cytolysins (CDCs). Oligonucleotides were designed to amplify a specific ~1 kb segment of the *pfo* gene (nucleotides 380 - 1479) from *C. perfringens*, and products obtained from these amplifications are referred to as *cdc*. Oligonucleotide sequences were as follows: *cdc* forward primer = 5'-GTACATATCCAGGAGCATTACAAC-3' and *cdc* reverse primer = 5'-CCACCATTCCCAAGCAAGACCTGT-3'. pRT20 (a generous gift of Dr. Rodney K. Tweten, University of Oklahoma Health Sciences Center), a plasmid containing the *pfo* gene, was included in a separate PCR reaction as a control. An annealing temperature of 57°C was used in each of the PCR amplifications.

PCR ribotyping of *C. sordellii* isolates. Oligonucleotides (Integrated DNA Technologies, Inc.) were designed to amplify the region between the 16S and 23S rRNA-encoding genes (33) in each isolate. Primer sequences were as follows: forward primer = 5'-GCTAACCTTTTAGGAGGCGGC-3' and reverse primer = 5'-GGCTACTTCCTGCACTATTCG-3'. These oligonucleotide sequences were designed based on the 3' end of the 16S rRNA gene and the 5' end of the 23S rRNA gene of *C. sordellii*. Temperature cycling was performed as described above with an annealing temperature of 55°C. Following amplification, the entire PCR reaction was separated via 2% agarose gel electrophoresis for 4 h at 4°C and 100 V. Following electrophoresis, DNA banding patterns were visualized via ethidium bromide staining. Isolates were assigned to ribotype groups under the criteria of possessing at least one differing band when compared to *C. sordellii* ATCC9714.

Transmission electron microscopy of *C. sordellii* isolates. Approximately 10 μl of mid-log phase culture of each *C. sordellii* isolate was applied to Formvar-coated grids for 5 min. Grids were stained with 2% phosphotungstic acid for 15 sec and subsequently observed via transmission electron microscopy (TEM) using a Hitachi H-7600 microscope. Samples were observed at a magnification of 4000 – 6000 X and images were captured using a Kodak 2K X 2K digital camera.

Antibiotic susceptibility of *C. sordellii* isolates. A lawn of each *C. sordellii* isolate was plated on Brucella Agar plates containing 5% sheep blood, vitamin K, and hemin (Remel). Following plating, antibiotic disks (Remel) were dispensed onto plates with four antibiotics per plate. Plates were subsequently incubated anaerobically at 37°C for ~ 18 h, at which point, zones of clearing around each antibiotic disk were measured and compared to the zones of clearing observed in each of the isolates to determine relative susceptibility. Antibiotics tested were cefoxitin (30 μg), ceftriaxone (30 μg), gentamicin (10 μg), erythromycin (15 μg), clindamycin (2 μg), ampicillin (10 μg), penicillin G (10 U), amoxicillin/clavulanic acid (20/10 μg), ciprofloxacin (5 μg), levofloxacin (5 μg), vancomycin (30 μg), and tetracycline (30 μg). Results from these initial antibiotic assays were compared only between *C. sordellii* strains to obtain relative susceptibility. Clindamycin resistance was further examined using the E-test MIC determination strip method according to the manufacturer's instructions (AB Biodisk). The results from the E-test were compared to the known standards for anaerobes as specified by the manufacturer (AB Biodisk). These standards designate MIC values above 2 μg clindamycin/ml as resistant.

Neuraminidase activity assay. Neuraminidase activity was examined using the Amplex Red Neuraminidase Assay Kit (Molecular Probes). Culture supernatant (48 h) from each *C. sordellii* isolate was incubated with the Amplex Red reaction mixture and incubated for 30 min at 37°C. The reaction was

monitored spectrophotometrically at A_{560} to detect released sialic acid, which reacts with Amplex Red to increase absorbance at this wavelength. Purified neuraminidase from *C. perfringens* (Molecular Probes) and hydrogen peroxide were included as positive controls.

Cytotoxicity assay. Each *C. sordellii* isolate was grown anaerobically in BHI broth (Difco) for 24 h and 48 h, at which point, 1 ml of culture supernatant was harvested by centrifugation for 10 min at 9,000 X g. Following centrifugation and concentration of supernatants using 10 kDa molecular weight cutoff Centricons (Millipore), 5 μg of total protein of the resulting supernatant was added in triplicate to a 96-well plate containing 4 X 10^4 mammalian cells/well in a confluent monolayer. Cells were monitored for at least 72 h post-treatment for signs of morphological changes indicative of cytopathic effects (CPE). Control cells were incubated with BHI. Cells were observed at a magnification of 140 X using a 1X-51 Olympus inverted microscope and images were captured with a DP-70 Olympus digital camera.

In addition to visualization of cell viability, cytotoxicity was monitored using the colorimetric CCK-8 Cell Viability Assay (Dojindo, Inc.). This viability assay uses WST-8 [2-(2-methoxy-4-nitrophenyl)-3-(4-nitrophenyl)-5-(2,4-disulphophenyl)-2H-tetrazolium, monosodium salt], which is reduced to a formazan derivative by dehydrogenases from viable cells. This reaction is monitored by reading the A_{450}, which increases proportionally to the level of

dehydrogenases. Following addition of WST-8 to cells treated in a 96-well plate, percent viability relative to the control was calculated using the formula (A_{test} – $A_{background}$)/($A_{control}$ - $A_{background}$), where A = absorbance at A_{450}, test = cells treated with supernatant, background = media only, and control = cells treated with BHI only.

Southern blot analysis of *tcsl*. To analyze *C. sordellii* chromosomal DNA for presence of the *tcsl* gene, a randomly digoxigenin (DIG)-labeled probe was constructed via PCR amplification. DNA was amplified from *C. sordellii* ATCC9714 in a 50 µl reaction, as described above, using the following primers (Integrated DNA Technologies, Inc.): 3592F = 5'-TTATCTATATATGATGTATTAAATATA-3' for the forward primer and 5331R = 5'-TATCGCTTTTAAAGACATTAACAA-3' for the reverse primer. The resulting PCR product represented the ~ 1.7 kb DNA segment present between the *Nco*I (bp 3592) and *Pst*I (bp 5331) sites located on the *tcsl* gene. Temperature cycling was performed as described above with an annealing temperature of 55°C. Following amplification, the product was denatured by boiling for 10 min and was subsequently randomly labeled with DIG using the DIG High Prime DNA Labeling Kit according to the manufacturer's instructions (Roche Diagnostics). Chromosomal DNA was isolated from mid-log phase cultures of *C. sordellii* ATCC9714 and UMC164 using the DNeasy Tissue Kit (Qiagen) and was subsequently restricted overnight at 37°C with *Nco*I and *Pst*I (New England

Biolabs). Following restriction, chromosomal DNA was separated via 1% agarose gel electrophoresis, denatured with buffer containing 0.5 M NaOH and 1.5 M NaCl, and subsequently neutralized with buffer containing 1.0 M Tris pH 8.0 and 1.5 M NaCl. Following neutralization, DNA was transferred to a nylon membrane via capillary transfer for 2 h in 10X SSC buffer (1.5 M NaCl, 150 mM sodium citrate pH 7.0). The membrane was subsequently UV-crosslinked for ~ 1 min, after which, it was incubated overnight at 60°C with ~ 600 ng of the denatured, DIG-labeled probe for hybridization. Following overnight hybridization, the membrane was washed twice with 2X SSC buffer containing 0.1% SDS at room temperature and then washed twice with 0.5X SSC buffer containing 0.1% SDS at 65°C. The membrane was subsequently blocked for 30 min in milk buffer (Roche Diagnostics), incubated with an anti-DIG alkaline phosphatase conjugate (Roche Diagnostics), and observed via chemiluminescence, following exposure to film, for visualization of hybridized DNA.

Immunoblot analysis of *C. sordellii* isolates. Culture supernatants (10 μg) from *C. sordellii* ATCC9714 and UMC164 were separated via 10% SDS-PAGE and subsequently electro-transferred to a poly(vinylidene difluoride) membrane (Amersham Pharmacia). For Western blotting, the membrane was probed with anti-TcsL antiserum and reacting proteins were detected via chemiluminescence using the ECL plus detection kit (Amersham Pharmacia).

Anti-TcsL antiserum was isolated following immunization of New Zealand White rabbits with a KLH-conjugated synthetic peptide (TcsL240-260) along with Complete Freund's adjuvant. This 15-residue peptide, IRNLEKFADEDLVRC, represents a putatively exposed hydrophilic region (residues 240-253) located at the N-terminus of TcsL. Following initial immunization, the immune response was boosted once a month for three months with Incomplete Freund's adjuvant plus TcsL240-260 prior to serum collection. Immunization and serum collection were performed by Sigma Genosys.

Glucosylation assay. TcsL-9714 or TcsL-UMC164 were incubated in a standard glucosylation assay for 2 h at 37°C as previously described (159). Following incubation, samples were separated via 15% SDS-PAGE and the gel was dried and exposed to film for visualization of ^{14}C-labeled proteins.

Hemolytic activity assay. Total protein from the supernatant of each *C. sordellii* strain was quantified via the Bradford protein assay (BioRad). Following quantification, 7 μg of total protein in a final volume of 50 μl PBS (Gibco) containing 1 mM dithiothreitol was used as the undiluted sample in a standard hemolysis assay performed in a U-bottomed 96-well plate. Eight 1:2 dilutions were performed for each isolate supernatant and 50 μl of a human erythrocyte solution (3 X 10^7 cells/ml) in PBS was added to each well and mixed. The plate was subsequently incubated at 37°C for 4 h. Following incubation, the plate was centrifuged at 1000 X g for 5 min to pellet non-lysed erythrocytes.

Resulting supernatants were assayed spectrophotometrically analyzed at A_{540} to detect hemolytic activity.

LD_{50} determination using BALB/c mice. For LD_{50} measurements, 8 wk old female BALB/c mice were injected i.v. with specific concentrations of supernatant from either *C. sordellii* UMC164 ($TcsL^+$, SDL^-) or *C. sordellii* PS4404 ($TcsL^-$, SDL^+). Mice were injected via the tail vein using a 26.5 gauge needle. Six mice were injected with each test concentration to determine the correct LD_{50} value. Sterile, filtered BHI was used for control injections in each experiment.

CHAPTER IV

CLOSTRIDIUM SORDELLII LETHAL TOXIN IS MAINTAINED IN A MULTIMERIC PROTEIN COMPLEX

Clostridium sordellii Lethal Toxin is Maintained in a Multimeric Protein Complex. (Daniel E. Voth, Maen Qa'dan, Elaine E. Hamm, Joy M. Pelfrey, and Jimmy D. Ballard. _Infection and Immunity_. 72:3366-3372)

Clostridium sordellii is a Gram-positive, spore-forming, anaerobic pathogen, which causes a variety of diseases including postpartum toxic shock syndrome, septic arthritis, neonatal omphalitis, and sudden death syndrome (2, 68, 100, 101, 143, 151, 169, 170). This list of diseases has recently been expanded with the implication of *C. sordellii* in the deaths of intravenous drug users following injection of contaminated heroin (111). In addition, *C. sordellii* has been identified as a possible cause of death in recent cases of patients receiving musculoskeletal allografts (99). Indeed, *C. sordellii* appears to have the capacity to cause a diverse number of diseases. For example, 16 different types of disease have been reported in the approximately 30 publications regarding *C. sordellii* infections. Unfortunately, very little is known about *C. sordellii's* mechanism of pathogenesis, making it difficult to provide tenable explanations for this organism's multi-faceted role in disease.

Prior to the results described in Chapter III of this dissertation, only three putative virulence factors from *C. sordellii* had been studied. *C. sordellii* produces a lecithinase (phospholipase-C), which is similar to alpha-toxin, a major virulence factor from *Clostridium perfringens* (93). Two *C. sordellii* virulence factors, TcsL and TcsH, have also been studied in some detail. Toxoids of TcsL and TcsH are effective vaccines against *C. sordellii* spore challenge in a guinea pig model (10), indicating these toxins may play a pivotal role in disease progression.

TcsL and TcsH are members of the family of LCTs, which is composed of at least five toxins possessing glycosyltransferase activity (25). Members of the LCT family of toxins, in addition to TcsL and TcsH, include TcdA and TcdB from *Clostridium difficile* and Tcnα from *Clostridium novyi*. Each LCT induces pronounced cytopathic effects (CPE) in cultured mammalian cells, and these effects are apparently a prelude to cell death. For induction of CPE, LCTs glycosylate, and thereby inactivate, members of the Ras family of small GTPases. TcdA, TcdB, TcsH, and Tcnα preferentially inactivate Rho, Rac, and Cdc42 (4) by transfer of sugar moieties derived from UDP-glucose or n-acetylglucosamine to reactive threonines in the effector-binding loop of target GTPases. TcsL also glycosylates small GTPases, but differs from other LCTs by targeting Ras, Rac, Rap, and Ral (4).

The enzymatic domain of LCTs has been narrowed to the amino-terminal 546 residues. The difference in substrate specificity between TcsL and TcdB is

due to sequence variation in the region of residues 364 to 516 within the enzymatic fragment (79). Residues important for binding UDP-glucose are found at D286 and D288, while glucosyltransferase activity requires D270 and R273 (32). Further studies have also implicated W102 in interaction with UDP-glucose by TcdB and TcsL (31). Despite these similarities, TcsL induces delayed CPE relative to TcdB (39, 137) and it has been suggested that the slower cytotoxicity could be due to delays in TcsL cell entry (39). In addition, we recently reported on the enhanced cytotoxicity of TcsL following exposure to pH 4.0 conditions (137). This finding indicated that TcsL might be substantially more active at pH 4.0, and this could be due to enhanced interactions with the cell following acid-induced conformational changes.

To better understand the connection between cell entry and activation of TcsL at pH 4.0, we analyzed the cytotoxic effects of TcsL's enzymatic domain using a surrogate cell entry system and found that alternative mechanisms of cell entry markedly increased the rate of intoxication. In addition, direct analysis of TcsL at pH 4.0 revealed dissociation of a high-molecular weight complex containing polypeptides of the toxin. Findings from the current study indicate that intoxication by TcsL is limited by the need for dissociation of a multimeric complex, which occurs optimally under acid pH conditions.

RESULTS

Normalized cell entry confers similar rates of CPE for TcdB and TcsL. Under normal cell culture conditions, TcsL induces cytopathic effects at a rate substantially slower than TcdB (107). In earlier work, it was reported that providing an extracellular pH 4.0 pulse quickened TcsL's otherwise slow time-course of intoxication (137). pH 4.0-activated TcsL induced CPE at a rate similar to that of TcdB, changing the time-point of 50% CPE from approximately 7 h to 90 min. At pH 8.0, cells could be protected from TcsL by the extracellular addition of anti-serum up to 2 h following treatment with the toxin. These data further indicated that TcsL intoxication is limited at the stage of cell entry, but this is overcome by an extracellular acid pH. Thus, in an effort to show directly that TcsL's slow rate of cytotoxicity was due to events at the point of cell entry, we designed constructs of the enzymatic domains of TcsL and TcdB, which allowed these fragments to enter cells in an identical manner.

To normalize cell entry for the enzymatic domains of TcdB ($TcdB^{1-556}$) and TcsL ($TcsL^{1-556}$), we utilized a nontoxic derivative of anthrax lethal toxin, which consists of protective antigen (PA) plus lethal factor (LF). In past studies involving cytosolic delivery of $TcdB^{1-556}$, we used a derivative of anthrax lethal toxin consisting of PA and a truncated form of LF (LFn), which is inactive but can interact with PA and be translocated to the cytosol (159). Genetic fusions were constructed and used as a source of $LFnTcdB^{1-556}$ in the earlier work, and a

similar approach was used for constructing LFnTcsL$^{1-556}$ in the current study. Similar to our report on acid pH-pulsed entry of TcsL (137), glucosylation profiles from extracts of cells treated with LFnTcsL$^{1-556}$ plus PA showed that all TcsL substrates were modified by the fusion (data not shown). Thus the fusion appeared suitable for making comparisons between the enzymatic domains of TcsL and TcdB.

As shown in Fig. 10, LFnTcdB$^{1-556}$ and LFnTcsL$^{1-556}$ delivered to the cytosol with PA demonstrated similar time-courses of CPE in HeLa cells. Wild-type TcdB induced 100% CPE by 3 h as compared to 9 h required by TcsL for full induction of CPE. Both LFnTcdB$^{1-556}$ and LFnTcsL$^{1-556}$ induced 100% CPE by 4.5 h. These data further suggests that TcsL's major barrier to intoxication occurred at steps in cell entry.

TcsL forms an acid pH-dissociable complex. Under the described conditions, TcsL from *C. sordellii* ATCC 9714 purified as a protein doublet even after three rounds of anion exchange chromatography. This observation is in agreement with Martinez and Wilkins, who reported a doublet in their preparation of TcsL from *C. sordellii* VPI 9048 (107). In addition to the doublet, we also observed the presence of ~5 smaller proteins co-purifying with TcsL. These smaller proteins, ranging in size from 45-55 kDa, cross-reacted with antiserum that recognizes TcsL and became more prominent following long-term storage of the toxin (data not shown), suggesting these were products of TcsL.

Figure. 10. Time course of CPE in TcsL and LFnTcsL$^{1-556}$ treated cells. HeLa cells were grown to confluence in a 96-well plate to ~ 5 x 10^4 cells/well. Cells were treated with either TcdB (100 fmol), TcsL (100 fmol), LFnTcsL$^{1-556}$ (1 pmol) or LFnTcdB$^{1-556}$ (1 pmol) in a volume of 100 μl. PA (30 pmol) was included with the fusion proteins. Control cells were treated with media, 20 mM Tris, heat-inactivated toxin, or PA + LFn alone. Following treatment, CPE were observed for 10 h and calculated by visualizing the number of rounded cells from a field of at least 100 cells. The corresponding lines for each sample are labeled within the figure. Samples were analyzed in triplicate and error bars represent the standard deviation from the mean.

Figure 10.

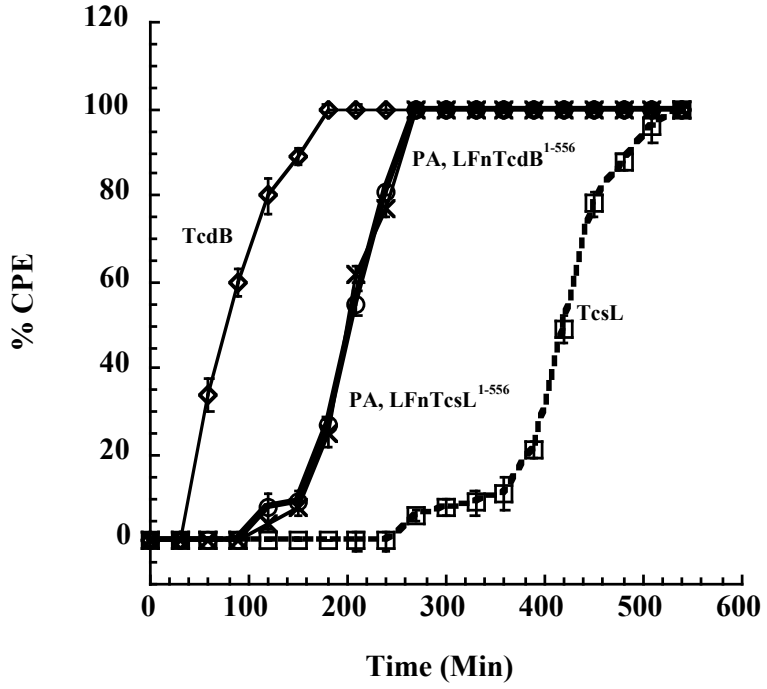
120
100
80
60
40
20
0
% CPE
0
100
200
300
400
500
600
Time (Min)
TcdB
PA, LFnTcdB1-556
PA, LFnTcsL1-556
TcsL

Given the observations of TcsL dissociation, we investigated whether this dissociation event might be related to TcsL's unique requirement of acid pH for activation. As shown in Fig. 11, following incubation of TcsL at pH 4.0, the toxin dissociates into a group of 45-55 kDa proteins. Inclusion of protease inhibitors, reducing agents, and buffers across a range of ionic strengths did not alter the dissociation profile (data not shown).

Interestingly, TcsL was able to reassemble when the sample was raised back to pH 8.0, indicating that dissociation was reversible (Fig. 12). To confirm the close association required for a complex of this kind, we cross-linked TcsL at pH 8.0 with Sulfo-EGS, a homobifunctional cross-linking reagent that cross-links proteins with lysine residues within a 16 Å proximity. As shown in Fig. 12, when TcsL/Sulfo-EGS was placed under pH 4.0 conditions, no dissociation was observed, indicating the close proximity of the complex components to each other. As shown in Fig. 13, TcsL/Sulfo-EGS, was no longer cytotoxic when incubated with HeLa cells up to 72 h and was no longer able to glucosylate Ras *in vitro*, while TcdB, cross-linked under the same conditions, retained full cytotoxicity. Additionally, as shown in Fig. 13B, TcsL/Sulfo-EGS did not compete with TcsL for binding in a HeLa cell cytotoxicity assay. These results further suggest dissociation of this complex is required for interaction at the cell surface and complete cytotoxic activity.

Figure. 11. Acid pH-induced dissociation of TcsL. Samples of purified TcsL (10 μg) were incubated for 30 min with varying amounts of 100 mM ammonium acetate buffer pH 3.8 to attain the indicated pH. Indicated samples were then supplemented with 250 mM Tris pH 9.0 to regain pH 8.0. Proteins were separated via 10% SDS-PAGE and observed using Coomassie Blue staining. pH range is indicated above gel.

Figure 11.

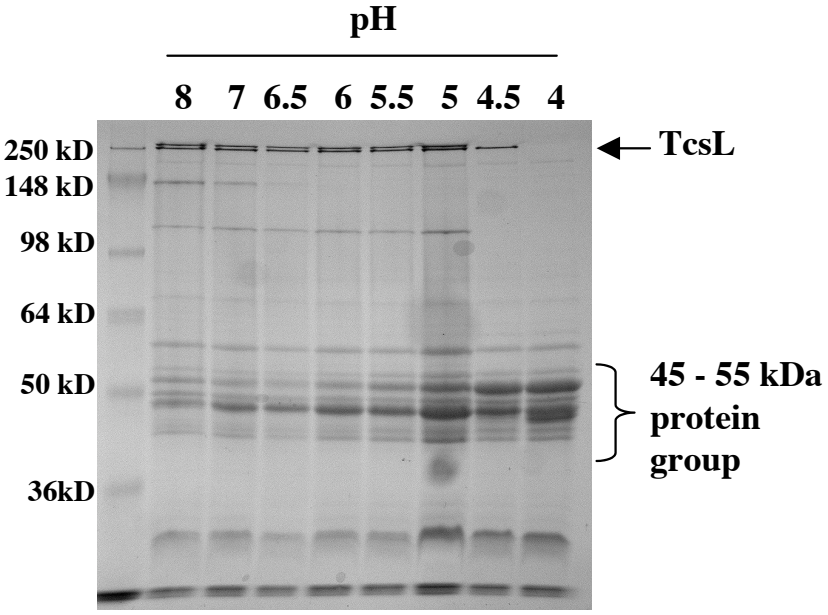
pH
8 7 6.5 6 5.5 5 4.5 4
250 kD
148 kD
98 kD
64 kD
50 kD
36kD
TcsL
45 - 55 kDa
protein
group

Figure. 12. Impact of pH shifts and cross-linking on TcsL stability. TcsL samples (10 μg) were analyzed via 10% SDS-PAGE and observed using Coomassie Blue staining following incubation under various pH conditions. Lane 1 = TcsL pH 8.0, Lane 2 = TcsL pH 4.0, Lane 3 = pH 4.0 TcsL shifted back to pH 8.0, Lane 4 = TcsL/Sulfo-EGS pH 8.0, Lane 5 = TcsL/Sulfo-EGS pH 4.0, Lane 6 = pH 4.0 TcsL/Sulfo-EGS shifted back to pH 8.0.

Figure 12.

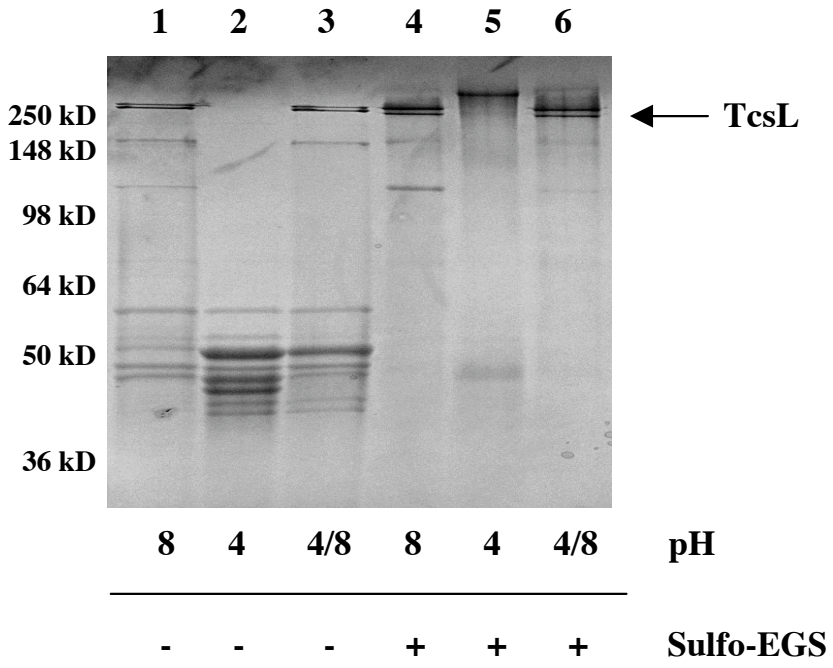
1 2 3 4 5 6
250 kD
148 kD
98 kD
64 kD
50 kD
36 kD
TcsL
8 4 4/8 8 4 4/8
pH
- - - + + +
Sulfo-EGS

Figure 13. Toxicity, cell binding, and enzymatic activity of cross-linked TcsL. HeLa cells were incubated with TcsL, TcsL/Sulfo-EGS, or TcsL + TcsL/Sulfo-EGS (2μg/ml) for up to 72 h and observed for morphological changes associated with TcsL-induced cytotoxicity. As a comparison, HeLa cells were also incubated with TcdB or TcdB/Sulfo-EGS (2μg/ml) and observed for morphological changes. TcsL or TcsL/Sulfo-EGS were also incubated in a Ras glucosylation assay as described in Materials and Methods. (A) Control untreated cells, (B) % Viability of TcsL, TcsL/Sulfo-EGS, and TcsL + TcsL/Sulfo-EGS-treated HeLa Cells. Inset compares glucosyltransferase activity of TcsL and TcsL/Sulfo-EGS, Lane 1 = TcsL and Lane 2 = TcsL/Sulfo-EGS, (C) TcsL-treated cells, (D) TcsL/Sulfo-EGS-treated cells, (E) TcdB-treated cells, (F) TcdB/Sulfo-EGS-treated cells. Samples were analyzed in triplicate and error bars indicate the standard deviation from the mean.

Figure 13.

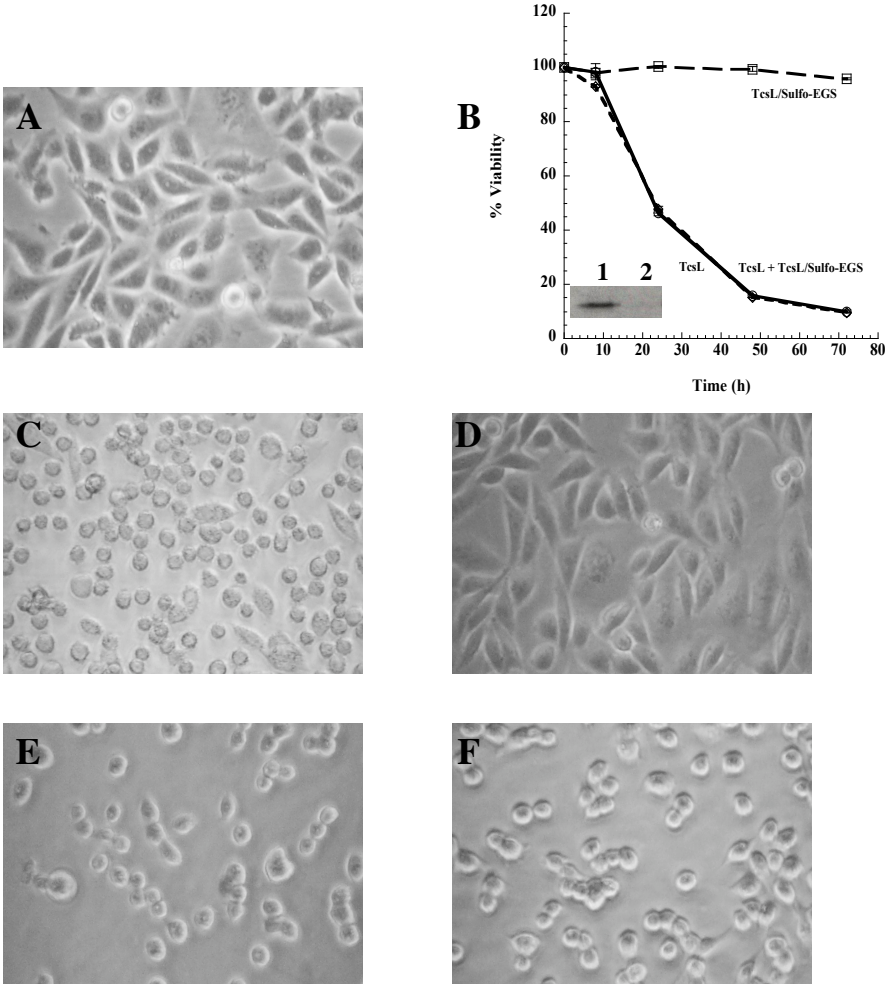
A
B
% Viability
120
100
80
60
40
20
0
0 10 20 30 40 50 60 70 80
Time (h)
TcsL/Sulfo-EGS
TcsL
TcsL + TcsL/Sulfo-EGS
1 2
C
D
E
F

Protease resistance at pH 8.0. To determine if TcsL dissociation was specific for pH 4.0 conditions, the protein was submitted to a series of protease digestions and high temperature incubation. As shown in Fig. 14, proteases including trypsin, α-chymotrypsin, V8 protease, and proteinase K, added in excess, were unable to induce TcsL dissociation similar to that observed at pH 4.0. However, the smaller polypeptides were sensitive to the various proteases, as these fell below the level of detection following protease treatment. As reported by Popoff (131), we confirmed that only α-chymotrypsin had any effect on TcsL activity, with CPE occurring ~50% slower than untreated TcsL (data not shown). TcsL was also subjected to incubation at 100°C to determine if dissociation occurs under elevated temperatures. Boiling TcsL for 15 min resulted in complete degradation of the protein, distinct from the dissociation observed in pH 4.0 samples (data not shown).

TcsL forms high molecular weight oligomeric structures at pH 8.0. Interestingly, the intensity of the 45-55 kDa proteins present in the pH 4.0-dissociated TcsL was higher than that expected if these proteins were derived from dissociation of TcsL alone. Among the possible explanations for the incongruent association between intensity of the smaller bands and levels of TcsL was that some of the 45-55 kDa proteins were derived from a larger complex not detected by standard 10% SDS-PAGE. For this reason, we analyzed samples of TcsL for high molecular weight complexes (>750 kDa) using SDS-agarose gel

Figure. 14. Protease treatment of TcsL. TcsL (10 μg) was incubated with an excess of each indicated protease (15 μg) overnight prior to SDS-PAGE analysis. pH is indicated above the gel and each pH section follows this order of protease treatment: Lanes 2 and 7 = TcsL, Lanes 3 and 8 = TcsL + trypsin, Lanes 4 and 9 = TcsL + α-chymotrypsin, Lanes 5 and 10 = TcsL + V8 protease, and Lanes 6 and 11 = TcsL + proteinase K. Lane 1 indicates the molecular weight marker.

Figure 14.

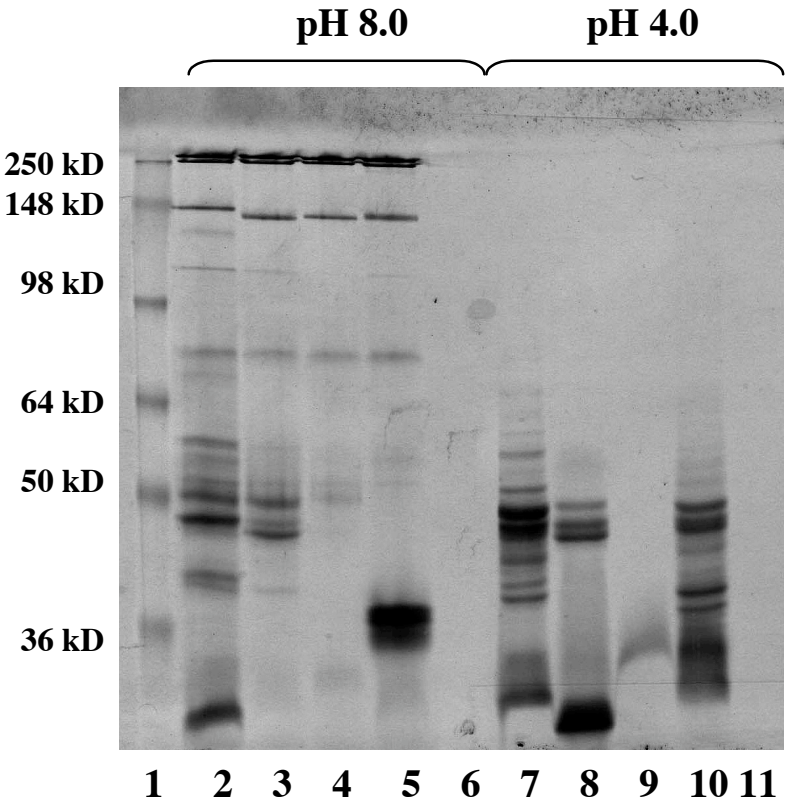

electrophoresis (SDS-AGE). As shown in Fig. 15A, a high molecular weight protein was observed in TcsL samples at pH 8.0 which also dissociated under pH 4.0 conditions similar to TcsL. Although TcsL reassembled when the sample was brought back to pH 8.0, this larger protein was not detected following the pH shift.

As shown in Fig. 15, high molecular weight proteins were not observed when two related LCTs, TcdB (Fig. 15B) and Tcnα (Fig. 15C), were subjected to the same pH conditions. Because high molecular weight proteins often represent the presence of oligomeric structures, TcsL was observed via TEM at pH 8.0 and pH 4.0. As shown in Fig. 15D, protein aggregates were observed in TcsL samples at pH 8.0, suggesting the formation of oligomers under these conditions. These oligomers, however, were not observed under pH 4.0 conditions (Fig. 15E), which supports the previous observations of the protein sample on SDS-PAGE.

These findings suggested that the larger protein complex might account for the protease resistance and protection to TcsL, and is dissociated at pH 4.0. Based on this possibility, we predicted that TcsL not maintained in the complex would be unstable. Thus, the protein mixture was resolved via SDS-PAGE and the protein resolving at ~ 280 kDa was electroeluted from the gel. In addition, the large protein complex was electroeluted following resolution by SDS-AGE. Both samples were then subsequently examined by SDS-PAGE. As shown in Fig. 16, following electroelution, TcsL spontaneously dissociated into the smaller 45-55

Figure. 15. SDS-AGE analysis of TcsL, TcdB, and Tcnα and TEM analysis of TcsL. Each respective toxin was separated using 1.5% SDS-AGE following incubation under the indicated pH conditions. Each lane represents 15 μg of protein. Each respective toxin is labeled in the figure. TcsL at pH 8.0 was stained with PTA and subsequently analyzed by TEM at $1X10^5$ X magnification. Arrows indicate examples of oligomeric structures. A) TcsL, B) TcdB, C) Tcnα, D) TEM analysis of TcsL at pH 8.0, E) TEM analysis of TcsL at pH 4.0.

Figure 15.

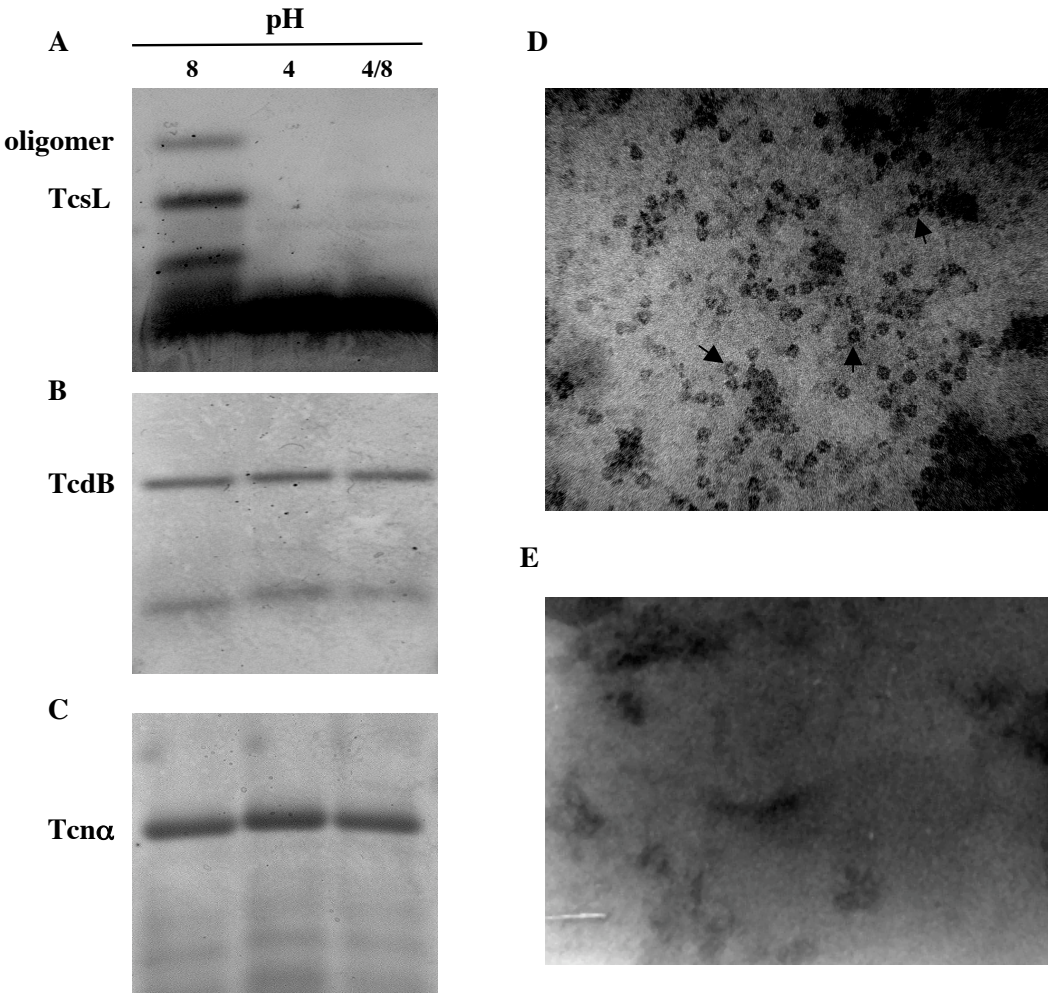

Figure. 16. Electroelution of TcsL and TcsL complex proteins. Protein bands representing TcsL and the TcsL complex were subjected to electroelution in the presence of SDS for 2 h at room temperature. Following electroelution, proteins were separated via 10% SDS-PAGE and observed using Coomassie Blue staining. Lane 1 = molecular weight marker, Lane 2 = protein electroeluted from TcsL, Lane 3 = protein electroeluted from the oligomer.

Figure 16.

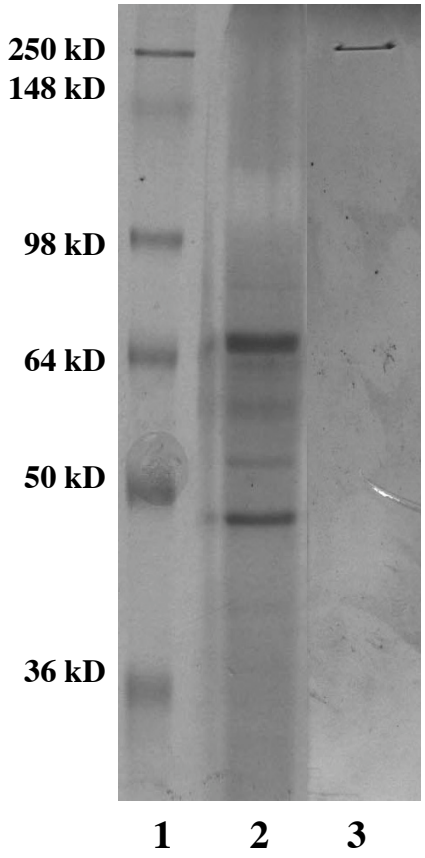

kDa proteins, similar to those observed following incubation at pH 4.0. Electroelution of the larger complex from SDS-AGE resulted in slight dissociation and the appearance of trace amounts of a protein resolving at the size of TcsL. Findings from the electroelution experiment indicate that TcsL outside of the larger complex is unstable and subject to degradation even under mild conditions. Furthermore, this analysis suggests that TcsL is part of the larger protein complex.

DISCUSSION

TcsL shares several common characteristics with other members of the LCT family of virulence factors. Among these attributes is the fact that TcsL is a notably large, single polypeptide relative to other bacterial toxins, acts as an intracellular toxin, and glycosylates small GTPases in order to alter target cell physiology. Yet, based on results from the current study, it appears that TcsL may be unique among the LCTs, as this toxin is maintained in a dissociable high molecular weight complex. Dissociation of this complex may be the major rate-limiting step in TcsL activity, and this barrier is overcome most effectively at acid pH. The need for dissociation of this complex prior to intoxication may explain our earlier observations (137) and the predictions of Chaves-Olarte (39). Both studies suggested TcsL's slow rate of inducing CPE was due to limitations at the point of cell entry.

Acid-induced activation is not uncommon to bacterial toxins; however, we believe the mechanism by which TcsL is activated at low pH is distinct from other reports. For example, the cholesterol-dependent cytolysin, listeriolysin-O, produced by *Listeria monocytogenes*, is optimally active within the acidified endosome (133). Unlike TcsL, listeriolysin-O is activated at low pH by direct conformational changes in the protein, which leads to more efficient membrane insertion, pore-formation, and, possibly, protein stability. Yet, unlike TcsL, activation of listeriolysin-O does not involve the dissociation of a multi-protein complex. Vacuolating cytotoxin from *Helicobacter pylori* is also reportedly activated by acid pH (109), but differs in several ways from activation of TcsL. Although vacuolating activity is enhanced at low pH, this does not apparently involve dissociation of a multimeric complex. Furthermore, unlike TcsL, activation of vacuolating cytotoxin is not reversible, as shifting the protein sample back to pH 8.0 does not reduce activity.

In our experiments and in previous reports (131), TcsL was resistant to a wide variety of active proteases including trypsin, V8 protease, and α-chymotrypsin. Each of these proteases had little effect on TcsL activity with only α-chymotrypsin reducing the rate of CPE. Proteinase-K cleaved and inactivated TcsL, but this only occurred following extended incubations. TcsL and the 45-55 kDa proteins were susceptible to these proteases when not associated with the complex, further indicating that the high molecular weight complex provides

protease resistance. In this way, TcsL is similar to botulinum toxin, which also resides in a multimeric complex. Similar to the TcsL-complex, botulinum toxin exists in a high molecular weight aggregate which is highly resistant to multiple proteases (40). However, unlike the TcsL complex, the botulinum toxin complex does not dissociate under acidic conditions.

Recent studies by Pfeifer et al. indicate that TcdB is proteolytically processed while entering the cytosol of target cells in early endocytic vesicles (130). This was also shown to be directly related to acidification within early endosomes. Thus, TcdB processing and disassembly of the monomer is intimately linked to cell entry. Likewise, our model for TcsL indicates that processing of the toxin may be necessary for intoxication. Yet, dissociation of TcsL proceeds differently and, perhaps, at earlier stages than that found for TcdB. The current model suggests TcsL dissociation requires extracellular low pH to enhance cytotoxicity through breakdown of the high molecular weight complex. It is unclear whether this also leads to translocation of a fragment of the toxin into the cytosol as was reported for TcdB.

Investigations are underway to determine the mechanism behind multimer formation and acid pH-induced dissociation of the complex. It will be important to differentiate between physical dissociation of the complex, proteolysis and autocatalysis. As mentioned in the results, inclusion of protease inhibitors does not alter the dissociation profile, suggesting this event may not result from

activation of proteases at acid-pH. Furthermore, spiking the sample with other proteins, such as BSA, does not result in degradation of these added proteins when the pH is lowered (data not shown). Thus, the current data indicates protease activation is not a tenable explanation for dissociation of the complex. However, the sequence of the gene encoding TcsL indicates this protein is expressed as a single polypeptide, suggesting the protein must be proteolyzed at some point. Collectively, these data suggest two possibilities. First, the toxin co-purifies with a protease, which is highly specific for TcsL and is not blocked by protease inhibitors that are currently available. Alternatively, dissociation of the multimer is due to a yet undefined mechanism of autocatalysis. This would be in line with the findings on the light chain of botulinum toxin, where studies demonstrated this polypeptide showed autocatalysis over an extended period of time at low pH (3).

The stability of the TcsL complex may influence *C. sordellii* disease. As one example, in a recent study of tissue from 795 donors, samples were analyzed for the presence of *C. sordellii* (104). Of these 795 donors, 8% were contaminated with *Clostridia* and 37.7% of these were found to be *C. sordellii*. Thus, contamination of allograft material by *C. sordellii* is a growing concern. Furthermore, approaches to decontaminate tissue prior to transplantation may also need to include methods to remove toxin. Indeed, TcsL's protease-resistant multimer may allow this toxin to be effective in a variety of environments and

explain in part how *C. sordellii* is capable of causing such a broad range of diseases.

MATERIALS AND METHODS

Cell culture and toxin purification. Human epitheloid carcinoma (HeLa) cells were obtained from the American Type Culture Collection and maintained in RPMI 1640 medium supplemented with 10% fetal bovine serum (Gibco). Cells were grown at 37°C in the presence of 6% CO_2 and were used between passages 10 and 20. *C. sordellii* ATCC 9714, *C. difficile* ATCC 10463, and *C. novyi* ATCC 19402 strains were used in this study for purification of TcsL, TcdB, and Tcnα, respectively. TcsL, TcdB, Tcnα, PA, and LFnTcdB$^{1\text{-}556}$ were isolated as previously described (137, 159).

Construction, expression, and isolation of LFnTcsL$^{1\text{-}556}$. The region encoding the enzymatic domain of TcsL was amplified from *C. sordellii* ATCC 9714 genomic DNA by PCR using the forward primer 5'-GCGCGCGGATCCATGAACTTAGTTAACAAAGCCCAA-3' and the reverse primer 5'-GCGCGCGGATCCTTATTATAATATTTTTTTAGAAACATAATC-3' to generate *tcsL*$^{1\text{-}1668}$ with a 5' and 3' *Bam*HI site. *tcsL*$^{1\text{-}1668}$ was then restricted with *Bam*HI, and *lfn* was genetically fused to *tcsL*$^{1\text{-}1668}$ by ligation overnight at 16°C with *Bam*HI restricted pABII, a derivative of pET15b containing *lfn*. This

construct generated an in-frame fusion of *lfn* and *tcsL*$^{1\text{-}1668}$ and the resulting plasmid was labeled pMQ101. The correct genetic fusion resulted in joining the 3' end of *lfn* at the codon TCC encoding S254, followed by sequences within the multiple cloning site that encoded the linker region and a string of residues (PGGGGGS), with the 5' end of *tcsL*$^{1\text{-}1668}$ at the ATG codon encoding M1. pMQ101 was then transformed into *Escherichia coli* DH5α (CLONTECH), and candidate clones were screened by mini-prep analysis. In-frame, correctly oriented clones were identified by restriction analysis and DNA sequencing and were subsequently transformed into *E. coli* BL-21 (DE3) (Stratagene). For protein expression, cells were grown at 37°C until an OD_{600} of 1.0 was reached, at which point expression was induced with 0.1 mM Isopropyl-B-D-Thiolgalactopyranoside (Denville Scientific, Inc.) at 16°C for 16 h. LFnTcsL$^{1\text{-}556}$ was purified using Ni^{2+} affinity chromatography according to the manufacturer's instructions (Novagen). The purified protein migrated within the predicted size range (~94 kD) as analyzed by SDS-PAGE and was reactive to both anti-LF and TcdB polyclonal antisera.

Glucosylation, cell viability, and quantification of cytopathic effects. Differential glucosylation assays were performed in a similar manner to those previously described (137), except PA (300 pmol) plus LFnTcsL$^{1\text{-}556}$ (300 pmol) was substituted for acid-pulsed TcsL. Ras glucosylation assays were also performed as previously described (137), with the substitution of Ras

(Calbiochem) in place of cell extracts. Cell viability assays were performed using the WST-8 (2-(2-methoxy-4-nitrophenyl)-3-(4-nitrophenyl)-5-(2,4-disulfophenyl)-2H-tetrazolium, monosodium salt) colorimetric assay according to the manufacturer's instructions (Dojindo Laboratories). The following formula was used to determine % cell viability: $\{(A_{test}-A_{background})/(A_{control}-A_{background})*100\}$, where A = absorbance at OD_{450}, background = media alone, and control = cells treated with media alone. Percent cytopathic effects (% CPE) were calculated by counting a minimum of 100 cells in 3 fields for each sample. Fully rounded cells were scored positive for CPE and the final % CPE was calculated as % rounded $cells_{test}$ - % rounded $cells_{control}$, where control sample = cells treated with media alone. In a standard assay, cells were treated with 100 fmol of TcdB or TcsL in a volume of 100 μl. For assays with the fusion proteins, cells were treated with 30 pmol of PA and 1 pmol of either $LFnTcsL^{1-556}$ or $LFnTcdB^{1-556}$ in a volume of 100 μl.

Electrophoretic analysis of TcsL, TcdB, and Tcnα, and immunoblot analysis of TcsL. 100 mM ammonium acetate buffer pH 3.8 was added to 10 μg of TcsL, TcdB, or Tcnα in varying amounts to obtain the indicated pH in each sample. Samples were incubated with this buffer for 30 min at room temperature, at which point the indicated samples were raised back to pH 8.0 using 250 mM Tris pH 9.0 and incubated for 30 min at room temperature. Samples were then separated using either 10% SDS-PAGE or 1.5% SDS-agarose gel electrophoresis

(SDS-AGE) as indicated and observed using Coomassie Blue staining. Indicated TcsL samples were subjected to western blot analysis using a *C. difficile* TcdB-specific primary antibody (TechLab, Inc.).

Electroelution. Following separation via 10% SDS-PAGE or 1.5% SDS-AGE, the band representing TcsL or the high molecular weight complex was excised from the gel and subjected to electroelution in the presence of SDS using the Centrilutor® Micro-electroeluter (Millipore). Proteins were allowed to electroelute for 2 h at room temperature. Following elution and concentration, the protein samples were again analyzed via 10% SDS-PAGE to determine content of protein complexes. Initial gels contained 15 μg of protein per lane and were visualized using Coomassie Blue staining.

Transmission electron microscopy analysis of TcsL. TcsL samples at pH 8.0 were observed via transmission electron microscopy (TEM) using a negative staining procedure. Briefly, TcsL (300 ng/μl) was placed on a copper support surface and allowed to adhere for 2 min. Following adherence, 100 μl of Phosphotungstic Acid (PTA) was applied to the grid for a 1 min incubation. Subsequently, the PTA was removed and the support was allowed to dry. Following drying, the protein was observed via TEM at $1X10^5$ X magnification. Additional samples were incubated at pH 4.0 for 30 min and subsequently observed using TEM.

TcsL cross-linking with Sulfo-EGS. TcsL at pH 8.0 was cross-linked using Sulfo-EGS, a homobifunctional cross-linking reagent, according to the manufacturer's instructions (Pierce Biotechnology, Inc.). Briefly, TcsL (200 μg) was buffer-exchanged into 50 mM HEPES pH 8.0 and subsequently incubated with Sulfo-EGS in a volume of 100 μl at room temperature for 30 min. Cross-linking reactions were stopped by the addition of 50 mM Tris pH 8.0 for 15 min at room temperature. A decreasing range of Sulfo-EGS concentrations was used from 2.5 mM to 250 pM to account for the effects of excess Sulfo-EGS. Following cross-linking, samples were analyzed via 10% SDS-PAGE, and observed using Coomassie Blue staining following incubation at the indicated pH. Each sample cross-linked with a varied concentration of Sulfo-EGS was tested in a routine HeLa cell cytotoxicity assay. Briefly, HeLa cells at 75% confluence were incubated with TcsL/Sulfo-EGS (2 μg/ml) and observed for 72 h. Cell viability was determined via the WST-8 assay as described above. As a control, TcdB was subjected to the same cross-linking conditions and Sulfo-EGS concentrations described above. HeLa cells were also incubated with TcdB/Sulfo-EGS to determine effects of Sulfo-EGS on TcdB-induced cytotoxicity.

Protease treatments and heat treatment of TcsL. TcsL (10 μg) was incubated with 15 μg of the following proteases in a final volume of 25 μl: proteinase K (Geno Technology, Inc.), α-chymotrypsin (Sigma-Aldrich), V8

protease (Sigma-Aldrich), and trypsin (Sigma-Aldrich). Indicated samples were placed under pH 4.0 conditions as described above, prior to protease treatment. All incubations were performed at room temperature and 37°C for 16 h except proteinase K, which was incubated at 55°C for 16 h. Additionally, protease-treated TcsL samples (2μg/ml) were incubated with HeLa cells up to 72 h and observed visually for CPE. Indicated TcsL samples were heated at 100°C for 15 min prior to electrophoretic analysis.

CHAPTER V

MODULATION OF HOST CELL PHYSIOLOGY VIA INDUCTION OF APOPTOSIS BY *CLOSTRIDIUM SORDELLII* LETHAL TOXIN

Clostridium sordellii lethal toxin (TcsL) is a member of the family of large clostridial toxins (LCTs), which inactivate small GTPases in the cytoplasm of mammalian cells. LCTs share functional and sequence homology, but vary in substrate specificity and co-substrate utilization (4). In the case of TcsL, the toxin hydrolyzes UDP-glucose and transfers the liberated sugar moiety to a reactive threonine (Thr-35) found in the effector-binding loop 1 of Ras, Rac, Ral, and Rap (82, 89, 132). TcsL also differs from other LCTs in that TcsL produced by *C. sordellii* reference strain ATCC9714 is maintained in a multi-protein complex, and acid pH-induced dissociation from this multimer enhances cytotoxic activity (shown and discussed in Chapter IV of this dissertation).

In earlier work, we demonstrated that cell rounding and death are temporally distinct events that occur in TcsL-intoxicated cells (137). While cell rounding occurs relatively early in intoxication (< 6 h), loss of viability is delayed for up to 24 h. Indeed, there are several complex steps during TcsL intoxication that precede both cell rounding and death of the targeted cell. The most immediate, post-translocation activities include localization of TcsL to the inner

plasma membrane and substrate modification, followed by modulation of mitochondrial membrane integrity (112, 129). However, the individual contribution of substrate modification, mitochondrial membrane disruption, and cell rounding to the ultimate death of the cell are not known.

Changes in cellular ultrastructure, while important, do not completely explain loss in cell viability. Indeed, incubation of mammalian cells with actin depolymerizing agents, such as cytochalasin D, does not result in a similar mode of cell death as that observed upon treatment with the LCTs (129). It also seems unlikely that cell death is due to a direct modulation of the mitochondrial membrane by TcsL, since recent work has shown localization of the toxin to the inner plasma membrane (112). This activity is accomplished through a sequence, encoded within the N-terminal 18 residues of TcsL, which specifically binds to phosphatidylserine. It is thought that this localization sequence allows TcsL to traffic to the inner plasma membrane of the cell, where active GTPases accumulate. Deletion of this 18-residue domain prevents TcsL from causing cytopathic effects, suggesting this short amino acid sequence is essential for cytotoxicity.

Petit et al. also reported that TcsL modulates the mitochondria of intoxicated cells within 2 h following treatment of HL-60 cells (129). By disrupting mitochondrial membrane integrity, TcsL triggers the release of cytochrome c and subsequent downstream events in apoptosis. Thus, TcsL

intoxication is bimodal, in that the toxin inactivates specific small GTPases followed by modulation of the mitochondria.

Based on these observations, the current model of TcsL intoxication suggests the toxin first localizes to the inner plasma membrane and glucosylates substrates, leading to cell rounding, modulation of mitochondrial integrity, activation of apoptosis, and finally death of the cell. Yet, the signaling events, or loss thereof, that lead to changes in mitochondrial integrity, and eventual cell death, in TcsL-intoxicated cells are poorly defined. However, based on published studies of Ras-regulated signaling pathways, the protein kinase Akt should be one of the signaling proteins impacted by TcsL immediately following inactivation of small GTPase substrates.

Akt is a prominent cell survival protein found in mammalian cells that acts downstream of, and in response to, Ras activation (49, 128). Following activation of Ras, via extracellular growth factors, phosphatidylinositol-3-kinase (PI3K) triggers the phosphorylation of PDK1, which subsequently aids in the phosphorylation of Akt at Thr-308 and Ser-473, resulting in the active form of the protein (7). Active Akt can then modulate downstream pro-survival pathway proteins, including ERK, MDM2, Forkhead transcription factors (FKHRs), and mTOR, and has been shown to phosphorylate, and inactivate, the pro-apoptotic protein Bad (49, 128). Active Akt is also responsible for phosphorylating

glycogen synthase kinase 3-beta (GSK-3β) (45), which is involved in cell cycle regulation and apoptosis.

Therefore, TcsL-mediated inactivation of Ras could have an immediate effect on Akt signaling, leading to downstream changes in mitochondrial integrity and, perhaps, activation of apoptosis. For this reason, in the current study, experiments examined the temporal effects of TcsL intoxication on Akt signaling. The results from this study suggest that TcsL induces rapid declines in the levels of phosphorylated Akt, followed by dephosphorylation and loss of GSK-3β, without dramatically influencing mitochondrial apoptotic effectors, such as Bad.

In addition to determining early Akt-dependent events involved in TcsL cytotoxicity, late-stage mitochondrial-associated apoptotic events were also examined. The results of these studies suggest that TcsL activity results in late-stage changes in the mitochondrial-dependent apoptotic pathway, including Bid and Bcl-x_L cleavage. In total, the current data suggest TcsL intoxication of mammalian cells results in an apoptotic feedback mechanism that ensures death of the affected cell.

RESULTS

TcsL intoxication results in late induction of apoptosis. While late stage apoptotic markers have been reported in TcsL-treated HL-60 cells (129), a temporal analysis of apoptosis, in HeLa cells, was required for interpretation of

results in the current study. In particular, caspase-3 activation and poly-ADP-ribose polymerase (PARP) inactivation, two proteins that are classical markers for the late stages of death in cells undergoing apoptosis (127), were analyzed in lysates collected from TcsL-treated HeLa cells.

As shown in Fig. 17A, caspase-3 was activated between 8-12 h post-treatment in HeLa cells incubated with TcsL. Cleaved, inactivated PARP was subsequently apparent by 12-24 h (Fig. 17B). These results also correlate with those previously shown (129) and provide a timing of the late events in TcsL-induced apoptosis. These results also indicate that each of these apoptotic steps occur downstream of GTPase inactivation, which is thought to occur shortly (< 1 h) following toxin entry into the target cell and subsequent escape from an endosomal compartment.

TcsL intoxication results in a rapid decline in the levels of activated Akt. Since TcsL was found to induce classical apoptotic events at least 8 h following glucosylation, and inactivation, of GTPases, components upstream of the caspases and pro-apoptotic mitochondrial proteins were examined in order to further understand the contribution of Ras inactivation to TcsL-induced cell death. A strong candidate for involvement in the pathway between Ras and apoptosis is Akt. This signaling protein is a vital regulatory component central to multiple cell survival networks in healthy cells (49). Additionally, Akt activity can be influenced by Ras activity via phosphorylation by PI3K. For functional Akt

Figure 17. Late stage apoptotic events occurring in TcsL-treated HeLa cells. (A) HeLa cells (4 X 10^4 cells/ml) were cultured in a 96-well black plate prior to analysis of caspase-3 activity. Following incubation with TcsL-W (1 μg/ml) for the indicated time points, cells were analyzed using the Apo-ONE® Homomgeneous Caspase-3/7 Assay as described in Materials and Methods. Control samples were incubated with 20 mM Tris, pH 8.0, for the indicated time points. Samples were analyzed in triplicate and error bars represent the standard deviation from the mean. ■ = TcsL-W-treated cells and ● = control cells. (B) HeLa cells were cultured in 25-cm^2 flasks and treated with TcsL-W (1 μg/ml) at ~ 75% confluence. Following treatments, cells were harvested, lysed, and total protein was separated via 4-15% SDS-PAGE and analyzed via Western blotting using a PARP-specific primary antibody. Control cells were incubated with 20 mM Tris, pH 8.0, and times of treatment are indicated above the gel.

Figure 17.

A

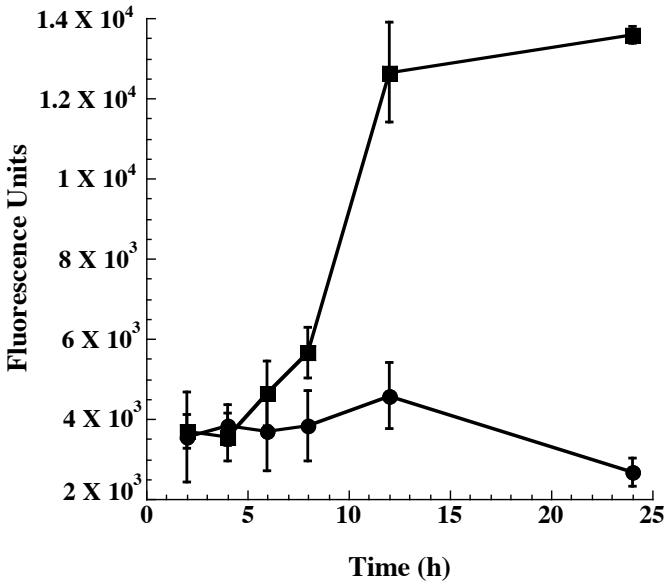
1.4 X 10^4
1.2 X 10^4
1 X 10^4
8 X 10^3
6 X 10^3
4 X 10^3
2 X 10^3
Fluorescence Units
0
5
10
15
20
25
Time (h)

B

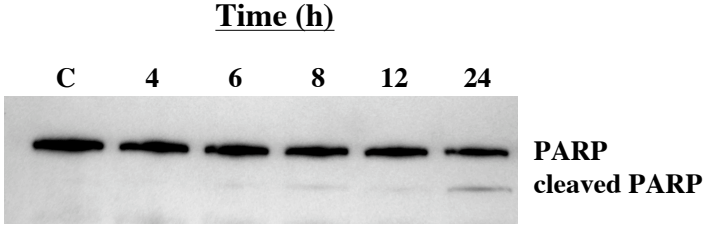
Time (h)
C
4
6
8
12
24
PARP
cleaved PARP

activity, the protein must be phosphorylated at Ser-473 by upstream factors, such as PI3K or PDK1 (7). Therefore, it was hypothesized that TcsL inactivation of Ras would result in a decline in the levels of phosphorylated Akt, resulting in a pro-apoptotic phenotype in TcsL-treated cells.

Using Western blot analysis, a rapid decline in the levels of phosphorylated Akt was observed early in routine TcsL treatment of HeLa cells, with an ~ 65% decrease in this form of the protein by 1 h post-treatment (Fig. 18A). This decline was in contrast total levels of Akt in TcsL-treated cells, which remained constant across the same time course (Fig. 18B). To determine whether this loss in phosphorylated Akt was dependent on TcsL-specific GTPase inactivation, the activation status of Akt was analyzed in lysates collected from HeLa cells treated with *Clostridium difficile* Toxin B (TcdB), a homologous glucosyltransferase that inactivates Rho, Rac, and Cdc42, but not Ras (4). As shown in Fig. 18C, treatment of HeLa cells with TcdB, for the same time course as TcsL, had no detectable negative effect on the levels of phosphorylated Akt, suggesting this effect was dependent on the inactivation of TcsL-specific substrates.

TcsL glucosyltransferase activity is required to induce rapid declines in active Akt. As mentioned above, some debate exists as to whether GTPase modification is a required step in the initiation of apoptosis in TcsL-treated cells (129). To better understand GTPase involvement in this process, we took

Figure 18. Levels of phosphorylated Akt in TcsL-treated HeLa cells. Following incubation with either 1 μg/ml TcsL-W (A and B) or 1 μg/ml TcdB (C) for the indicated time points, cells were harvested, lysed, and total protein was separated via 4-15% SDS-PAGE and analyzed via Western blotting using a phospho-Akt-specific primary antibody. Times of treatment are indicated above the gel. (A) Levels of phosphorylated Akt in TcsL-W-treated cells. (B) Levels of total Akt in TcsL-W-treated cells. (C) Levels of phosphorylated Akt in TcdB-treated cells.

Figure 18.

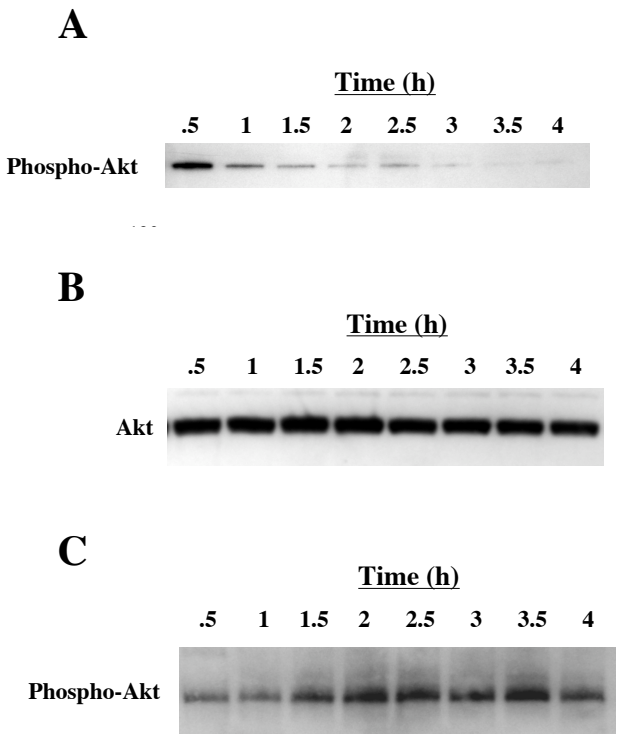
A
Time (h)
.5 1 1.5 2 2.5 3 3.5 4
Phospho-Akt
B
Time (h)
.5 1 1.5 2 2.5 3 3.5 4
Akt
C
Time (h)
.5 1 1.5 2 2.5 3 3.5 4
Phospho-Akt

advantage of a fusion protein delivery system based on the cellular entry of anthrax toxin that was described in Chapter IV of this dissertation. Using this fusion protein, LFnTcsL$^{1-556}$, along with protective antigen (PA) from *Bacillus anthracis*, we were able to analyze the effects of the enzymatic domain of TcsL alone on the levels of phosphorylated Akt. As shown in Fig. 19A, treatment of cells with PA plus LFnTcsL$^{1-556}$ resulted in a decline in phosphorylated Akt by ~ 4 h, suggesting the toxin's glucosyltransferase activity is sufficient to influence the levels of active Akt.

To further examine the requirement for glucosyltransferase activity in TcsL-induced declines in active Akt, the toxin was inactivated by incubation with the UDP derivative UDP-2',3'-dialdehyde as previously reported (64). Inactivation of the toxin in this manner results in a form of the protein that still binds and enters the cell but is no longer able to modify GTPases due to its inability to bind UDP-glucose and, thus, can no longer induce CPE (Fig. 19). As shown in Fig. 19B, HeLa cells incubated with derivatized TcsL exhibited no decline in the levels of phosphorylated Akt, further indicating the glucosyltransferase activity of the toxin is required for mediating these early events.

Downstream effects of TcsL inactivation of Akt. Downstream effectors of active Akt were next examined following TcsL intoxication. In this study, the phosphorylation state of Bad and GSK-3β was examined in HeLa cells following

Figure 19. Effects of TcsL glucosyltransferase activity on Akt activation. Following incubation with either 1 μg/ml LFnTcsL$^{1-556}$ + 1 μg/ml PA (A) or 1 μg/ml derivatized TcsL-W (B) for the indicated time points, cells were harvested, lysed, and total protein was separated via 4-15% SDS-PAGE and analyzed via Western blotting using a phospho-Akt-specific primary antibody. Times of treatment are indicated above the gel. (A) Levels of phosphorylated Akt in cells incubated with LFnTcsL$^{1-556}$ + PA. (B) Levels of phosphorylated Akt in cells incubated with derivatized TcsL-W. (C-E) HeLa cells were cultured in 96-well plates and subsequently incubated with either 20 mM Tris, pH 8.0 (C), TcsL-W (D), or derviatized TcsL (E) for 24 h. Pictures are representative of cells observed in multiple treatments.

Figure 19.

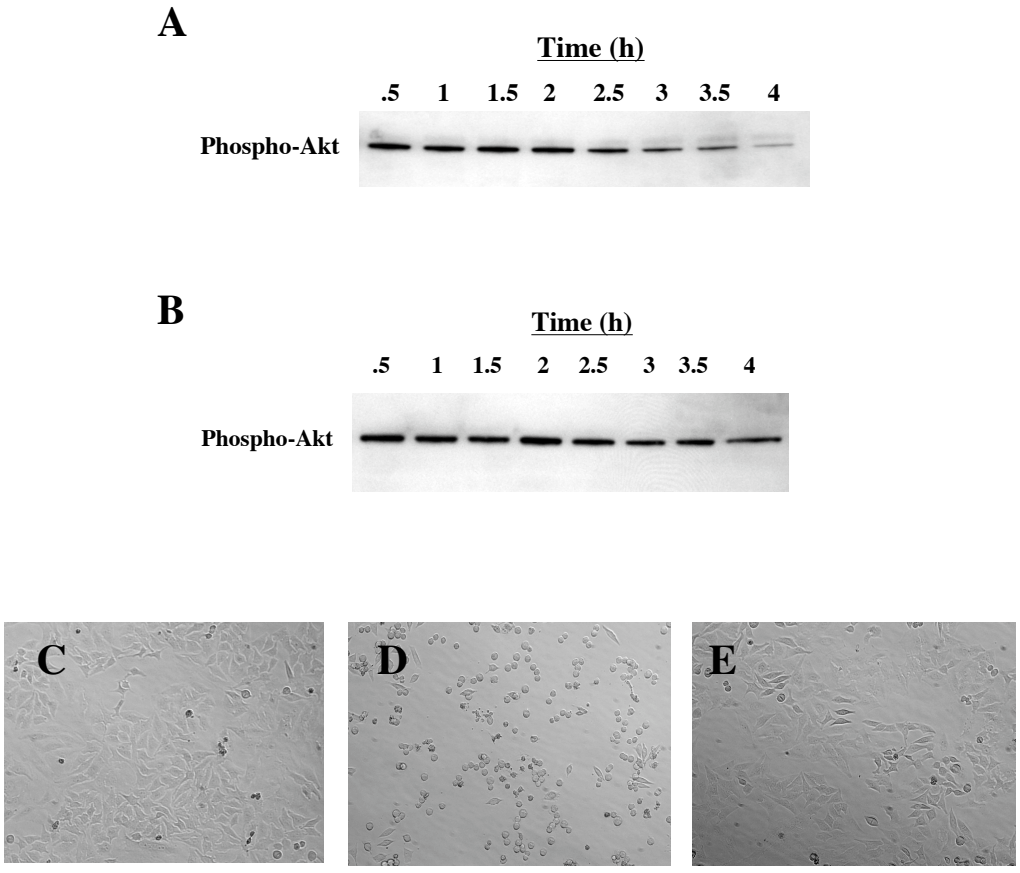
A
Time (h)
.5 1 1.5 2 2.5 3 3.5 4
Phospho-Akt
B
Time (h)
.5 1 1.5 2 2.5 3 3.5 4
Phospho-Akt
C
D
E

incubation with TcsL. As shown in Fig. 20, TcsL-intoxicated HeLa cells showed decreases in the phosphorylated form of GSK-3β (Fig. 20A) at 8 – 12 h post-intoxication and a corresponding decline in levels of total GSK-3β (Fig. 20B). These declines did not, however, result from a global loss in cellular protein (Fig. 20C). This condition represents a pro-apoptotic phenotype late in intoxication due to activation of GSK-3β, which is known to influence cell cycle regulation and apoptosis (45, 78). Surprisingly, no detectable loss in phosphorylated Bad was observed under these conditions (data not shown). While Bad has been shown to be involved in apoptotic responses in specific cells following Akt inactivation (148), it is possible that other, unidentified factors function at the mitochondrial surface following Akt inactivation in TcsL-intoxicated cells.

Since TcsL inactivation of Akt affected specific downstream effectors of this pro-survival pathway, Wortmannin, an inhibitor of PI3K and, consequently, Akt (Fig. 21A), was employed to examine the global response in cells lacking active Akt. As shown in Fig. 21B, treatment of cells with Wortmannin resulted in a rapid decline in phosphorylated GSK-3β; however, no corresponding loss in GSK-3β was observed, with total levels of this protein remaining constant through 24 h (Fig. 21B). These results further suggested TcsL-specific and glucosylation-specific effects were occurring in the cells treated with this LCT.

Late apoptotic events occurring in cells intoxicated by TcsL. To further understand the apoptotic events occurring in cells treated with TcsL,

Figure 20. Downstream effects of Akt inactivation by TcsL. Following incubation with TcsL-W (1 μg/ml) for the indicated time points, cells were harvested, lysed, and total protein was separated via 4-15% SDS-PAGE and stained with Coomassie Blue or analyzed via Western blotting using a phospho-GSK-3β-specific primary antibody. Times of treatment are indicated above the gel. (A) Levels of phosphorylated GSK-3β in TcsL-W-treated cells. (B) Levels of total GSK-3β in TcsL-W-treated cells. (C) Levels of total protein in TcsL-W-treated cells.

Figure 20.

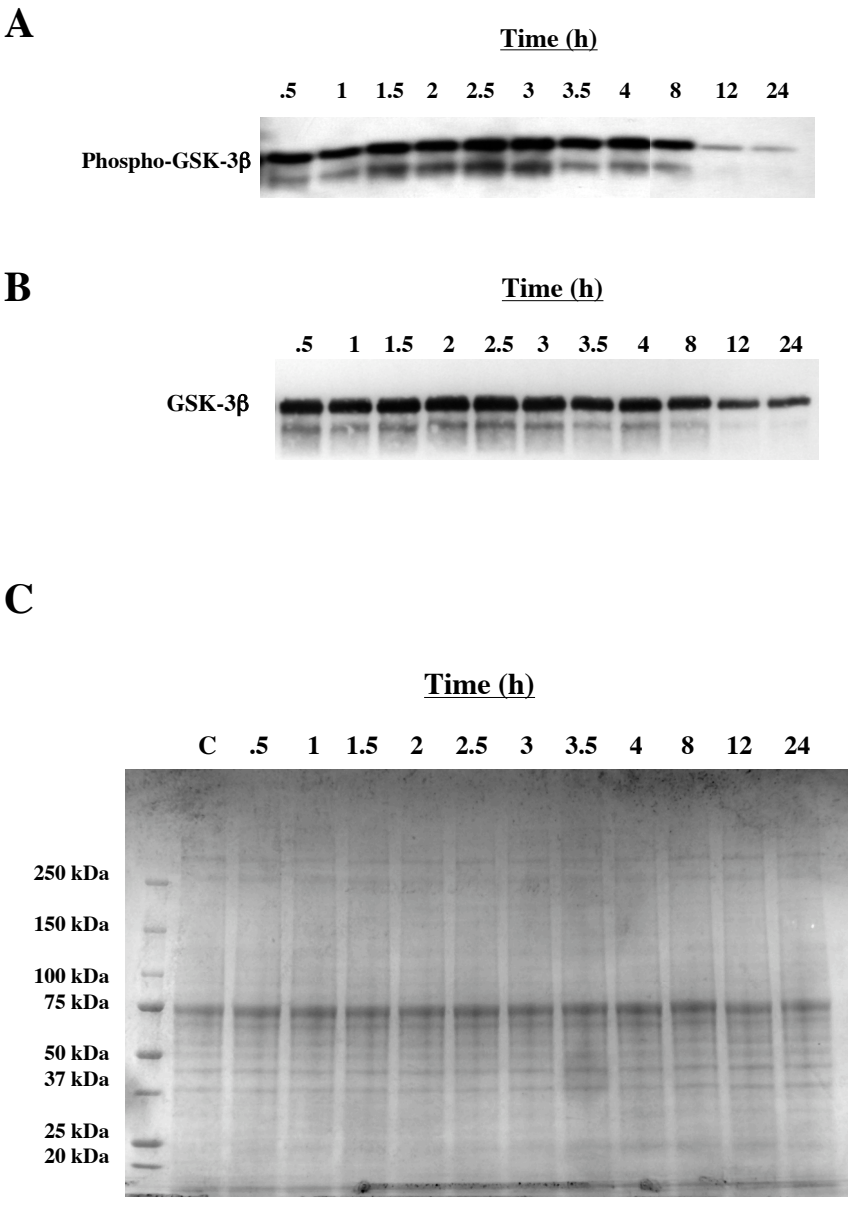
A
Time (h)
.5 1 1.5 2 2.5 3 3.5 4 8 12 24
Phospho-GSK-3β
B
Time (h)
.5 1 1.5 2 2.5 3 3.5 4 8 12 24
GSK-3β
C
Time (h)
C .5 1 1.5 2 2.5 3 3.5 4 8 12 24
250 kDa
150 kDa
100 kDa
75 kDa
50 kDa
37 kDa
25 kDa
20 kDa

Figure 21. Levels of phosphorylated Akt and phosphorylated GSK-3β in Wortmannin-treated HeLa cells. Following incubation with Wortmannin (1 μM) for the indicated time points, cells were harvested, lysed, and total protein was separated via 4-15% SDS-PAGE and analyzed via Western blotting using a phospho-Akt-specific, Akt-specific, phospho-GSK-3β-specific, or GSK-3β-specific primary antibody. Times of treatment are indicated above the gel. (A) Levels of phosphorylated Akt and total Akt in Wortmannin-treated cells. (B) Levels of phosphorylated GSK-3β and total GSK-3β in Wortmannin-treated cells.

Figure 21.

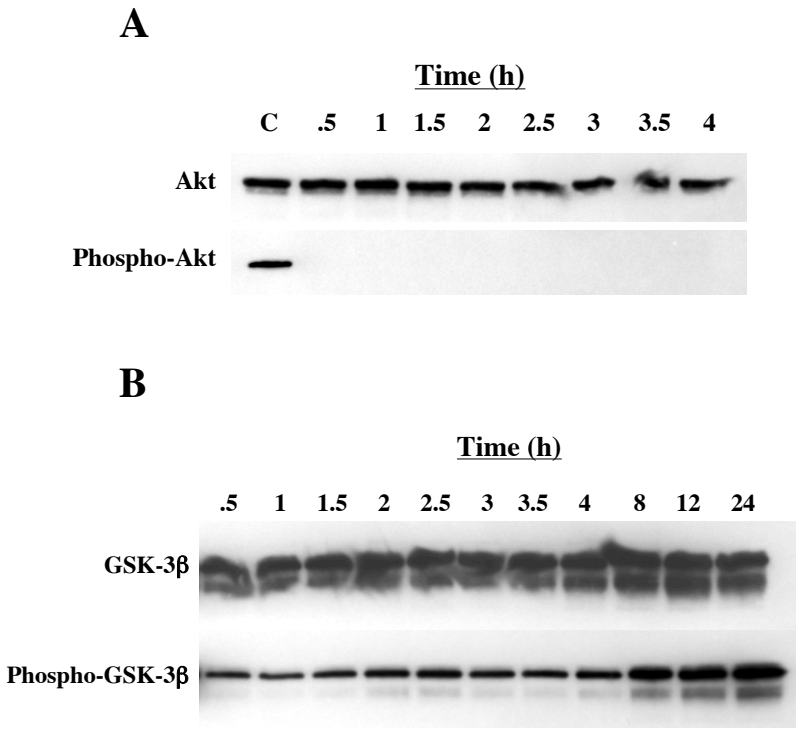
A
Time (h)
C .5 1 1.5 2 2.5 3 3.5 4
Akt
Phospho-Akt
B
Time (h)
.5 1 1.5 2 2.5 3 3.5 4 8 12 24
GSK-3β
Phospho-GSK-3β

specific mitochondrial effectors were examined to determine their potential role in TcsL cytotoxicity. In particular, Bid, Bcl-2, and Bcl-x_L were examined in this study, as these are three well-known mitochondrial proteins involved in apoptotic responses (94, 164). As shown in Fig. 22, total levels of Bcl-2, an anti-apoptotic protein, were unaffected following intoxication of NIH/3T3 cells by TcsL. In contrast, both Bid and Bcl-x_L underwent cleavage by 8 – 12 h, indicative of pro-apoptotic conditions (94). Interestingly, this cleavage event was not observed in lysates taken from cells incubated in the presence of TcsL and a pan-caspase inhibitor (Fig. 22). Active caspase-3 has been previously shown to cleave other proteins, including Bid and Bcl-x_L, resulting in an amplification/feedback apoptotic response that ensures the death of the affected cell (94, 152). This evidence, in combination with the current results, suggests that TcsL intoxication of NIH/3T3 cells results in specific caspase-dependent, late stage apoptotic events that create an amplification response involving specific mitochondrial apoptotic effector proteins (summarized in Fig. 23).

DISCUSSION

In the current study, we examined the pre-mitochondrial events leading to apoptosis in cells intoxicated by the bacterial glucosyltransferase TcsL. These results indicate that TcsL activity causes the rapid inactivation of a major cell survival regulator, Akt. Akt is a serine/threonine kinase that functions

Figure 22. Effects of TcsL intoxication on mitochondrial apoptotic effector proteins. Following incubation with TcsL-W (1 μg/ml) for the indicated time points, cells were harvested, lysed, and total protein was separated via 4-15% SDS-PAGE and analyzed via Western blotting using either Bcl-2-, Bcl-x_L-, or Bid-specific primary antibody. Times of treatment are indicated above the gel. C.I. = cells pretreated for 1 h with a pancaspase inhibitor (50 μM).

Figure 22.

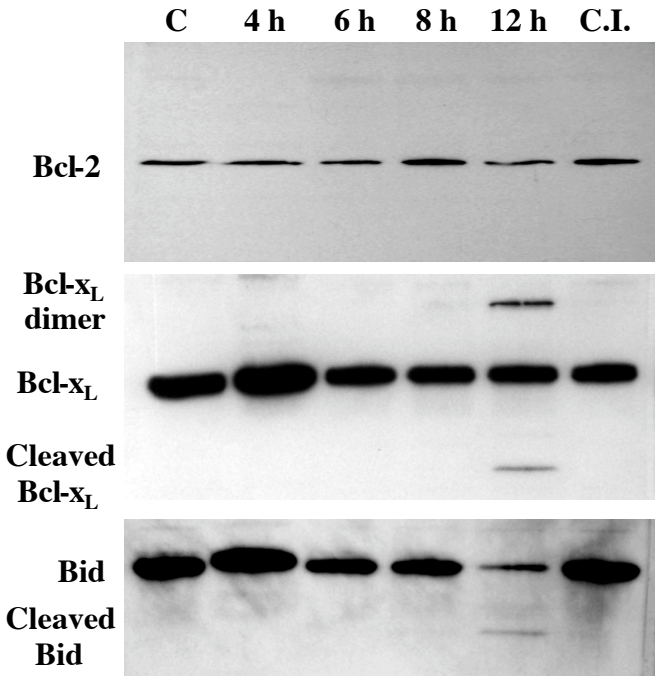
C
4 h
6 h
8 h
12 h
C.I.
Bcl-2
Bcl-x$_L$ dimer
Bcl-x$_L$
Cleaved Bcl-x$_L$
Bid
Cleaved Bid

Figure 23. Model of TcsL-induced apoptosis involving early glucosylation-specific events and an amplification/feedback response. Following cell entry, TcsL glucosylates Ras at the inner cell membrane, resulting in an inactive form of the protein. Inactivated Ras results in the inactivation of Akt, a major cell survival regulator that controls multiple signaling pathways. The absence of active Akt triggers a cell death response via downstream effectors, such as GSK-3β and the mitochondrial effector Bad. Once the mitochondrial membrane potential has been perturbed, cytochrome c is released into the cytosol, where it forms a complex with caspase-9 termed the apoptosome. This complex is then responsible for downstream processing of caspases, such as caspase-3. Caspase-3 then functions as an executioner caspase that cleaves additional proteins, including Bid and Bcl-x_L. Processing of these mitochondrial effectors enhances the apoptotic response via a feedback/amplification loop. These processes ultimately result in PARP inactivation, DNA fragmentation, and, consequently, cell death.

Figure 23.

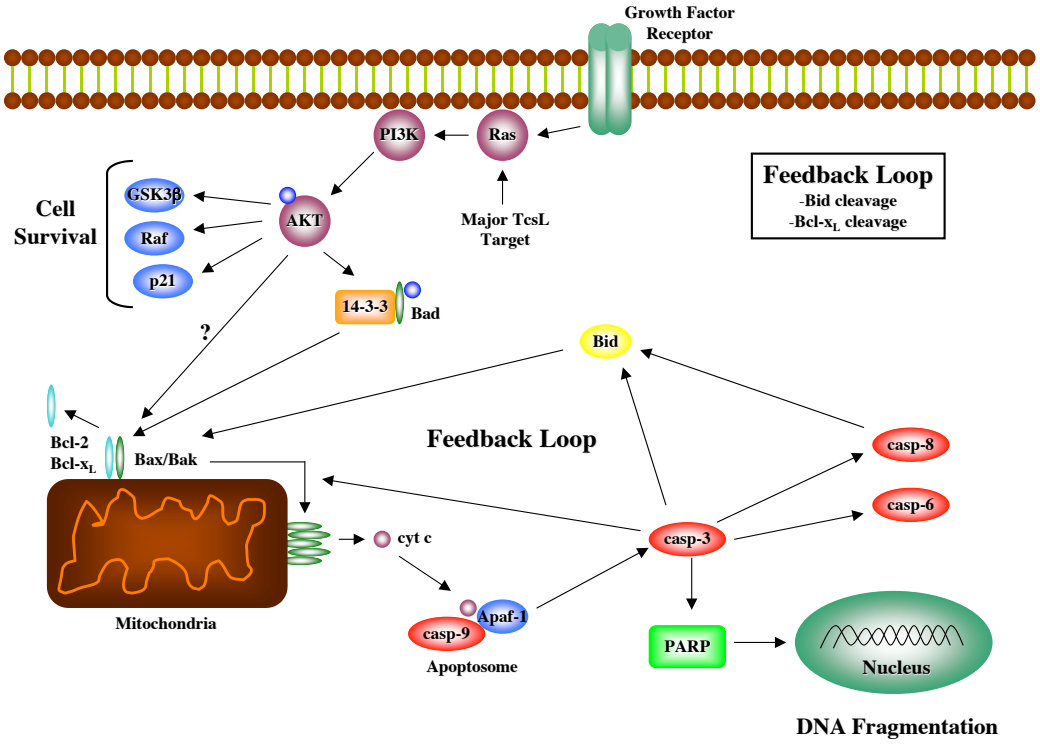
Growth Factor
Receptor
PI3K
Ras
Feedback Loop
-Bid cleavage
-Bcl-xL cleavage
Cell
Survival
GSK3β
Raf
p21
AKT
Major TcsL
Target
14-3-3
Bad
?
Bid
Bcl-2
Bcl-xL
Bax/Bak
Feedback Loop
casp-8
casp-6
casp-3
cyt c
Mitochondria
Apaf-1
casp-9
Apoptosome
PARP
Nucleus
DNA Fragmentation

downstream of Ras, a TcsL substrate, to enhance cell survival (49, 128, 146) via multiple phosphorylation cascades. Akt itself is activated via phosphorylation at Ser-473, following which, the protein participates in multiple signaling pathways including, but not limited to, ERK, GSK-3β, and p53, and regulates transcriptional activators, such as the FKHR family, in order to prevent apoptosis (49, 128). The current results indicate that TcsL inactivation of Akt, via GTPase glucosylation, leads to mitochondrial- and caspase-dependent events that ensure death of the target cell.

While unique among the LCTs, exploitation of Akt signaling, through inactivation, by at least three bacterial pathogens, including *Pseudomonas aeruginosa* (74), *Serratia marcescens* (52), and *Yersinia enterocolitica* (147), has been previously demonstrated. Most notably, Exoenzyme S, a Type III effector protein produced by *Pseudomonas aeruginosa*, is an ADP-ribosyltransferase that inactivates Ras in target cells (74). The ADP-ribosyltransferase activity of this bacterial toxin leads to declines in active Akt, disruption of the actin cytoskeleton (58), and ultimately to death of the affected cell. Additionally, as with the current derivatized TcsL results, ExoS mutants lacking enzymatic activity are no longer able to modulate Akt activation and are rendered non-toxic (74). These studies, along with the current TcsL results, suggest Akt may be a common signaling protein targeted by bacterial toxins that impact small GTPase activation.

Although ExoS inactivation of Akt has been demonstrated in serum-starved cells subsequently exposed to growth factors (74), the current TcsL data indicate that this bacterial toxin induces the inactivation of Akt in cells growing in the presence of serum containing growth factors. Following incubation of HeLa cells, in the presence of serum, with TcsL, rapid (< 1 h) declines in the levels of phosphorylated Akt were observed. These declines were observed prior to the reported time of mitochondrial- and caspase-dependent events that eventually ensue due to TcsL activity. In studies examining mitochondrial protein- and caspase-related activity, cytochrome c release and caspase-9 activation were not observed until 2 h post-treatment with TcsL (129), suggesting that the toxin's effects on Akt may be a prerequisite for mitochondrial-dependent apoptosis. Additionally, studies of the TcsL enzymatic domain and derivatized TcsL indicate that these Akt-specific effects are dependent on catalytically active toxin. In total, these results suggest that glucosylation, and inactivation, of small GTPases is an essential step in TcsL cytotoxicity.

Due to the observed effects of TcsL on Akt activation, we also examined the activation status of downstream Akt effectors as a consequence of Akt inactivation. These results indicated that TcsL intoxication has specific effects on the downstream protein GSK-3β. In the current study, GSK-3β was dephosphorylated by 8 - 12 h post-intoxication, with a corresponding loss in total GSK-3β, further supporting an apoptotic phenotype late in intoxication. In

contrast, no detectable change in the activation state of Bad was observed in the current study. Subsequent experiments, using Wortmannin as a general Akt inhibitor, showed no effect on total GSK-3β, suggesting this is a TcsL-specific response.

Following examination of TcsL-specific early effects on Akt inactivation, specific mitochondrial effectors were also examined to determine their role in TcsL-induced cell death. In particular, the mitochondrial effectors Bcl-2, Bcl-x_L, and Bid were examined for their potential roles in TcsL-induced apoptosis. In healthy cells, both Bcl-2 and Bcl-x_L serve as anti-apoptotic factors that function to inhibit cytochrome c release from the mitochondria (164). The current results showed no detectable Bcl-2 involvement in TcsL cytotoxicity; however, TcsL-intoxicated cells demonstrated processing of Bcl-x_L, shown by cleavage of this mitochondrial-associated protein. This cleavage event has been reported to be caspase-3-dependent, resulting in a pro-apoptotic form of Bcl-x_L (22, 59). At the same time point of Bcl-x_L processing, cleaved Bid was also detected in TcsL-intoxicated cells. This cleavage has also been shown to be a pro-apoptotic response that results in a feedback response via caspase-3 activity (152). In line with these observations, the current results showed prevention of both Bcl-x_L and Bid processing when cells were incubated in the presence of TcsL and a pancaspase inhibitor, further suggesting the requirement of caspases to elicit a complete apoptotic response to the LCTs.

In total, the current data suggests TcsL induces an apoptotic program in target cells that involves early pre-mitochondrial, mitochondrial, and late stage caspase-mediated events that result in a feedback/amplification response to ensure cell death (Fig. 23). In studies of the LCT-producing clostridia, major emphasis is placed on the toxins, and their ability to cause cell death, as a major determinant in the severity of disease. While it has been established that mitochondrial proteins and caspases are important for apoptosis in LCT-intoxicated cells, the current study stresses the need to dissect the upstream components involved in these toxins' mechanisms of action. In particular, the link between GTPase glycosylation and the proteins responsible for cell death must be defined in order to halt toxin activity before apoptosis proceeds to a point of no return. The current results indicate that TcsL modulates a vital cell survival protein, Akt, prior to observation of cell rounding and mitochondrial-dependent apoptotic events. While TcdB, a related LCT, was not found to elicit similar effects, these results suggest that each of the LCTs could impact diverse cell survival signaling pathways prior to the induction of apoptosis.

MATERIALS AND METHODS

Mammalian cell culture, bacterial strains, and toxin purification. Human epitheloid carcinoma (HeLa) and NIH/3T3 mouse fibroblast cells were obtained from the American Type Culture Collection and maintained in RPMI

1640 medium (Gibco) containing 10% fetal calf serum (Gibco) at 37°C in the presence of 6% CO_2. All cells were used between passages 10 and 20. *C. sordellii* strain W (Dr. Dennis Stevens, VA Hospital, Boise, Idaho) was used for isolation of TcsL in this study and *C. difficile* ATCC 10463 was used for isolation of TcdB. For toxin purification, *C. sordellii* or *C. difficile* were cultured in 1 L dialysis bag cultures, and TcsL and TcdB were purified as previously described (138). $LfnTcsL^{1-556}$ and PA were expressed in *Escherichia coli* and isolated as described in Chapter IV of this dissertation. Unless otherwise indicated, all other chemical reagents were from Sigma.

Inactivation of TcsL. TcsL was inactivated via incubation with UDP-2',3'-dialdehyde using a modified version of the protocol described by Genth *et al.* for *C. difficile* TcdB (64). TcsL (0.5 μg/ml) was incubated in a 100 μl solution containing 1 mM UDP-2',3'-dialdehyde (Sigma) solubilized in 20 mM Tris, 150 mM NaCl, pH 7.5. The sample was incubated at 37°C for 3 h to inactivate the toxin. Following inactivation, the sample was passed over a 50 kDa MWCO filter using the Microcon system (Amicon). Using this system, the toxin was washed three times with 20 mM Tris, pH 8.0 for removal of excess UDP-2',3'-dialdehyde. Inactivated TcsL was subsequently incubated with HeLa cells in a 96-well plate overnight to determine loss of cytotoxic activity.

Western blot analysis. HeLa cells, grown to confluence in 6-well tissue culture plates, were incubated with TcsL (1 μg/ml), $LfnTcsL^{1-556}$ (1 μg/ml) +

protective antigen (1 μg/ml), TcdB (1 μg/ml), or Wortmannin (1 μM) for the indicated periods of time. In indicated samples, cells were pretreated for 1 h with a pancaspase inhibitor (50 μM) (Calbiochem) prior to toxin treatment. Following toxin treatment, cells were harvested via incubation on ice for 20 min in buffer containing 50 mM Tris-HCl (pH 5.7), 5 mM EDTA, 1% SDS, 100 mM NEM, and protease inhibitor cocktail. Cell lysates were subsequently passed through a 20 gauge needle 10 times. Total cell lysate protein was quantified using the DC Protein Assay method according to the manufacturer's instructions (BioRad). Cell lysates (10 μg) were separated via 4-20% SDS-PAGE and transferred to a poly(vinylidene) membrane. Following transfer, membranes were probed with the indicated primary antibodies (Cell Signaling Technologies). After overnight incubation in primary antibody, membranes were incubated with an HRP-conjugated secondary antibody (Cell Signaling Technologies) and reacting proteins were visualized via enhanced chemiluminescence using the ECL-plus kit (Amersham).

Caspase-3 activation assays. To analyze the activation state of caspase-3 in TcsL-treated cells, the Apo-ONE® Homogeneous Caspase-3/7 Assay (Promega) was utilized. HeLa cells were grown to ~ 75% confluence in a 96-well plate and subsequently incubated with TcsL (1 μg/ml) for the indicated time points. Following toxin treatment, the Apo-ONE® Caspase-3/7 Reagent was added to each well, including control cells and blank wells. Following incubation

at room temperature for 1 h, fluorescence intensity of each well was determined using a Fluostar Optima fluorimeter (BMG Labtechnologies). An excitation wavelength of 485 nm and an emission wavelength of 530 nm were used. Each sample was analyzed in triplicate and error bars represent the standard deviation from the mean.

CHAPTER VI

SUMMARY

The studies described in this dissertation were designed in order to gain a better understanding of the virulence mechanisms of *C. sordellii*, with particular emphasis on the soluble virulence factors produced by this organism. While *C. sordellii*-associated disease has been reported, in humans, for many years now, and appears to be on the rise, little is known regarding the virulence determinants responsible for this disease. As with many of the pathogenic clostridia, *C. sordellii* produces a number of soluble virulence proteins that are thought to be responsible for establishing infection and causing disease. To this end, the current studies involved analyzing a panel of *C. sordellii* isolates for virulence factor production and activity. Following this characterization, the primary *C. sordellii* virulence factor, TcsL, was studied at the biochemical and cell biology level to further understand the role of this toxin in *C. sordellii* pathogenesis.

In Chapter III of this dissertation, an extensive study of cadaver-derived *C. sordellii* strains was undertaken in order to determine the frequency at which this pathogen produces one, two, or more of its reported virulence factors. Surprisingly, only one of the examined strains produced TcsL, which is thought to be the major virulence determinant in *C. sordellii*-associated disease. Aside from

TcsL, five of the cadaver-derived strains produced an active hemolysin, termed sordellilysin (SDL). SDL lysed erythrocytes *in vitro* and was also cytolytic to a panel of cultured mammalian cells. Additionally, using Western blot analysis, we determined that SDL shares some homology with perfringolysin O produced by *C. perfringens*.

In order to better understand the importance of TcsL and SDL in *C. sordellii* pathogenesis, the mouse model of intravenous injection was employed. Using this model, supernatants from $TcsL^+$, SDL^- and $TcsL^-$, SDL^+ strains were compared via LD_{50} analysis. From these experiments, we found that supernatants containing TcsL demonstrated an ~ 10-fold lower LD_{50} than supernatants containing active SDL. Additionally, supernatants lacking these toxins, but containing other virulence factors, were not lethal in the mouse model. In total, these results suggest that a high percentage of strains of *C. sordellii* produce an active hemolytic protein that may aid in causing specific forms of disease; however, studies using the mouse model suggest that TcsL may be more important for the shock-like death observed in patients with *C. sordellii*-associated disease. These results also show a high degree of variability in virulence factor profiles among *C. sordellii* strains, which may be a key component of this organism's ability to cause many different types of disease.

In Chapter IV of this dissertation, a closer examination of the biochemical aspects of TcsL was performed, with an emphasis on the pH-specific effects on

the toxin. In these studies, we found that TcsL dissociates at acid pH (< pH 5.0), the same pH at which the toxin demonstrates enhanced cytopathic effects (CPE) when incubated with cultured mammalian cells. This acid pH triggers TcsL to dissociate into a group of 40 – 50 kDa proteins. The close association of these smaller proteins in the TcsL protein complex was confirmed using a chemical crosslinking reagent. In the presence of this reagent, TcsL no longer dissociated into the smaller protein group when placed in an acid pH environment, and crosslinked TcsL was no longer cytotoxic to cultured cells. In addition to toxin dissociation, we also found that TcsL samples contained a high molecular weight complex that was also subject to pH-induced dissociation. Using an electroelution technique, it was determined that TcsL was indeed a component of this multimeric complex. Suspecting that this complex may be a protective environment for TcsL, protease treatments of the toxin were also performed. The results of these studies indicated that TcsL is a highly stable protein that is not subject to common protease digestion unless elevated to high temperature. Collectively, the results from these studies suggest that TcsL is a stable toxin that is maintained in a protective complex and dissociates at acid pH to enhance cytotoxicity. These characteristics would likely offer a beneficial environment to the toxin in the context of the host disease setting.

In Chapter V of this dissertation, the impact of TcsL on cell physiology was examined, with a particular emphasis on signaling pathways affected by this

toxin. These studies were designed to gain a better understanding of the immediate downstream effects of glucosylation of small GTPases by TcsL. Due to its role in multiple cell survival pathways, and its activation via Ras, Akt was examined as a possible effector of GTPase glucosylation by TcsL. Results from these experiments indicate that TcsL's activity results in rapid declines in the levels of phosphorylated (activated) Akt in intoxicated cells. Following Akt inactivation a notable decrease in phosphorylated GSK-3β and total GSK-3β was observed. These results suggest that TcsL affects one of the cell's major survival response proteins, Akt, and elicits subsequent effects on downstream survival response pathways in order to ensure cell death. Additionally, these data provide a direct link between GTPase glucosylation and cell death induced by TcsL.

After examining the early events occurring in TcsL-intoxicated cells, we also studied some of the later apoptotic events in these cells, focusing on mitochondrial-dependent apoptotic effector proteins. The results from these studies suggest TcsL induces a late stage apoptotic feedback mechanism via Bid and Bcl-x_L. In TcsL-intoxicated cells, both Bid and Bcl-x_L were cleaved by 12 h post-intoxication. Cleavage of these two proteins represents a pro-apoptotic condition in these cells. This cleavage event, however, was not observed in the presence of a caspase inhibitor, suggesting caspase activation is required prior to activation of these mitochondrial proteins. Thus, the late stage phenotype of TcsL-intoxicated cells indicates that these cells are undergoing caspase-dependent

apoptosis that involves a feedback mechanism proceeding through the mitochondrial effector proteins, Bid and Bcl-x_L.

In total, the work described in this dissertation presents some important advances in the field of *C. sordellii* pathogenesis. In regard to the organism, the current results provide a better understanding of the versatility of this pathogen due to its ability to produce a variety of virulence factors. The virulence factor characterization also identified a potentially important virulence determinant in SDL, a hemolytic factor produced by a high percentage of the strains examined. In regard to TcsL, the current results have further defined the pH-dependent effects of this toxin on the cell and, additionally, show that TcsL exerts its effects on the Akt cell survival pathway prior to mitochondrial apoptotic events. It is my hope that the findings presented in the current dissertation would contribute to a better understanding of *C. sordellii* pathogenesis and provide a basic knowledge of the virulence characteristics of this pathogen in order to better understand *C. sordellii*-associated disease.

REFERENCES

1. **Abdulla, A. and L. Yee.** 2000. The clinical spectrum of *Clostridium sordellii* bacteraemia: two case reports and a review of the literature. *J Clin Pathol*. **53:** 709-712.

2. **Adamkiewicz, T.V., D. Goodman, B. Burke, D.M. Lyerly, J. Goswitz and P. Ferrieri.** 1993. Neonatal *Clostridium sordellii* toxic omphalitis. *Pediatr Infect Dis J*. **12:** 253-257.

3. **Ahmed, S.A., P. McPhie and L.A. Smith.** 2003. Autocatalytically fragmented light chain of botulinum a neurotoxin is enzymatically active. *Biochemistry*. **42:** 12539-12549.

4. **Aktories, K., G. Schmidt and I. Just.** 2000. Rho GTPases as targets of bacterial protein toxins. *Biol Chem*. **381:** 421-426.

5. **Al-Mashat, R.R. and D.J. Taylor.** 1983. *Clostridium sordellii* in enteritis in an adult sheep. *Vet Rec*. **112:** 19.

6. **Al-Mashat, R.R. and D.J. Taylor.** 1983. Production of diarrhoea and enteric lesions in calves by the oral inoculation of pure cultures of *Clostridium sordellii*. *Vet Rec*. **112:** 141-146.

7. **Alessi, D.R., M. Andjelkovic, B. Caudwell, P. Cron, N. Morrice, P. Cohen and B.A. Hemmings.** 1996. Mechanism of activation of protein kinase B by insulin and IGF-1. *Embo J*. **15:** 6541-6551.

8. **Allo, M., J. Silva, Jr., R. Fekety, G.D. Rifkin and H. Waskin.** 1979. Prevention of clindamycin-induced colitis in hamsters by *Clostridium sordellii* antitoxin. *Gastroenterology*. **76:** 351-355.

9. **Altschuler, D.L. and F. Ribeiro-Neto.** 1998. Mitogenic and oncogenic properties of the small G protein Rap1b. *Proc Natl Acad Sci U S A*. **95:** 7475-7479.

10. **Amimoto, K., E. Oishi, H. Yasuhar, O. Sasak, S. Katayama, T. Kitajima, A. Izumida and T. Hirahara.** 2001. Protective effects of *Clostridium sordellii* LT and HT toxoids against challenge with spores in guinea pigs. *J Vet Med Sci*. **63:** 879-883.

11. **Arseculeratne, S.N., R.G. Panabokke and S. Wijesundera.** 1969. The toxins responsible for the lesions of *Clostridium sordellii* gas gangrene. *J Med Microbiol*. **2:** 37-53.

12. **Awad, M.M., D.M. Ellemor, R.L. Boyd, J.J. Emmins and J.I. Rood.** 2001. Synergistic effects of alpha-toxin and perfringolysin O in *Clostridium perfringens*-mediated gas gangrene. *Infect Immun*. **69:** 7904-7910.

13. **Baldacini, O., R. Girardot, G.A. Green, B. Rihn and H. Monteil.** 1992. Comparative study of immunological properties and cytotoxic effects of *Clostridium difficile* toxin B and *Clostridium sordellii* toxin L. *Toxicon*. **30:** 129-140.

14. **Bangsberg, D.R., J.I. Rosen, T. Aragon, A. Campbell, L. Weir and F. Perdreau-Remington.** 2002. Clostridial myonecrosis cluster among injection drug users: a molecular epidemiology investigation. *Arch Intern Med*. **162:** 517-522.

15. **Barnes, P. and J.M. Leedom.** 1987. Infective endocarditis due to *Clostridium sordellii*. *Am J Med*. **83:** 605.

16. **Barth, H., G. Pfeifer, F. Hofmann, E. Maier, R. Benz and K. Aktories.** 2001. Low pH-induced formation of ion channels by *Clostridium difficile* toxin B in target cells. *J Biol Chem*. **276:**10670-10676.

17. **Bartlett, J.G.** 1979. Antibiotic-associated pseudomembranous colitis. *Rev Infect Dis*. **1:** 530-539.

18. **Bartlett, J.G.** 1981. Antimicrobial agents implicated in *Clostridium difficile* toxin-associated diarrhea of colitis. *Johns Hopkins Med J*. **149:** 6-9.

19. **Bartlett, J.G., T. Chang, N.S. Taylor and A.B. Onderdonk.** 1979. Colitis induced by *Clostridium difficile*. *Rev Infect Dis*. **1:** 370-378.

20. **Bartlett, J.G., N. Moon, T.W. Chang, N. Taylor and A.B. Onderdonk.** 1978. Role of *Clostridium difficile* in antibiotic-associated pseudomembranous colitis. *Gastroenterology*. **75:** 778-782.

21. **Bartlett, J.G., A.B. Onderdonk, E. Drude, C. Goldstein, M. Anderka, S. Alpert and W.M. McCormack.** 1977. Quantitative bacteriology of the vaginal flora. *J Infect Dis*. **136:** 271-277.

22. **Basanez, G., J. Zhang, B.N. Chau, G.I. Maksaev, V.A. Frolov, T.A. Brandt, J. Burch, J.M. Hardwick and J. Zimmerberg.** 2001. Pro-apoptotic cleavage products of Bcl-x_L form cytochrome c-conducting pores in pure lipid membranes. *J Biol Chem*. **276:** 31083-31091.

23. **Bette, P., A. Oksche, F. Mauler, C. von Eichel-Streiber, M.R. Popoff and E. Habermann.** 1991. A comparative biochemical, pharmacological and immunological study of *Clostridium novyi* alpha-toxin, *C. difficile* toxin B and *C. sordellii* lethal toxin. *Toxicon*. **29:** 877-887.

24. **Bitti, A., P. Mastrantonio, P. Spigaglia, G. Urru, A.I. Spano, G. Moretti and G.B. Cherchi.** 1997. A fatal postpartum *Clostridium sordellii*-associated toxic shock syndrome. *J Clin Pathol*. **50:** 259-260.

25. **Boquet, P.** 1999. Bacterial toxins inhibiting or activating small GTP-binding proteins. *Ann N Y Acad Sci*. **886:** 83-90.

26. **Borer, A., J. Gilad, E. Sikuler, K. Riesenberg, F. Schlaeffer and D. Buskila.** 1999. Fatal *Clostridium sordellii* ischio-rectal abscess with septicaemia complicating ultrasound-guided transrectal prostate biopsy. *J Infect*. **38:** 128-129.

27. **Brito, G.A., J. Fujji, B.A. Carneiro-Filho, A.A. Lima, T. Obrig and R.L. Guerrant.** 2002. Mechanism of *Clostridium difficile* toxin A-induced apoptosis in T84 cells. *J Infect Dis*. **186:** 1438-1447.

28. **Brooks, M.E. and H.B.G. Epps.** 1958. Taxonomic studies of the genus *Clostridium*: *Clostridium bifermentans* and *C. sordellii*. *J Med Microbiol*. **21:** 144-155.

29. **Browdie, D.A., J.H. Davis, M.J. Koplewitz, L. Corday and A.W. Leadbetter.** 1975. *Clostridium sordellii* infection. *J Trauma*. **15:** 515-518.

30. **Buchman, A.L., M. Ponsillo and P.H. Nagami.** 1991. Empyema caused by *Clostridium sordellii*, a rare form of pleuropulmonary disease. *J Infect*. **22:** 171-174.

31. **Busch, C., F. Hofmann, R. Gerhard and K. Aktories.** 2000. Involvement of a conserved tryptophan residue in the UDP-glucose binding of large clostridial cytotoxin glycosyltransferases. *J Biol Chem*. **275:** 13228-13234.

32. **Busch, C., F. Hofmann, J. Selzer, S. Munro, D. Jeckel and K. Aktories.** 1998. A common motif of eukaryotic glycosyltransferases is essential for the enzyme activity of large clostridial cytotoxins. *J Biol Chem*. **273:** 19566-19572.

33. **Cartwright, C.P., F. Stock, S.E. Beekmann, E.C. Williams and V.J. Gill.** 1995. PCR amplification of rRNA intergenic spacer regions as a method for epidemiologic typing of *Clostridium difficile*. *J Clin Microbiol*. **33:** 184-187.

34. **CDC.** 2005. *Clostridium sordellii* toxic shock syndrome after medical abortion with mifepristone and intravaginal misoprostol--United States and Canada, 2001-2005. *MMWR Morb Mortal Wkly Rep*. **54:** 724.

35. **CDC.** 2001. Unexplained deaths following knee surgery--Minnesota, November 2001. *MMWR Morb Mortal Wkly Rep*. **50:** 1035-1036.

36. **Chang, T.W., S.L. Gorbach and J.B. Bartlett.** 1978. Neutralization of *Clostridium difficile* toxin by *Clostridium sordellii* antitoxins. *Infect Immun*. **22:** 418-422.

37. **Chang, T.W., P.S. Lin, S.L. Gorbach and J.G. Bartlett.** 1979. Ultrastructural changes of cultured human amnion cells by *Clostridium difficile* toxin. *Infect Immun*. **23:** 795-798.

38. **Chaves-Olarte, E., I. Florin, P. Boquet, M. Popoff, C. von Eichel-Streiber and M. Thelestam.** 1996. UDP-glucose deficiency in a mutant cell line protects against glucosyltransferase toxins from *Clostridium difficile* and *Clostridium sordellii*. *J Biol Chem*. **271:** 6925-6932.

39. **Chaves-Olarte, E., M. Weidmann, C. Eichel-Streiber and M. Thelestam.** 1997. Toxins A and B from *Clostridium difficile* differ with respect to enzymatic potencies, cellular substrate specificities, and surface binding to cultured cells. *J Clin Invest*. **100:** 1734-1741.

40. **Chen, F., G.M. Kuziemko and R.C. Stevens.** 1998. Biophysical characterization of the stability of the 150-kilodalton botulinum toxin, the nontoxic component, and the 900-kilodalton botulinum toxin complex species. *Infect Immun*. **66:** 2420-2425.

41. **Clark, G.F., H.C. Krivan, T.D. Wilkins and D.F. Smith.** 1987. Toxin A from *Clostridium difficile* binds to rabbit erythrocyte glycolipids with terminal Galα1-3Galβ1-4GlcNAc sequences. *Arch Biochem Biophys*. **257:** 217-229.

42. **Clark, S.** 2003. Sudden death in periparturient sheep associated with *Clostridium sordellii*. *Vet Rec*. **153:** 340.

43. **Cohen, S.H., Y.J. Tang and J. Silva Jr.** 2000. Analysis of the pathogenicity locus in *Clostridium difficile* strains. *J Infect Dis*. **181:** 659-663.

44. **Cooke, D.L. and S.P. Borriello.** 1998. Non-specific binding of *Clostridium difficile* toxin A to murine immunoglobulins occurs via the Fab component. *Infect Immun*. **66:** 1981-1984.

45. **Cross, D.A., D.R. Alessi, P. Cohen, M. Andjelkovich and B.A. Hemmings.** 1995. Inhibition of glycogen synthase kinase-3 by insulin mediated by protein kinase B. *Nature*. **378:** 785-789.

46. **Cunniffe, J.G.** 1996. *Clostridium sordellii* bacteraemia. *J Infect*. **33:** 127-129.

47. **Dang, L.H., C. Bettegowda, N. Agrawal, I. Cheong, D. Huso, P. Frost, F. Loganzo, L. Greenberger, J. Barkoczy, G.R. Pettit, A.B. Smith, 3rd, H. Gurulingappa, S. Khan, G. Parmigiani, K.W. Kinzler, S. Zhou and B. Vogelstein.** 2004. Targeting vascular and avascular compartments of tumors with *C. novyi*-NT and anti-microtubule agents. *Cancer Biol Ther*. **3:** 326-337.

48. **Dang, L.H., C. Bettegowda, D.L. Huso, K.W. Kinzler and B. Vogelstein.** 2001. Combination bacteriolytic therapy for the treatment of experimental tumors. *Proc Natl Acad Sci U S A*. **98:** 15155-15160.

49. **Datta, S.R., A. Brunet and M.E. Greenberg.** 1999. Cellular survival: a play in three Akts. *Genes Dev*. **13:** 2905-2927.

50. **Donta, S.T., N. Sullivan and T.D. Wilkins.** 1982. Differential effects of *Clostridium difficile* toxins on tissue-cultured cells. *J Clin Microbiol*. **15:** 1157-1158.

51. **Ernst, M.E., M.E. Klepser, M. Fouts and M.N. Marangos.** 1997. Tetanus: pathophysiology and management. *Ann Pharmacother*. **31:** 1507-1513.

52. **Escobar-Diaz, E., E.M. Lopez-Martin, M. Hernandez del Cerro, A. Puig-Kroger, V. Soto-Cerrato, B. Montaner, E. Giralt, J.A. Garcia-Marco, R. Perez-Tomas and A. Garcia-Pardo.** 2005. AT514, a cyclic depsipeptide from *Serratia marcescens*, induces apoptosis of B-chronic lymphocytic leukemia cells: interference with the Akt/NF-kappaB survival pathway. *Leukemia*. **19:** 572-579.

53. **Fiorentini, C., W. Malorni, S. Paradisi, M. Giuliano, P. Mastrantonio and G. Donelli.** 1990. Interaction of *Clostridium difficile* toxin A with cultured cells: cytoskeletal changes and nuclear polarization. *Infect Immun*. **58:** 2329-2336.

54. **Florin, I. and M. Thelestam.** 1983. Internalization of *Clostridium difficile* cytotoxin into cultured human lung fibroblasts. *Biochim Biophys Acta*. **763:** 383-392.

55. **Florin, I. and M. Thelestam.** 1986. Lysosomal involvement in cellular intoxication with *Clostridium difficile* toxin B. *Microb Pathog*. **1:** 373-385.

56. **Frey, S.M. and T.D. Wilkins.** 1992. Localization of two epitopes recognized by monoclonal antibody PCG-4 on *Clostridium difficile* toxin A. *Infect Immun*. **60:** 2488-2492.

57. **Frisch, C., R. Gerhard, K. Aktories, F. Hofmann and I. Just.** 2003. The complete receptor-binding domain of *Clostridium difficile* toxin A is required for endocytosis. *Biochem Biophys Res Commun*. **300:** 706-711.

58. **Frithz-Lindsten, E., Y. Du, R. Rosqvist and A. Forsberg.** 1997. Intracellular targeting of exoenzyme S of *Pseudomonas aeruginosa* via type III-dependent translocation induces phagocytosis resistance,

cytotoxicity, and disruption of actin microfilaments. *Mol Microbiol*. **25:** 1125-1139.

59. **Fujita, N., A. Nagahashi, K. Nagashima, S. Rokudai and T. Tsuruo.** 1998. Acceleration of apoptotic cell death after the cleavage of Bcl-x_L protein by caspase-3-like proteases. *Oncogene*. **17:** 1295-1304.

60. **Fukumoto, Y., K. Kaibuchi, Y. Hori, H. Fujioka, S. Araki, T. Ueda, A. Kikuchi and Y. Takai.** 1990. Molecular cloning and characterization of a novel type of regulatory protein (GDI) for the rho proteins, ras p21-like small GTP-binding proteins. *Oncogene*. **5:** 1321-1328.

61. **Garrett, M.D., G.N. Major, N. Totty and A. Hall.** 1991. Purification and N-terminal sequence of the p21rho GTPase-activating protein, rho GAP. *Biochem J*. **276 (Pt 3):** 833-836.

62. **Garrett, M.D., A.J. Self, C. van Oers and A. Hall.** 1989. Identification of distinct cytoplasmic targets for ras/R-ras and rho regulatory proteins. *J Biol Chem*. **264:** 10-13.

63. **Genth, H., F. Hofmann, J. Selzer, G. Rex, K. Aktories and I. Just.** 1996. Difference in protein substrate specificity between hemorrhagic toxin and lethal toxin from *Clostridium sordellii*. *Biochem Biophys Res Commun*. **229:** 370-374.

64. **Genth, H., J. Selzer, C. Busch, J. Dumbach, F. Hofmann, K. Aktories and I. Just.** 2000. New method to generate enzymatically deficient *Clostridium difficile* toxin B as an antigen for immunization. *Infect Immun*. **68:** 1094-1101.

65. **Geric, B., M. Rupnik, D.N. Gerding, M. Grabnar and S. Johnson.** 2004. Distribution of *Clostridium difficile* variant toxinotypes and strains with binary toxin genes among clinical isolates in an American hospital. *J Med Microbiol*. **53:** 887-894.

66. **Geyer, M., C. Wilde, J. Selzer, K. Aktories and H.R. Kalbitzer.** 2003. Glucosylation of Ras by *Clostridium sordellii* lethal toxin: consequences for effector loop conformations observed by NMR spectroscopy. *Biochemistry*. **42:** 11951-11959.

67. **Giry, M., M.R. Popoff, C. von Eichel-Streiber and P. Boquet.** 1995. Transient expression of RhoA, -B, and -C GTPases in HeLa cells potentiates resistance to *Clostridium difficile* toxins A and B but not to *Clostridium sordellii* lethal toxin. *Infect Immun*. **63:** 4063-4071.

68. **Gredlein, C.M., M.L. Silverman and M.S. Downey.** 2000. Polymicrobial septic arthritis due to *Clostridium* species: case report and review. *Clin Infect Dis*. **30:** 590-594.

69. **Green, G.A., V. Schue and H. Monteil.** 1995. Cloning and characterization of the cytotoxin L-encoding gene of *Clostridium sordellii*: homology with *Clostridium difficile* cytotoxin B. *Gene*. **161:** 57-61.

70. **Hall, I.C. and J.P. Scott.** 1927. *Bacillus sordellii*, a cause of malignant edema in man. *J Infect Dis*. **41:** 329-335.

71. **Hammond, G.A. and J.L. Johnson.** 1995. The toxigenic element of *Clostridium difficile* strain VPI 10463. *Microb Pathog*. **19:** 203-213.

72. **Hatheway, C.L.** 1990. Toxigenic clostridia. *Clin Microbiol Rev*. **3:** 66-98.

73. **He, D., S.J. Hagen, C. Pothoulakis, M. Chen, N.D. Medina, M. Warny and J.T. LaMont.** 2000. *Clostridium difficile* toxin A causes early damage to mitochondria in cultured cells. *Gastroenterology*. **119:** 139-150.

74. **Henriksson, M.L., R. Rosqvist, M. Telepnev, H. Wolf-Watz and B. Hallberg.** 2000. Ras effector pathway activation by epidermal growth factor is inhibited *in vivo* by exoenzyme S ADP-ribosylation of Ras. *Biochem J*. **347 Pt 1:** 217-222.

75. **Henriques, B., I. Florin and M. Thelestam.** 1987. Cellular internalisation of *Clostridium difficile* toxin A. *Microb Pathog*. **2:** 455-463.

76. **Herrmann, C., M.R. Ahmadian, F. Hofmann and I. Just.** 1998. Functional consequences of monoglucosylation of Ha-Ras at effector domain amino acid threonine 35. *J Biol Chem*. **273:** 16134-16139.

77. **Hiraoka, K., K. Kaibuchi, S. Ando, T. Musha, K. Takaishi, T. Mizuno, M. Asada, L. Menard, E. Tomhave, J. Didsbury and et al.**

1992. Both stimulatory and inhibitory GDP/GTP exchange proteins, smg GDS and rho GDI, are active on multiple small GTP-binding proteins. *Biochem Biophys Res Commun*. **182:** 921-930.

78. **Hoeflich, K.P., J. Luo, E.A. Rubie, M.S. Tsao, O. Jin and J.R. Woodgett.** 2000. Requirement for glycogen synthase kinase-3beta in cell survival and NF-kappaB activation. *Nature*. **406:** 86-90.

79. **Hofmann, F., C. Busch and K. Aktories.** 1998. Chimeric clostridial cytotoxins: identification of the N-terminal region involved in protein substrate recognition. *Infect Immun*. **66:** 1076-1081.

80. **Hofmann, F., C. Busch, U. Prepens, I. Just and K. Aktories.** 1997. Localization of the glucosyltransferase activity of *Clostridium difficile* toxin B to the N-terminal part of the holotoxin. *J Biol Chem*. **272:** 11074-11078.

81. **Hofmann, F., A. Herrmann, E. Habermann and C. von Eichel-Streiber.** 1995. Sequencing and analysis of the gene encoding the alpha-toxin of *Clostridium novyi* proves its homology to toxins A and B of *Clostridium difficile*. *Mol Gen Genet*. **247:** 670-679.

82. **Hofmann, F., G. Rex, K. Aktories and I. Just.** 1996. The Ras-related protein Ral is monoglucosylated by *Clostridium sordellii* lethal toxin. *Biochem Biophys Res Commun*. **227:** 77-81.

83. **Hogan, S.F. and K. Ireland.** 1989. Fatal acute spontaneous endometritis resulting from *Clostridium sordellii*. *Am J Clin Pathol*. **91:** 104-106.

84. **Holtz, F. and E.W. Mauch.** 1962. Gas gangrene of uterus: survival following hysterectomy. *Obstet Gynecol*. **19:** 545-548.

85. **Hou, L. and S.K. Dutta.** 2000. Phylogenetic characterization of several para- and meta-PCB dechlorinating *Clostridium* species: 16s rDNA sequence analyses. *Lett Appl Microbiol*. **30:** 238-243.

86. **Hundsberger, T., V. Braun, M. Weidmann, P. Leukel, M. Sauerborn and C. von Eichel-Streiber.** 1997. Transcription analysis of the genes *tcdA-E* of the pathogenicity locus of *Clostridium difficile*. *Eur J Biochem*. **244:** 735-742.

87. **Ihara, K., S. Muraguchi, M. Kato, T. Shimizu, M. Shirakawa, S. Kuroda, K. Kaibuchi and T. Hakoshima.** 1998. Crystal structure of human RhoA in a dominantly active form complexed with a GTP analogue. *J Biol Chem*. **273:** 9656-9666.

88. **Just, I., G. Fritz, K. Aktories, M. Giry, M.R. Popoff, P. Boquet, S. Hegenbarth and C. von Eichel-Streiber.** 1994. *Clostridium difficile* toxin B acts on the GTP-binding protein Rho. *J Biol Chem*. **269:** 10706-10712.

89. **Just, I., J. Selzer, F. Hofmann, G.A. Green and K. Aktories.** 1996. Inactivation of Ras by *Clostridium sordellii* lethal toxin-catalyzed glucosylation. *J Biol Chem*. **271:** 10149-10153.

90. **Just, I., J. Selzer, C. von Eichel-Streiber and K. Aktories.** 1995. The low molecular mass GTP-binding protein Rho is affected by toxin A from *Clostridium difficile*. *J Clin Invest*. **95:** 1026-1031.

91. **Just, I., J. Selzer, M. Wilm, C. von Eichel-Streiber, M. Mann and K. Aktories.** 1995. Glucosylation of Rho proteins by *Clostridium difficile* toxin B. *Nature*. **375:** 500-503.

92. **Just, I., M. Wilm, J. Selzer, G. Rex, C. von Eichel-Streiber, M. Mann and K. Aktories.** 1995. The enterotoxin from *Clostridium difficile* (ToxA) monoglucosylates the Rho proteins. *J Biol Chem*. **270:** 13932-13936.

93. **Karasawa, T., X. Wang, T. Maegawa, Y. Michiwa, H. Kita, K. Miwa and S. Nakamura.** 2003. *Clostridium sordellii* phospholipase C: gene cloning and comparison of enzymatic and biological activities with those of *Clostridium perfringens* and *Clostridium bifermentans* phospholipase C. *Infect Immun*. **71:** 641-646.

94. **Karran, L. and M.J. Dyer.** 2001. Proteolytic cleavage of molecules involved in cell death or survival pathways: a role in the control of apoptosis? *Crit Rev Eukaryot Gene Expr*. **11:** 269-277.

95. **Kimura, A.C., J.I. Higa, R.M. Levin, G. Simpson, Y. Vargas and D.J. Vugia.** 2004. Outbreak of necrotizing fasciitis due to *Clostridium sordellii* among black-tar heroin users. *Clin Infect Dis*. **38:** e87-91.

96. **Krivan, H.C., G.F. Clark, D.F. Smith and T.D. Wilkins.** 1986. Cell surface binding site for *Clostridium difficile* enterotoxin: evidence for a glycoconjugate containing the sequence Galα1-3Galβ1-4GlcNAc. *Infect Immun*. **53:** 573-581.

97. **Lane, D.J.** *16S/23S rRNA sequencing*, in *Nucleic Acid Techniques in Bacterial Systematics*, E.S.M. Goodfellow, Editor. 1991, Wiley. p. 115-175.

98. **Larson, H.E. and A.B. Price.** 1977. Pseudomembranous colitis: Presence of clostridial toxin. *Lancet*. **2:** 1312-1314.

99. **LeDell, K.H., R. Lynfield, R.N. Danila and H.F. Hull.** 2001. Unexplained deaths following knee surgery. *Morb Mortal Wkly Rep*. **50:** 1080.

100. **Lewis, C.J. and R. Naylor.** 1996. Sudden death in lambs associated with *Clostridium sordellii* infection. *Vet Rec*. **138:** 262.

101. **Lewis, C.J. and R.D. Naylor.** 1998. Sudden death in sheep associated with *Clostridium sordellii*. *Vet Rec*. **142:** 417-421.

102. **Lynch, J.M., A. Anderson, F.R. Camacho, A.K. Winters, G.R. Hodges and W.G. Barnes.** 1980. Pseudobacteremia caused by *Clostridium sordellii*. *Arch Intern Med*. **140:** 65-68.

103. **Madihah, M.S., A.B. Ariff, M.S. Khalil, A.A. Suraini and M.I. Karim.** 2001. Anaerobic fermentation of gelatinized sago starch-derived sugars to acetone-1-butanol-ethanol solvent by *Clostridium acetobutylicum*. *Folia Microbiol (Praha)*. **46:** 197-204.

104. **Malinin, T.I., B.E. Buck, H.T. Temple, O.V. Martinez and W.P. Fox.** 2003. Incidence of clostridial contamination in donors' musculoskeletal tissue. *J Bone Joint Surg Br*. **85:** 1051-1054.

105. **Marshall, C.J.** 1996. Ras effectors. *Curr Opin Cell Biol*. **8:** 197-204.

106. **Martinez, O.V., B.E. Buck, M. Hernandez and T. Malinin.** 2003. Blood and marrow cultures as indicators of bone contamination in cadaver donors. *Clin Orthop*. **409:**317-324.

107. **Martinez, R.D. and T.D. Wilkins.** 1992. Comparison of *Clostridium sordellii* toxins HT and LT with toxins A and B of *C. difficile*. *J Med Microbiol*. **36:** 30-36.

108. **Martinez, R.D. and T.D. Wilkins.** 1988. Purification and characterization of *Clostridium sordellii* hemorrhagic toxin and cross-reactivity with *Clostridium difficile* toxin A (enterotoxin). *Infect Immun*. **56:** 1215-1221.

109. **McClain, M.S., W. Schraw, V. Ricci, P. Boquet and T.L. Cover.** 2000. Acid activation of *Helicobacter pylori* vacuolating cytotoxin (VacA) results in toxin internalization by eukaryotic cells. *Mol Microbiol*. **37:** 433-442.

110. **McGregor, J.A., D.E. Soper, G. Lovell and J.K. Todd.** 1989. Maternal deaths associated with *Clostridium sordellii* infection. *Am J Obstet Gynecol*. **161:** 987-995.

111. **McLauchlin, J., V. Mithani, F.J. Bolton, G.L. Nichols, M.A. Bellis, Q. Syed, R.P. Thomson and J.R. Ashton.** 2002. An investigation into the microflora of heroin. *J Med Microbiol*. **51:** 1001-1008.

112. **Mesmin, B., K. Robbe, B. Geny, F. Luton, G. Brandolin, M.R. Popoff and B. Antonny.** 2004. A phosphatidylserine-binding site in the cytosolic fragment of *Clostridium sordellii* lethal toxin facilitates glucosylation of membrane-bound Rac and is required for cytotoxicity. *J Biol Chem*. **279:** 49876-49882.

113. **Miech, R.P.** 2005. Pathophysiology of mifepristone-induced septic shock due to *Clostridium sordellii*. *Ann Pharmacother*. **39:** 1483-1488.

114. **Mitchell, M.J., B.E. Laughon and S. Lin.** 1987. Biochemical studies on the effect of *Clostridium difficile* toxin B on actin *in vivo* and *in vitro*. *Infect Immun*. **55:** 1610-1615.

115. **Mizuno, T., K. Kaibuchi, T. Yamamoto, M. Kawamura, T. Sakoda, H. Fujioka, Y. Matsuura and Y. Takai.** 1991. A stimulatory GDP/GTP exchange protein for smg p21 is active on the post-translationally processed form of c-Ki-ras p21 and rhoA p21. *Proc Natl Acad Sci U S A*. **88:** 6442-6446.

116. **Morris, W.E., F.A. Uzal, F.R. Fattorini and H. Terzolo.** 2002. Malignant oedema associated with blood sampling in sheep. *Aust Vet J*. **80:** 280-281.

117. **Mory, F., A. Lozniewski, M.N. Guirlet, D. Guidat, L. Bresler, M. Weber and P. Boissel.** 1995. Severe sepsis caused by *Clostridium sordellii* following liver biopsy in a liver transplant recipient. *Clin Infect Dis*. **21:** 1522-1523.

118. **Muller, S., C. von Eichel-Streiber and M. Moos.** 1999. Impact of amino acids 22-27 of Rho-subfamily GTPases on glucosylation by the large clostridial cytotoxins TcsL-1522, TcdB-1470, and TcdB-8864. *Eur J Biochem*. **266:** 1073-1080.

119. **Murai, H., M. Ikeda, S. Kishida, O. Ishida, M. Okazaki-Kishida, Y. Matsuura and A. Kikuchi.** 1997. Characterization of Ral GDP dissociation stimulator-like (RGL) activities to regulate c-fos promoter and the GDP/GTP exchange of Ral. *J Biol Chem*. **272:** 10483-10490.

120. **Nakamura, S., H. Ogura, J. Tanaka, N. Tanabe, K. Yamakawa, M. Hatano and S. Nishida.** 1984. Difference in susceptibility of various cell cultures to cytotoxic culture filtrates of *Clostridium sordellii*. *Microbiol Immunol*. **28:** 493-497.

121. **Nakamura, S., N. Tanabe, K. Yamakawa and S. Nishida.** 1983. Cytotoxin production by *Clostridium sordellii* strains. *Microbiol Immunol*. **27:** 495-502.

122. **Nakamura, S., K. Yamakawa and S. Nishida.** 1986. Antibacterial susceptibility of *Clostridium sordellii* strains. *Zentralbl Bakteriol Mikrobiol Hyg [A]*. **261:** 345-349.

123. **Nimcevic, D., M. Schuster and J.R. Gapes.** 1998. Solvent production by *Clostridium beijerinckii* NRRL B592 growing on different potato media. *Appl Microbiol Biotechnol*. **50:** 426-428.

124. **Nishida, S., K. Tamai and T. Yamagishi.** 1964. Taxonomy of *Clostridium bifermentans* and *Clostridium sordellii*: Their toxigenicity, urease activity, and sporulating potency. *J Bacteriol*. **88:** 1641-1646.

125. **Nobes, C.D. and A. Hall.** 1995. Rho, rac, and cdc42 GTPases regulate the assembly of multimolecular focal complexes associated with actin stress fibers, lamellipodia, and filopodia. *Cell*. **81:** 53-62.

126. **Okeke, B.C., Y.C. Chang, M. Hatsu, T. Suzuki and K. Takamizawa.** 2001. Purification, cloning, and sequencing of an enzyme mediating the reductive dechlorination of tetrachloroethylene (PCE) from *Clostridium bifermentans* DPH-1. *Can J Microbiol*. **47:** 448-456.

127. **Oliver, F.J., G. de la Rubia, V. Rolli, M.C. Ruiz-Ruiz, G. de Murcia and J.M. Murcia.** 1998. Importance of poly(ADP-ribose) polymerase and its cleavage in apoptosis. Lesson from an uncleavable mutant. *J Biol Chem*. **273:** 33533-33539.

128. **Osaki, M., M. Oshimura and H. Ito.** 2004. PI3K-Akt pathway: its functions and alterations in human cancer. *Apoptosis*. **9:** 667-676.

129. **Petit, P., J. Breard, V. Montalescot, N.B. El Hadj, T. Levade, M. Popoff and B. Geny.** 2003. Lethal toxin from *Clostridium sordellii* induces apoptotic cell death by disruption of mitochondrial homeostasis in HL-60 cells. *Cell Microbiol*. **5:** 761-771.

130. **Pfeifer, G., J. Schirmer, J. Leemhuis, C. Busch, D.K. Meyer, K. Aktories and H. Barth.** 2003. Cellular uptake of *Clostridium difficile* toxin B. Translocation of the N-terminal catalytic domain into the cytosol of eukaryotic cells. *J Biol Chem*. **278:** 44535-44541.

131. **Popoff, M.R.** 1987. Purification and characterization of *Clostridium sordellii* lethal toxin and cross-reactivity with *Clostridium difficile* cytotoxin. *Infect Immun*. **55:** 35-43.

132. **Popoff, M.R., E. Chaves-Olarte, E. Lemichez, C. von Eichel-Streiber, M. Thelestam, P. Chardin, D. Cussac, B. Antonny, P. Chavrier, G. Flatau, M. Giry, J. de Gunzburg and P. Boquet.** 1996. Ras, Rap, and Rac small GTP-binding proteins are targets for *Clostridium sordellii* lethal toxin glucosylation. *J Biol Chem*. **271:** 10217-10224.

133. **Portnoy, D.A., V. Auerbuch and I.J. Glomski.** 2002. The cell biology of *Listeria monocytogenes* infection: the intersection of bacterial pathogenesis and cell-mediated immunity. *J Cell Biol*. **158:** 409-414.

134. **Pothoulakis, C., R.J. Gilbert, C. Cladaras, I. Castagliuolo, G. Semenza, Y. Hitti, J.S. Montcrief, J. Linevsky, C.P. Kelly, S. Nikulasson, H.P. Desai, T.D. Wilkins and J.T. LaMont.** 1996. Rabbit sucrase-isomaltase contains a functional intestinal receptor for *Clostridium difficile* toxin A. *J Clin Invest*. **98:** 641-649.

135. **Present, D.A., R. Meislin and B. Shaffer.** 1990. Gas gangrene. A review. *Orthop Rev*. **19:** 333-341.

136. **Qa'Dan, M., M. Ramsey, J. Daniel, L.M. Spyres, B. Safiejko-Mroczka, W. Ortiz-Leduc and J.D. Ballard.** 2002. *Clostridium difficile* toxin B activates dual caspase-dependent and caspase-independent apoptosis in intoxicated cells. *Cell Microbiol*. **4:** 425-434.

137. **Qa'Dan, M., L.M. Spyres and J.D. Ballard.** 2001. pH-enhanced cytopathic effects of *Clostridium sordellii* lethal toxin. *Infect Immun*. **69:** 5487-5493.

138. **Qa'Dan, M., L.M. Spyres and J.D. Ballard.** 2000. pH-induced conformational changes in *Clostridium difficile* toxin B. *Infect Immun*. **68:** 2470-2474.

139. **Richards, S.M. and B.W. Hunt.** 1982. *Clostridium sordellii* in lambs. *Vet Rec*. **111:** 22.

140. **Rifkin, G.D., F.R. Fekety and J. Silva, Jr.** 1977. Antibiotic-induced colitis implication of a toxin neutralized by *Clostridium sordellii* antitoxin. *Lancet*. **2:** 1103-1106.

141. **Rode, L.J., L. Pope, C. Filip and L.D. Smith.** 1971. Spore appendages and taxonomy of *Clostridium sordellii*. *J Bacteriol*. **108:** 1384-1389.

142. **Roggentin, P., G. Gutschker-Gdaniec, R. Schauer and R. Hobrecht.** 1985. Correlative properties for a differentiation of two *Clostridium sordellii* phenotypes and their distinction from *Clostridium bifermentans*. *Zentralbl Bakteriol Mikrobiol Hyg [A]*. **260:** 319-328.

143. **Rorbye, C., I.S. Petersen and L. Nilas.** 2000. Postpartum *Clostridium sordellii* infection associated with fatal toxic shock syndrome. *Acta Obstet Gynecol Scand*. **79:** 1134-1135.

144. **Rupnik, M., V. Avesani, M. Janc, C. von Eichel-Streiber and M. Delmee.** 1998. A novel toxinotyping scheme and correlation of toxinotypes with serogroups of *Clostridium difficile* isolates. *J Clin Microbiol*. **36:** 2240-2247.

145. **Sauerborn, M., P. Leukel and C. von Eichel-Streiber.** 1997. The C-terminal ligand-binding domain of *Clostridium difficile* toxin A (TcdA) abrogates TcdA-specific binding to cells and prevents mouse lethality. *FEMS Microbiol Lett*. **155:** 45-54.

146. **Sautin, Y.Y., J.M. Crawford and S.I. Svetlov.** 2001. Enhancement of survival by LPA via Erk1/Erk2 and PI 3-kinase/Akt pathways in a murine hepatocyte cell line. *Am J Physiol Cell Physiol*. **281:** C2010-2019.

147. **Sauvonnet, N., I. Lambermont, P. van der Bruggen and G.R. Cornelis.** 2002. YopH prevents monocyte chemoattractant protein 1 expression in macrophages and T-cell proliferation through inactivation of the phosphatidylinositol 3-kinase pathway. *Mol Microbiol*. **45:** 805-815.

148. **Schurmann, A., A.F. Mooney, L.C. Sanders, M.A. Sells, H.G. Wang, J.C. Reed and G.M. Bokoch.** 2000. p21-activated kinase 1 phosphorylates the death agonist bad and protects cells from apoptosis. *Mol Cell Biol*. **20:** 453-461.

149. **Sekine, A., M. Fujiwara and S. Narumiya.** 1989. Asparagine residue in the rho gene product is the modification site for botulinum ADP-ribosyltransferase. *J Biol Chem*. **264:** 8602-8605.

150. **Shapiro, R.L., C. Hatheway and D.L. Swerdlow.** 1998. Botulism in the United States: a clinical and epidemiologic review. *Ann Intern Med*. **129:** 221-228.

151. **Sinave, C., G. Le Templier, D. Blouin, F. Leveille and E. Deland.** 2002. Toxic shock syndrome due to *Clostridium sordellii*: a dramatic postpartum and post-abortion disease. *Clin Infect Dis*. **35:** 1441-1443.

152. **Slee, E.A., S.A. Keogh and S.J. Martin.** 2000. Cleavage of Bid during cytotoxic drug and UV radiation-induced apoptosis occurs downstream of the point of Bcl-2 action and is catalysed by caspase-3: a potential feedback loop for amplification of apoptosis-associated mitochondrial cytochrome c release. *Cell Death Differ*. **7:** 556-565.

153. **Smedley, J.G., 3rd, D.J. Fisher, S. Sayeed, G. Chakrabarti and B.A. McClane.** 2004. The enteric toxins of *Clostridium perfringens*. *Rev Physiol Biochem Pharmacol*. **152:** 183-204.

154. **Smith, J.A., D.L. Cooke, S. Hyde, S.P. Borriello and R.G. Long.** 1997. *Clostridium difficile* toxin A binding to human intestinal epithelial cells. *J Med Microbiol*. **46:** 953-958.

155. **Soper, D.E.** 1986. Clostridial myonecrosis arising from an episiotomy. *Obstet Gynecol*. **68:** 26S-28S.

156. **Sordelli, A.** 1923. Flore anaerobe de Buenos Aires. *C R Soc Biol Paris*. **88:** 53-55.

157. **Spera, R.V., Jr., M.H. Kaplan and S.L. Allen.** 1992. *Clostridium sordellii* bacteremia: case report and review. *Clin Infect Dis*. **15:** 950-954.

158. **Spyres, L.M., J. Daniel, A. Hensley, M. Qa'Dan, W. Ortiz-Leduc and J.D. Ballard.** 2003. Mutational analysis of the enzymatic domain of *Clostridium difficile* toxin B reveals novel inhibitors of the wild-type toxin. *Infect Immun*. **71:** 3294-3301.

159. **Spyres, L.M., M. Qa'Dan, A. Meader, J.J. Tomasek, E.W. Howard and J.D. Ballard.** 2001. Cytosolic delivery and characterization of the TcdB glucosylating domain by using a heterologous protein fusion. *Infect Immun*. **69:** 599-601.

160. **Tan, K.S., B.Y. Wee and K.P. Song.** 2001. Evidence for holin function of *tcdE* gene in the pathogenicity of *Clostridium difficile*. *J Med Microbiol*. **50:** 613-619.

161. **Thelestam, M. and M. Bronnegard.** 1980. Interaction of cytopathogenic toxin from *Clostridium difficile* with cells in tissue culture. *Scand J Infect Dis Suppl*. **22:**16-29.

162. **Thys, J.P., P. Ectors and P. Noel.** 1980. Non-traumatic clostridial myositis: an unusual feature of brain death. *Postgrad Med J*. **56:** 501-503.

163. **Troxel, T.R., M.S. Gadberry, W.T. Wallace, D.L. Kreider, J.D. Shockey, E.A. Colburn, P. Widel and I. Nicholson.** 2001. Clostridial

antibody response from injection-site lesions in beef cattle, long-term response to single or multiple doses, and response in newborn beef calves. *J Anim Sci*. **79:** 2558-2564.

164. **Tsujimoto, Y.** 1998. Role of Bcl-2 family proteins in apoptosis: apoptosomes or mitochondria? *Genes Cells*. **3:** 697-707.

165. **Tucker, K.D., P.E. Carrig and T.D. Wilkins.** 1990. Toxin A of *Clostridium difficile* is a potent cytotoxin. *J Clin Microbiol*. **28:** 869-871.

166. **Tucker, K.D. and T.D. Wilkins.** 1991. Toxin A of *Clostridium difficile* binds to the human carbohydrate antigens I, X, and Y. *Infect Immun*. **59:** 73-78.

167. **Tweten, R.K.** 2005. Cholesterol-dependent cytolysins, a family of versatile pore-forming toxins. *Infect Immun*. **73:** 6199-6209.

168. **Useh, N.M., A.J. Nok and K.A. Esievo.** 2003. Pathogenesis and pathology of blackleg in ruminants: the role of toxins and neuraminidase. A short review. *Vet Q*. **25:** 155-159.

169. **Vatn, S., O.V. Sjaastad and M.J. Ulvund.** 2000. Histamine in lambs with abomasal bloat, haemorrhage, and ulcers. *J Vet Med A Physiol Pathol Clin Med*. **47:** 251-255.

170. **Vatn, S., M.A. Tranulis and M. Hofshagen.** 2000. *Sarcina*-like bacteria, *Clostridium fallax* and *Clostridium sordellii* in lambs with abomasal bloat, haemorrhage, and ulcers. *J Comp Pathol*. **122:** 193-200.

171. **Vetter, I.R., F. Hofmann, S. Wohlgemuth, C. Herrmann and I. Just.** 2000. Structural consequences of mono-glucosylation of Ha-Ras by *Clostridium sordellii* lethal toxin. *J Mol Biol*. **301:** 1091-1095.

172. **von Eichel-Streiber, C., R. Laufenberg-Feldmann, S. Sartingen, J. Schulze and M. Sauerborn.** 1992. Comparative sequence analysis of the *Clostridium difficile* toxins A and B. *Mol Gen Genet*. **233:** 260-268.

173. **von Eichel-Streiber, C. and M. Sauerborn.** 1990. *Clostridium difficile* toxin A carries a C-terminal repetitive structure homologous to the carbohydrate binding region of streptococcal glycosyltransferases. *Gene*. **96:** 107-113.

174. **Wagenknecht-Wiesner, A., M. Weidmann, V. Braun, P. Leukel, M. Moos and C. von Eichel-Streiber.** 1997. Delineation of the catalytic domain of *Clostridium difficile* toxin B-10463 to an enzymatically active N-terminal 467 amino acid fragment. *FEMS Microbiol Lett*. **152:** 109-116.

175. **Wedel, N., P. Toselli, C. Pothoulakis, B. Faris, P. Oliver, C. Franzblau and T. LaMont.** 1983. Ultrastructural effects of *Clostridium difficile* toxin B on smooth muscle cells and fibroblasts. *Exp Cell Res*. **148:** 413-422.

176. **Wei, Y., Y. Zhang, U. Derewenda, X. Liu, W. Minor, R.K. Nakamoto, A.V. Somlyo, A.P. Somlyo and Z.S. Derewenda.** 1997. Crystal structure of RhoA-GDP and its functional implications. *Nat Struct Biol*. **4:** 699-703.

177. **Wilson, K.H., R. Blitchington, B. Hindenach and R.C. Greene.** 1988. Species-specific oligonucleotide probes for rRNA of *Clostridium difficile* and related species. *J Clin Microbiol*. **26:** 2484-2488.\

178. **Wren, B.W.** 1991. A family of clostridial and streptococcal ligand-binding proteins with conserved C-terminal repeat sequences. *Mol Microbiol*. **5:** 797-803.

179. **Wren, B.W., R.R. Russell and S. Tabaqchali.** 1991. Antigenic cross-reactivity and functional inhibition by antibodies to *Clostridium difficile* toxin A, *Streptococcus mutans* glucan-binding protein, and a synthetic peptide. *Infect Immun*. **59:** 3151-3155.

180. **Yoshida, Y., M. Kawata, Y. Miura, T. Musha, T. Sasaki, A. Kikuchi and Y. Takai.** 1992. Microinjection of smg/rap1/Krev-1 p21 into Swiss 3T3 cells induces DNA synthesis and morphological changes. *Mol Cell Biol*. **12:** 3407-3414.

181. **Zhou, K., Y. Wang, J.L. Gorski, N. Nomura, J. Collard and G.M. Bokoch.** 1998. Guanine nucleotide exchange factors regulate specificity of downstream signaling from Rac and Cdc42. *J Biol Chem*. **273:** 16782-16786.

APPENDIX

In addition to the LCT studies described in this dissertation, a period of my graduate career involved studies designed to better understand the mechanism of action of two of the components of anthrax toxin, the bacterial toxin produced by *Bacillus anthracis*. *B. anthracis* produces a tripartite toxin composed of lethal factor (LF), edema factor (EF), and protective antigen (PA). The combination of LF and PA yields lethal toxin (LT), and EF plus PA yields edema toxin (ET). While anthrax toxin has been studied for many years, the majority of research has focused on understanding LT activity and its effects on host cells. Thus, the two chapters of this appendix include two studies detailing previously undescribed functions of PA and EF. The results of each of these studies suggest a larger, cytotoxic role for these two components of anthrax toxin in the disease and will be discussed in the discussion sections of each chapter. These two studies are presented in their peer-reviewed form in this appendix.

BACILLUS ANTHRACIS OEDEMA TOXIN AS A CAUSE OF CELL TYPE-SPECIFIC CYTOTOXICITY

Bacillus anthracis Oedema Toxin as a Cause of Tissue Necrosis and Cell-Type Specific Cytotoxicity. (Daniel E. Voth*, Elaine E. Hamm*, Lan G. Nguyen, Amy E. Tucker, Isabelle I. Salles, William Ortiz-Leduc, and Jimmy D. Ballard. *Cellular Microbiology*. 7:1139-1149. *D.E.V. and E.E.H. contributed equally to this work.)

Bacillus anthracis produces three proteins that work in binary combination to induce edema and lethality. During intoxication, protective antigen (PA) mediates the cellular entry of edema factor (EF) and lethal factor (LF), yielding edema toxin (ET) and lethal toxin (LT), respectively (13). Once in the cytosol, LF, a zinc-dependent metalloprotease, cleaves mitogen-activated protein kinase kinases, consequently disrupting signaling pathways modulated by extracellular signal regulated kinases 1 and 2, c-jun N-terminal kinase, and p38 (14). EF is a Ca^{2+}- and calmodulin-dependent adenylate cyclase that generates high levels of cAMP in the cell (29, 30). This rapid rise in cAMP levels has been implicated in the inhibition of phagocytosis in neutrophils and may provide an initial defense from the host immune system during infection (43). Furthermore, isogenic strains of *B. anthracis* lacking LF or EF are reduced in virulence (44), indicating both ET and LT play an important role during the disease process.

EF is a member of the class of adenylate cyclase toxins, which modify cell physiology by the rapid conversion of cellular ATP to cAMP. First described by

Leppla as an adenylate cyclase (29), EF shares sequence homology with the adenylate cyclase toxin (CyaA) from *Bordetella pertussis* (15) and ExoY from *Pseudomonas aeruginosa* (65). These virulence factors alter cell physiology through the supraphysiological accumulation of cAMP. Additionally, CyaA has been reported to contribute to apoptosis in macrophages during *B. pertussis* infection *in vivo* (21). While ET has been shown to disrupt neutrophil function and alter cytokine production (23), the full impact of this toxin on the host, or on specific cell physiology, is not understood. In fact, Moayeri and colleagues recently reported on the ability of LT to cause tissue damage and hypoxia (37) in a murine model, but whether or not ET also contributes to cell death and tissue necrosis is unclear.

In order to examine potential ET-induced tissue damage, we have taken advantage of the developing zebrafish embryo as a model system to study this toxin. The zebrafish embryo model proved useful in earlier studies on LT, wherein we confirmed the ability of LF to disrupt glycogen synthase kinase-3β activity (59). The developing zebrafish model presents several distinct advantages for the study of intracellular bacterial toxins. In addition to their ability to develop during a short time-period, zebrafish embryos are optically transparent for a week past fertilization, allowing for convenient visualization of multi-organ systems (25). Unlike other models, whole animal histopathological analysis of zebrafish is simple, as longitudinal cross-sections of the entire fish can

be prepared and visualized. Furthermore, a complete immune system is absent during initial stages of development, and this allows assessment of tissue damage without major inflammatory responses (58). Thus, one can assess the direct impact of a bacterial toxin on specific organs and tissue using this model. For these reasons, we utilized the developing zebrafish embryo as a model to improve our understanding of ET and determine if this toxin demonstrates organ-specific activity and causes tissue necrosis. Results from these treatments indicate ET effectively caused tissue necrosis and cell death, as well as, lethality in the zebrafish model. Based on these observations further experiments were performed to determine if ET is cytotoxic to a variety of mammalian cell types, the results of which indicate the impact of this toxin is cell-type specific and cAMP levels do not correlate with death in all cells.

RESULTS

ET induces cytotoxic effects in zebrafish Pac2 embryonic fibroblasts. Prior to treatment of live embryos, we sought to determine if ET was capable of intoxicating zebrafish-derived cells. Based on the reported sequences from the partially completed zebrafish genome, we were able to identify homologs of the EF cofactor calmodulin (NP_892012*)* and zebrafish cDNA clones homologous to the two known PA receptors, ANTXR1 (BI866712.1) and ANTXR2 (CA471164).

As shown in Fig. A-1A, treatment of Pac2 cells resulted in an increase in cAMP levels compared to cells treated with buffer alone or the enzymatically inactive EF-K346R mutant plus PA. Furthermore, ET treatments resulted in a decrease in cell viability, with a ~50% reduction in the number of live cells at 48 h following treatment (Fig. A-1A). Finally, when compared to control Pac2 cells (Fig. A-1B), Pac2 cells treated with ET demonstrated distinct morphological changes, including cell elongation and eventual rounding (Fig. A-1C).

Treatment of zebrafish embryos with ET results in widespread tissue damage. With the preliminary results indicating ET could intoxicate zebrafish cells, experiments were performed to determine the effect of ET on intact zebrafish embryos. Exposure to ET caused notable pleiotropic effects in the developing embryos, including tissue damage, and swimbladder defects. Notable discoloration of the head and trunk regions and degeneration of the cranial epithelium, both phenotypes that are likely indicative of tissue damage and decay, were observed in a majority of the embryos. A small population of affected fish experienced moderate retention of the yolk sac (Fig. A-2). Additionally, most of the larvae were unable to inflate their swim bladder. Although the ET-treated embryos survived through all seven stages of development, most of the embryos succumbed to the toxin 7 days post-treatment. Interestingly, among all of the diverse defects, we were unable to detect any pronounced edema among the

Figure A-1. Impact of ET on cAMP levels and cell survival in zebrafish Pac2 embryonic fibroblasts. Pac2 fibroblasts were incubated with ET for the indicated periods of time. Cells were subsequently analyzed for morphological changes, cell viability via WST-8 staining, or changes in the levels of intracellular cAMP via the BioTrak EIA. cAMP levels are reported in pmol/mg of total protein. Samples were analyzed in triplicate and error bars indicate the standard deviation from the mean. (A) cAMP levels and cell viability in ET-treated Pac2 cells. (B and C) Representative morphological changes demonstrated by (C) ET-treated Pac2 cells as compared to (B) control Pac2 cells.

Figure A-1.

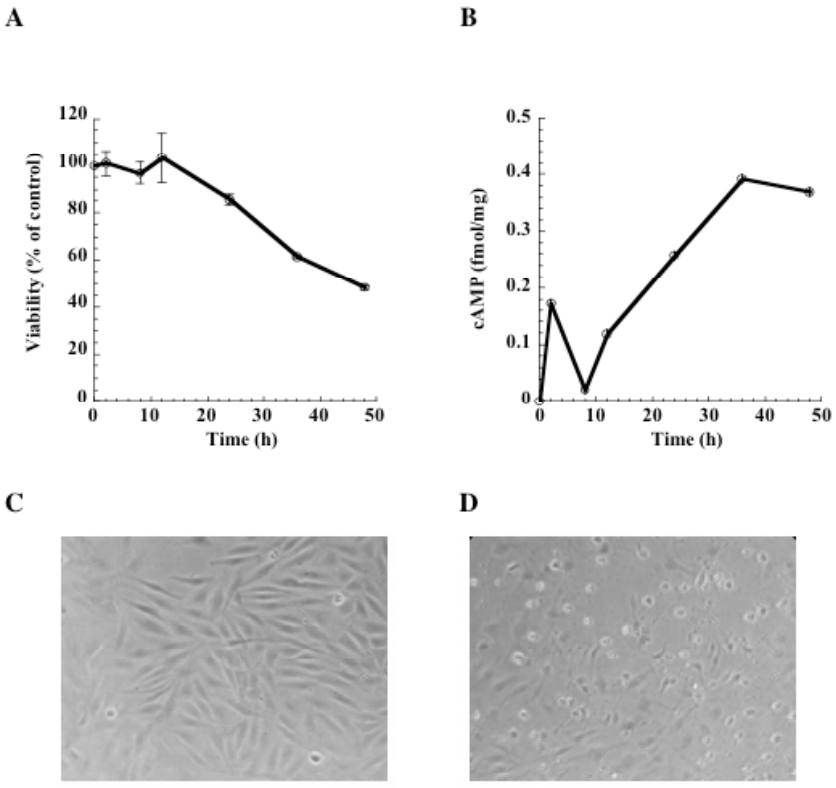
A
B
Viability (% of control)
120
100
80
60
40
20
0
0
10
20
30
40
50
Time (h)
cAMP (fmol/mg)
0.5
0.4
0.3
0.2
0.1
0
0
10
20
30
40
50
Time (h)
C
D

Figure A-2. Impact of ET on developing zebrafish embryos. Following treatment of zebrafish during blastula stage with EF alone (left panel) or with ET (right panel), changes in development were observed. (A) Arrows indicate regions of defects: uninflated swimbladder (arrow 1), discoloration (arrow 2), and internal bleeding (arrow 3). (B) Arrows demark regions of abnormalities: discoloration (arrow 1) and uninflated swimbladder (arrow 2). (C) Arrows indicate regions of abnormalities: discoloration (arrow 1), uninflated swimbladder (arrow 2), and degeneration of cranial epithelium (arrow 3). Photographs were taken 6 days following treatment with ET.

Figure A-2.

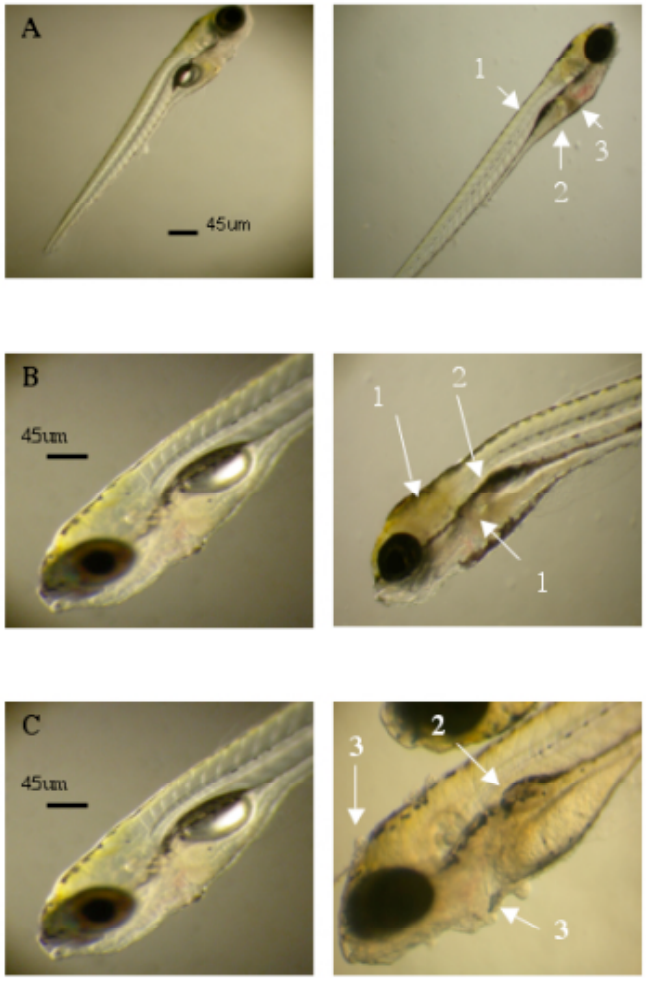

several hundred ET-treated embryos examined throughout the course of these studies.

ET-treated embryos were further examined by histopathology to determine the degree of cell death and tissue necrosis. The histological examination revealed regions of acute tissue damage of the gill epithelia (Fig. A-3A) and gill chamber, gastrointestinal tract (Fig. A-3B), and moderate, acute damage of the liver (Fig. A-3C). The entire gut appeared necrotic with substantial cell death and sloughing of cells within this region (see boxed area Fig. A-3B).

It is important to note that sensitivity to ET was not stage-dependent, as the aforementioned defects could be detected in all treatments regardless of stage of exposure. Additionally, each concentration of toxin caused the same types of defects (tissue and organ damage, yolk sac retention, swimbladder defects, and animal death); however, tissue damage was more extensive in zebrafish exposed to the highest dose of toxin.

ET induces cell death in murine macrophage-like cells. Results from the zebrafish embryo analysis suggested ET could induce cytotoxic effects and tissue necrosis in this model. Yet, it was unclear whether ET could also cause cell death in mammalian cells. For this reason, we first examined the impact of ET on RAW 264.7 and IC-21 murine macrophage-like cells. Prior studies on LT have shown RAW 264.7 and IC-21 cells to be highly susceptible to PA-mediated intoxication (although only RAW 264.7 cells are killed by LT), allowing us to

Figure A-3. Marked tissue necrosis following ET treatment of zebrafish embryos. Cross-sections of zebrafish treated with ET at the blastula stage were stained with hematoxylin and eosin. (A) Section of the gill epithelia. Arrows denote cells of necrotic tissue. (B) Section of the gastrointestinal tract. Black box demarks regions of tissue necrosis. (C) Cross-section of liver. Arrows indicate the presence of necrotic parenchymal cells in the liver.

Figure A-3.

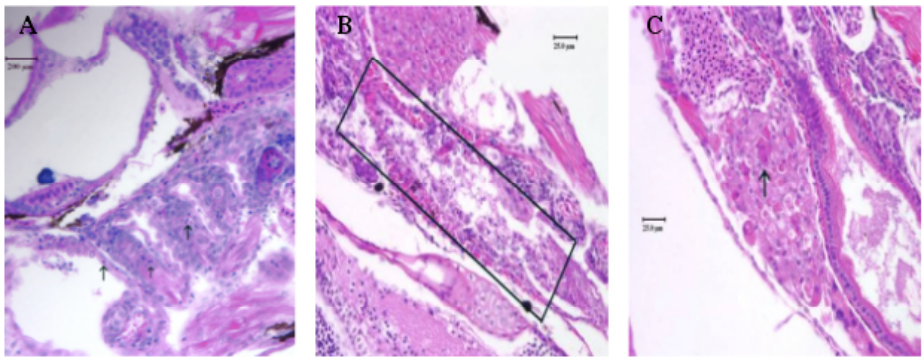

predict these cells would be effectively targeted by ET. As shown in Fig. A-4A, in RAW 264.7 cells, levels of cAMP approached 1000 pmol per mg of cell lysate by 24 h and showed a decline to basal level by 48 h. As shown in Fig. A-4B, the increased cAMP levels correlated with the time of death observed in this cell line, with ~ 80% death occurring by 48 h. RAW 264.7 cells also demonstrated rounding and eventual lysis at the later times of intoxication (Fig. A-4C and A-4D).

IC-21 cells also exhibited an increase in cAMP surpassing that observed in RAW 264.7 cells when incubated in the presence of ET (Fig. A-4A). cAMP levels approached 7000 pmol per mg of cell lysate by 24 h and, in contrast to the RAW 264.7 cells, exhibited a steady decline in total cAMP up to 48 h. As shown in Fig. A-4B, these increases in cAMP also correlated with cytotoxicity, resulting in ~ 70% cell death by 72 h. IC-21 cells also showed rounding and eventual lysis at the late time points of intoxication (Fig. A-4E and A-4F).

Analysis of apoptosis profiles in ET-treated macrophages. We next examined the type of cell death occurring in ET-treated macrophages. Although ET-treated macrophages did not demonstrate visual apoptotic hallmarks, such as membrane blebbing and apoptotic body formation, cAMP regulation has been reported in several cases to have differential effects on apoptotic cell death (19, 48); therefore, apoptosis was examined as a possible mechanism of death in these ET-sensitive cells. Both RAW 264.7 and IC-21 cells were pretreated for 1 h with

Figure A-4. Levels of cAMP and cell survival in cells treated with ET. RAW 264.7 macrophages, IC-21 macrophages, and NIH/3T3 fibroblasts were incubated with ET and, at the indicated time points, examined to determine cAMP levels and cell viability. cAMP was measured via the Biotrak EIA and reported as pmol/mg of total protein. Cell viability was determined via WST-8 staining and reported as % viability compared to the control. Samples were analyzed in triplicate and error bars indicate the standard deviation from the mean. (A) cAMP levels following incubation with ET. (B) Cell viability following incubation with ET. (C – H) Morphological changes in RAW 264.7, IC-21, and NIH/3T3 cells treated with Tris control and ET. Each picture is representative of a routine ET treatment. (C and D) RAW 264.7. (E and F) IC-21. (G and H) NIH/3T3.

Figure A-4.

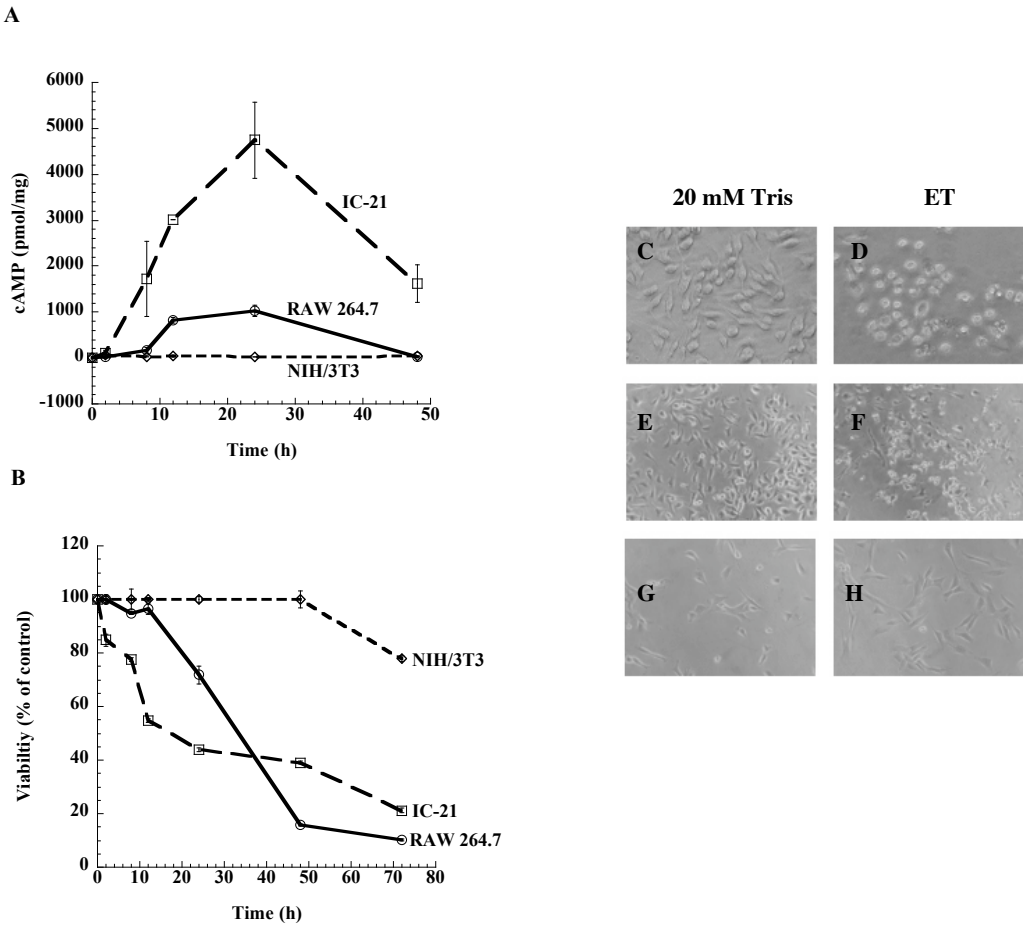
A
cAMP (pmol/mg)
6000
5000
4000
3000
2000
1000
0
-1000
0
10
20
30
40
50
Time (h)
IC-21
RAW 264.7
NIH/3T3
B
Viabiltiy (% of control)
120
100
80
60
40
20
0
0
10
20
30
40
50
60
70
80
Time (h)
NIH/3T3
IC-21
RAW 264.7
20 mM Tris
ET
C
D
E
F
G
H

a pan-caspase inhibitor, ZVAD-FMK, prior to treatment with ET. As shown in Fig. 5, RAW 264.7 (Fig. A-5A) and IC-21 (Fig. A-5B) cells were not protected from ET-induced death in the presence of ZVAD-FMK. Corresponding to apoptosis inhibitor results, there was no discernible increase in cleaved caspase-3 (Fig. A-5C) or poly-ADP-ribose polymerase (PARP) (Fig. A-5D). In contrast, control cells treated with LFn/TcsL$^{1-556}$, a fusion protein that consists of LFn (the PA-binding domain of LF) fused to the enzymatic domain of *Clostridium sordellii* lethal toxin and a potent inducer of apoptosis (60), revealed activation of both caspase-3 and PARP. Finally, in line with these results, TUNEL staining for 3' nicked DNA did not reveal any notable chromosomal fragmentation in ET-treated macrophages (Fig. A-5F and A-5G).

The time-course of cell death in ET-treated macrophages was indicative of apoptosis, yet we were unable to detect any of the standard hallmarks of this pathway. For this reason, oncosis was also investigated as a possible mechanism of ET-induced cell death. Toxin-induced oncosis generally occurs within a short time-period (< 4 h) and can be blocked by the addition of extracellular glycine (9, 12). Thus, we reasoned that ET-induced cell death should be blocked by the addition of glycine if these cells were dying by oncosis. Addition of up to 10 mM glycine to ET-treated cells did not protect either IC-21 or RAW 264.7 macrophages from cell death (data not shown), further suggesting these toxin-

Figure A-5. Effect of ET on apoptosis in RAW 264.7 macrophages. (A and B) Influence of caspase inhibitors on ET-induced cytotoxicity. RAW 264.7 and IC-21 cells were pre-treated with ZVAD-FMK (30 μM for RAW 264.7 and 50 μM for IC-21 cells) for 1 h prior to treatment with ET. At the indicated time points, cell viability was determined via WST-8 staining. Samples were analyzed in triplicate and error bars indicate the standard deviation from the mean. (A) RAW 264.7 cell viability. (B) IC-21 cell viability. (C – G) RAW 264.7 cells were treated with ET (2μg/ml), harvested, and evaluated via western blotting and TUNEL staining. For western blotting, cells lysates were collected, separated via 10 % SDS-PAGE, and analyzed using the indicated primary antibody. (C) Anti-caspase-3 western blot of RAW 264.7 cell lysates. (D) Anti-PARP western blot of RAW 264.7 cell lysates. In each western blot, times and treatment conditions are indicated above the panel. In each panel, C = Tris control and L = PA + LfnTcsL$^{1-556}$. At 24 h post-treatment, cells were collected and processed via TUNEL staining as described in Experimental Procedures. (E) 20 mM Tris. (F) ET. (G) 50 nM staurosporine. Brackets designate the areas of apoptotic cells.

Figure A-5.

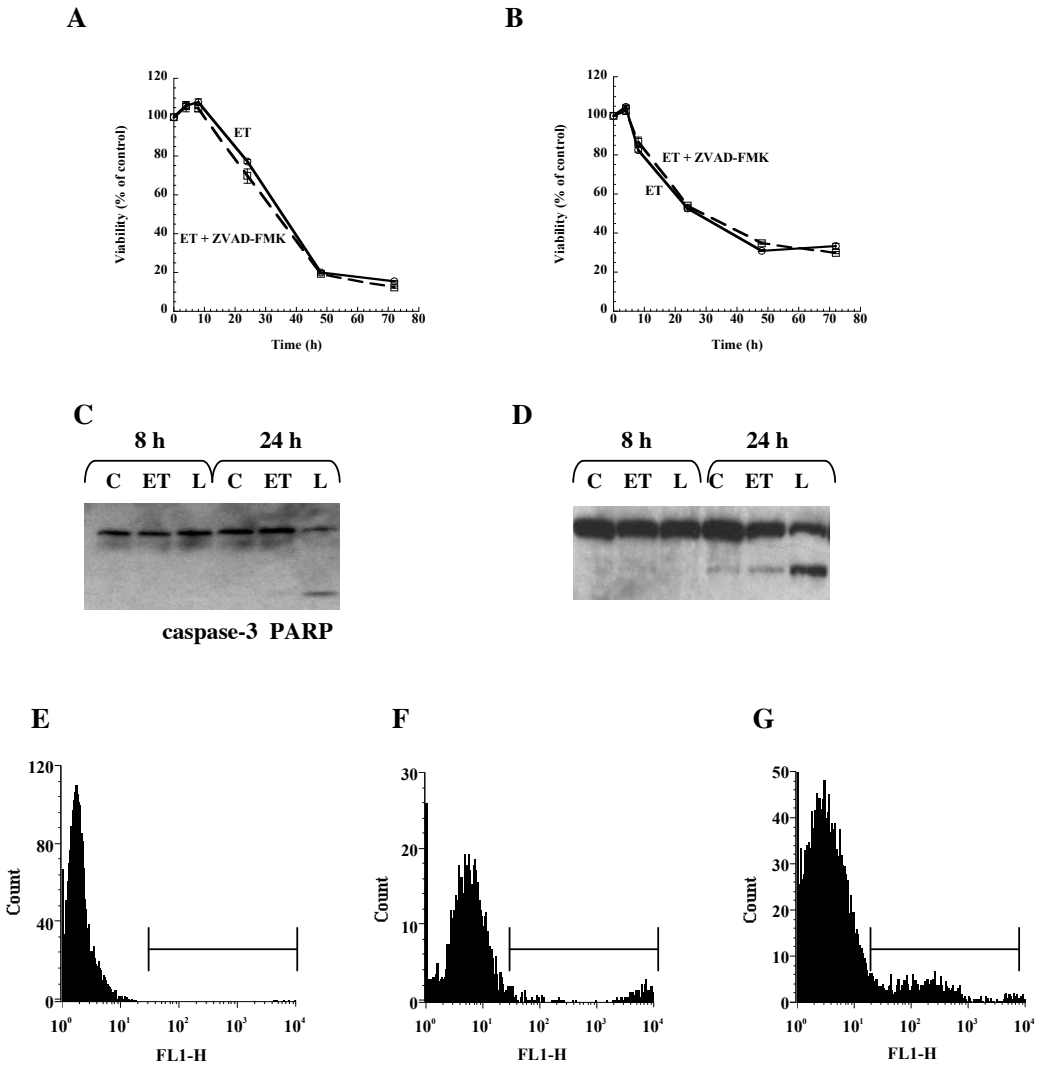
A
B
Viability (% of control)
Time (h)
ET
ET + ZVAD-FMK
C
D
8 h
24 h
C ET L C ET L
caspase-3 PARP
E
F
G
Count
FL1-H

treated cells did not die by either of the classically defined apoptosis or oncosis pathways.

Non-macrophage cells are differentially sensitive to ET intoxication. In light of the above results regarding macrophage sensitivity to ET, we investigated the cytotoxic effects of this toxin on NIH/3T3 murine fibroblast cells, a non-macrophage murine fibroblast cell line, to determine whether the effects of ET were macrophage-specific. NIH/3T3 cells were incubated in the presence of ET, as in the macrophage experiments described above, and observed for intracellular cAMP accumulation, changes in cell viability, and morphological changes. As shown in Fig. A-4A, in contrast to the macrophage cell lines, NIH/3T3 cells showed no increase in cAMP above basal level in the presence of ET. As shown in Fig. A-4B, these cells also did not exhibit any loss in viability up to 48 h. Additionally, these cells showed no change in morphology over the time course of treatment (Fig. A-4G and A-4H). Treatment with 10-fold more ET also had no detectable impact on NIH/3T3 cell physiology, viability, or levels of cAMP (data not shown).

In order to determine if defects in cell entry might account for the resistance of NIH/3T3 cells to ET, we again utilized LFn/TcsL$^{1\text{-}556}$ to examine the susceptibility of NIH/3T3 cells intoxicated through a PA-dependent mechanism. As shown in Fig. A-6, following treatment with PA and LFn/TcsL$^{1\text{-}556}$, NIH/3T3

Figure A-6. Cytopathic effects and cell death caused by LFnTcsL$^{1-556}$ in both IC-21 and NIH/3T3 cells. Each cell type indicated was incubated with LFnTcsL$^{1-556}$ (2μg/ml) plus PA (2μg/ml) for the indicated time points, at which point cell viability was determined via WST-8 staining. Samples were analyzed in triplicate and error bars indicate the standard deviation from the mean.

Figure A-6.

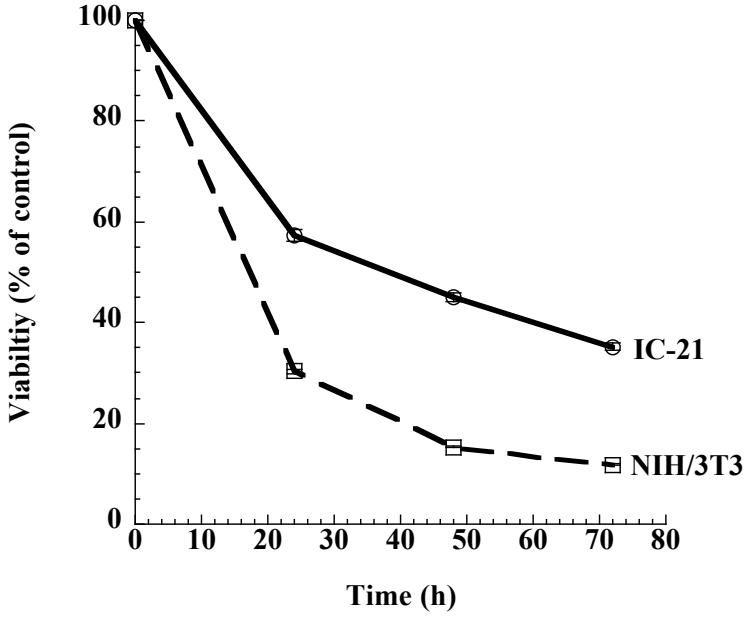
100
80
60
40
20
0
Viabiltiy (% of control)
0
10
20
30
40
50
60
70
80
Time (h)
IC-21
NIH/3T3

cells appeared more sensitive to the fusion than IC-21 macrophages, indicating reduced cell entry was an unlikely explanation for NIH/3T3 resistance to ET.

We next sought to determine if EF was capable of modifying NIH/3T3 cells when provided access to the cytosol in a PA-independent manner. To address this issue, we generated a transfected NIH/3T3 cell line containing the EF-encoding gene (*cya*) under the control of a mifepristone-inducible promoter. Following addition of mifepristone, the *cya*-transfected NIH/3T3 cells showed a rapid rise in cAMP levels. As shown in Fig. A-7A, the amount of cAMP in NIH/3T3-*cya* cells reached a high level (~ 740 pmol per mg of cell lysate at 24 h) comparable to that observed in the RAW 264.7 cell line. As shown in Fig. A-7B, this rise in cAMP was also accompanied by a decrease in cell viability, indicating that EF, under these conditions, was able to induce cell death in a non-macrophage cell line when steps in cell entry were by-passed. As shown in Fig. A-7D, induction with mifepristone also resulted in marked morphological changes, including cell elongation and bladdering. Plasmid and mock controls of NIH/3T3 cells demonstrated no noticeable changes in morphology (Fig. A-7C).

Having observed three different cell type-specific effects of ET, CHO cells, which were first used to define the activity of EF (29), were examined to determine correlations between cAMP levels and cell viability. As shown in Fig. A-8A, when CHO cells are incubated with ET there is a rapid rise in cAMP, with peak levels of ~ 2600 pmol per mg of cell lysate between 2 and 12 hours. While

Figure A-7. Morphological changes, cAMP accumulation, and cell viability following induction of NIH/3T3 fibroblasts, transfected with the *cya* gene (NIH/3T3-*cya*), with mifepristone. NIH/3T3-*cya* fibroblasts were plated at 50,000 cells/well and, following overnight incubation, were incubated in the presence of the indicated concentrations of mifepristone and observed for 24 h for observation of morphological changes, cAMP accumulation, and changes in cell viability. At this point, cells were either lysed and supernatants processed using the cAMP EIA or viability was determined via WST-8 staining. Samples were analyzed in triplicate and error bars indicate the standard deviation from the mean. (A) cAMP levels of mifepristone-induced NIH/3T3-*cya* cells. (B) Cell viability of mifepristone-induced NIH/3T3-*cya* cells. (C and D) The pictures shown are representative of a routine assay in which cells were induced with 1 X 10^{-9} M mifepristone. (C) Uninduced NIH/3T3-*cya* cells. (D) Mifepristone-induced NIH/3T3-*cya* cells.

Figure A-7.

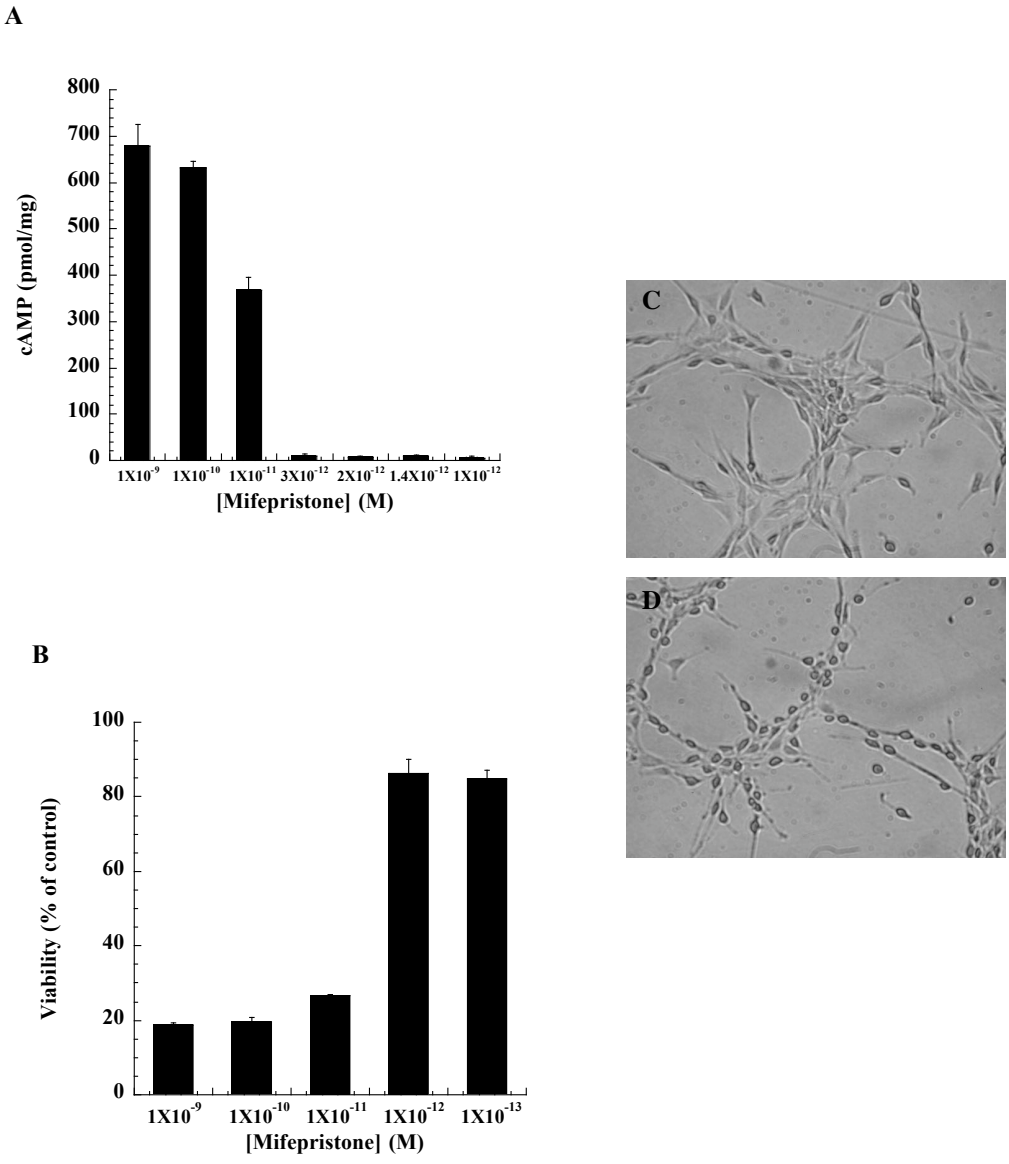
A
cAMP (pmol/mg)
800
700
600
500
400
300
200
100
0
1X10-9
1X10-10
1X10-11
3X10-12
2X10-12
1.4X10-12
1X10-12
[Mifepristone] (M)
B
Viability (% of control)
100
80
60
40
20
0
1X10-9
1X10-10
1X10-11
1X10-12
1X10-13
[Mifepristone] (M)
C
D

Figure A-8. cAMP accumulation and cell viability in ET-treated CHO cells. CHO cells were incubated with ET and at the indicated time points were examined to determine cAMP levels and cell viability. cAMP was measured via the Biotrak EIA and reported as pmol/mg of total protein. Cell viability was determined via WST-8 staining and reported as % viability compared to the control. Samples were analyzed in triplicate and error bars indicate the standard deviation from the mean. (A) cAMP levels and cell viability following incubation with ET. (B) Morphological changes observed in ET-treated CHO cells. (C) Control, untreated CHO cells.

Figure A-8.

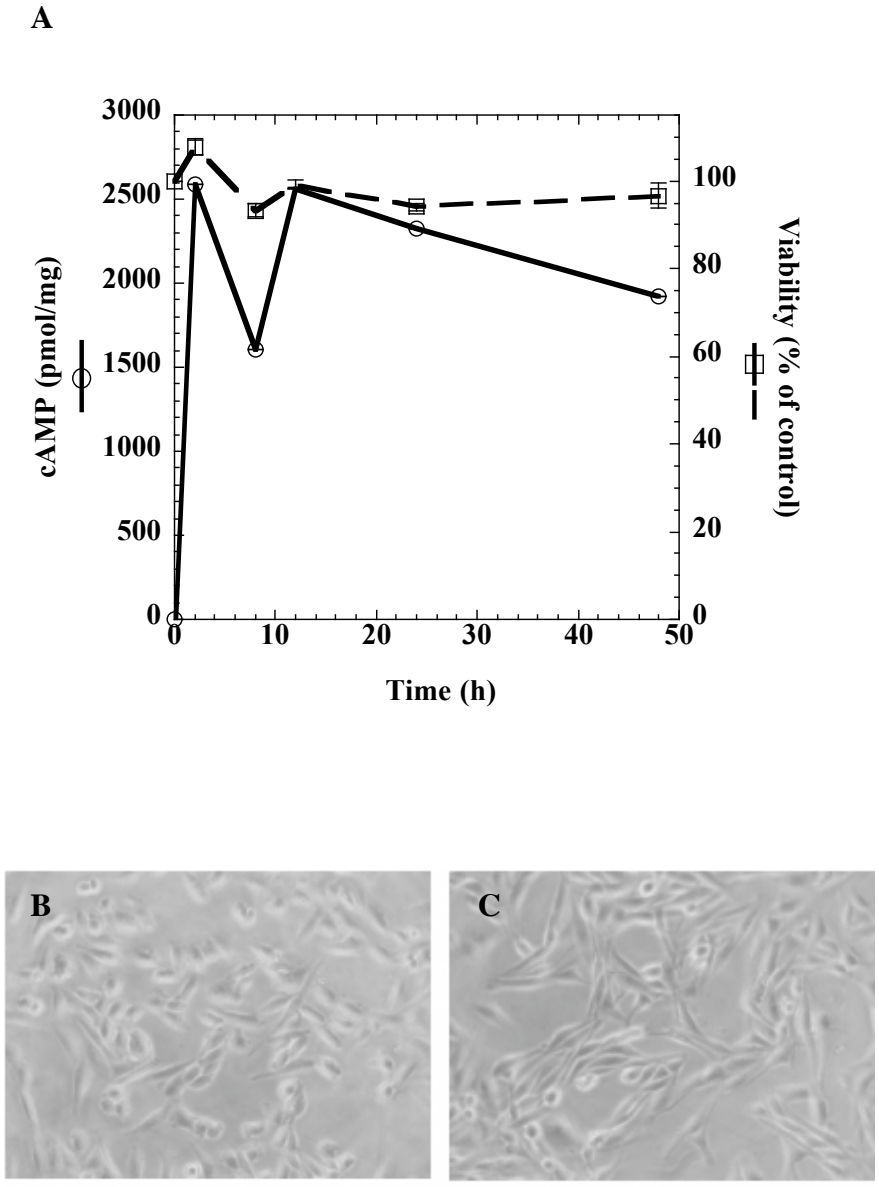
A
3000
2500
2000
1500
1000
500
0
cAMP (pmol/mg)
0
10
20
30
40
50
Time (h)
100
80
60
40
20
0
Viability (% of control)
B
C

these levels are higher than those observed for the RAW 264.7 cells, which experience a loss in viability, CHO cells showed no significant loss in cell viability over a 72 h period (Fig. A-8A). Distinct morphological changes are seen between ~ 2 – 6 h, with cell elongation being the major feature (Fig. A-8B and A-8C); however, following this morphological change, CHO cells exhibited no further effects due to ET treatment, even following repeated additions of ET over an extended time period (data not shown).

The survival of ET-treated CHO cells was unexpected based on the levels of cAMP observed and what had been found from the macrophage and NIH/3T3-*cya* experiments. Despite the sustained levels of cAMP, CHO cells adapt and appear to grow normally following exposure to ET. This survival event could be due to cAMP's reported ability to promote the expression of anti-apoptotic factors in certain cell types (19, 24). To address this experimentally, CHO cells were pretreated for 45 min with ET and then exposed to staurosporine, a potent inducer of apoptosis. As shown in Fig. A-9, ET did not protect CHO cells from staurosporine, but in fact made these cells even more sensitive to this factor. This effect was dependent on the enzymatic activity of EF, as the EF-K346R mutant did not increase the sensitivity of CHO cells to staurosporine. These results indicate that it is unlikely that ET is triggering an anti-apoptotic effect, and the more plausible explanation is that these cells have adapted to this supraphysiological level of cAMP.

Figure A-9. ET effects on CHO cell sensitivity to staurosporine. CHO cells were pretreated with ET (2 μg/ml) or EF-K346R (2 μg/ml) + PA (2 μg/ml) for 45 min, at which point staurosporine (500 mM) was added to the cells. Cell viability was determined via WST-8 staining and reported as % viability compared to the control. Samples were analyzed in triplicate and error bars indicate the standard deviation from the mean.

Figure A-9.

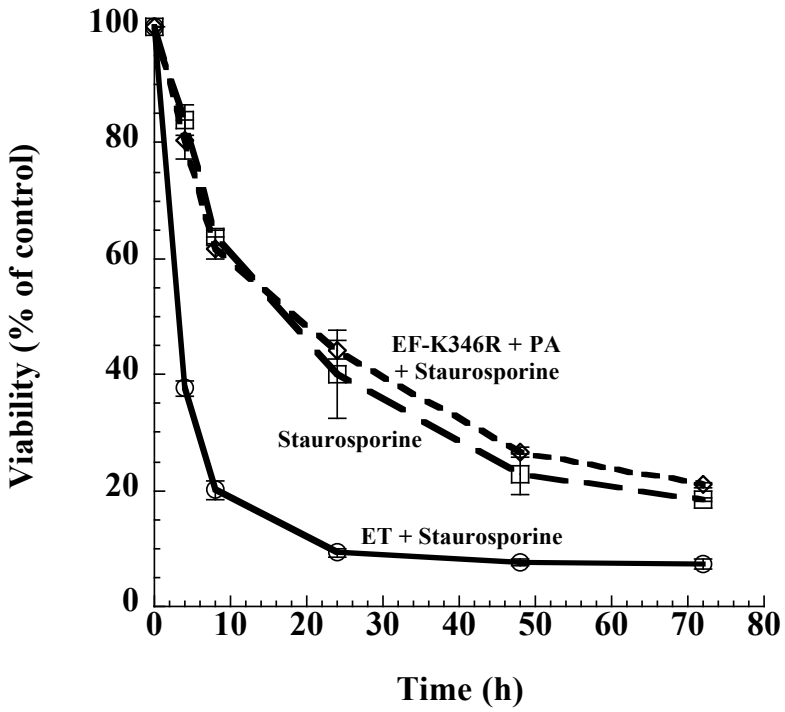
Viability (% of control)
Time (h)
EF-K346R + PA
+ Staurosporine
Staurosporine
ET + Staurosporine
0
20
40
60
80
100
0
10
20
30
40
50
60
70
80

DISCUSSION

Results from the current study reveal ET's capacity for inducing tissue damage and cell-type specific cytotoxicity. While the majority of work has focused on LT as the primary *B. anthracis* virulence factor, there is no reason why this should be so. Isogenic strains with disruptions in *cya* demonstrate an increased LD_{50} (44) and are less effective attenuated vaccines than strains expressing EF and PA (45). Thus, it is reasonable to assume that ET plays an integral part in anthrax disease. In addition, adenylate cyclases from several pathogens, including *B. pertussis* (21), *P. aeruginosa* (65), and *Yersinia pestis* (34) are also thought to be involved in their respective diseases. Therefore, dissecting the influence of ET on cell, tissue, and organ physiology should provide new insights into anthrax disease.

The developing zebrafish embryo provided an ideal vertebrate model for assessing the impact of ET on tissues and major organs. For these studies, the developing zebrafish embryo model was selected over more traditional animal models for several reasons. First, several hundred embryos can be collected from a single fertilization and these can be exposed to toxin in a single treatment. Second, laboratory zebrafish, including our Oklahoma strain, remain a relatively outbred population, and previous work on LT and *B. anthracis* found mouse sensitivities varied by several orders of magnitude depending on the strain of mice examined (17, 38). Thus, it was difficult to predict which mouse line would be

most appropriate for the study of ET. Third, zebrafish embryos are translucent for up to seven days following fertilization, making initial analysis possible by simple visualization (25). Fourth, whole sagittal plane slices can be prepared from the treated embryos, which allows for rapid, yet thorough analysis of multiple systems in a single pathology preparation. Finally, the immune system remains immature at points when major organ systems are in place (58). This was especially important to our studies because we wanted to implicate ET directly in the observed tissue damage and eliminate the possibility that damage was a result of inflammatory responses.

Given the broad impact of cAMP in cell physiology, and in light of the distinct pathologies observed in ET treated zebrafish, we expected cells of various lineages might respond differently to intoxication by ET. Indeed, the differential influence of cAMP on various cell types is extensively reported in the literature. For example, cAMP has been implicated in protection against apoptotic agents in hepatocytes (48), T84 colon cancer cells (42), neutrophils (26), and cardiac muscle cells (11). Conversely, cAMP has been implicated in the induction of apoptosis in endothelial cells (24), human glioma cells (19), rat leukemia cells (51), and lymphoma cells (66). Our findings reinforce this point, since various cell types responded to ET-induced changes in cAMP with distinct differences. ET induced cell death in two cell lines, RAW 264.7 and IC-21, while remaining

seemingly harmless to NIH/3T3 fibroblasts and causing only morphological changes in CHO cells, which survived ET intoxication.

The explanation for the absence of cAMP accumulation in ET-treated NIH/3T3 cells remains unclear, since our results indicate these cells support PA-mediated entry and show high levels of cAMP when EF is expressed from within the cell. It is formally possible that NIH/3T3 cells are defective in a previously undescribed step in cell entry, which is specific to ET. It is also possible that expression of EF from within the cell far exceeds levels that could be obtained by the normal modes of entry, and EF, in such excess, can overcome the resistance. Multiple attempts were made to quantify expression levels of EF within the cell, but were not successful. Despite this caveat, the data from the *cya*-transfected NIH3T3 cells does indicate that cofactors (e.g. accessible calmodulin and Ca^{2+}) are available in amounts sufficient to permit EF adenylate cyclase activity.

In contrast to NIH/3T3 cells, CHO cells clearly show a large increase in cAMP levels, yet survive intoxication. Since the levels of cAMP remain high in ET-treated CHO cells, the explanation for resistance is not the rapid turnover of this second-messenger, but more likely is due to cAMP effects, which are substantially different than those occurring in sensitive cells.

There are several possible explanations for ET's cell-specific cytotoxicity. First, EF may possess a yet undiscovered activity that contributes to cell death. Thus, changes in cAMP levels are of little consequence in the presence of other

activities. Arguing against this possibility is the fact that EF mutants defective in adenylate cyclase activity do not induce cytotoxic effects in our treatments. The second, and more likely, explanation is that some cells adapt to changes in levels of cAMP, even when these amounts become unusually high. In fact, an adaptive response seems a likely explanation in CHO cells, since we observe a dramatic change in cell morphology during the early stages of treatment with ET, yet these cells survive intoxication while the levels of cAMP remain high up to 48 h following treatment. However, other cell types, such as RAW 264.7 and IC-21 macrophages, which eventually die following ET treatment, are not capable of adapting to high levels of cAMP.

The mechanism of ET-induced cell death appears to be somewhat unique and does not fit the classic profile of apoptosis or oncosis. In previous work from our group on large clostridial toxins, we were able to use pancaspase inhibitors to partially protect cells against toxin-induced apoptosis. However, in the case of ET-treated macrophages, addition of a pancaspase inhibitor did not reduce toxicity. In line with this, we did not detect activated caspase-3 in the ET-treated cells. Other hallmarks of apoptosis, such as nuclear fragmentation and cleavage of PARP are also not detected in macrophages treated with ET. Additionally, microscopic examination of the cells treated with ET did not reveal characteristic blebbing or formation of apoptotic bodies, both of which occur in apoptotic cells.

Indeed, with the exception of the long time-course to death, these cells did not show any of the classic signs of apoptosis.

Collectively these findings indicate ET may contribute to *B. anthracis* pathogenesis through cytolysis of host cells. Clearly, this does not preclude the possibility that ET also disrupts important aspects of physiology in cells that do not eventually die from intoxication, but does suggest necrosis and cell death observed in anthrax disease could be attributed in part to ET.

MATERIALS AND METHODS

Cell culture. NIH/3T3 murine fibroblast cells (NIH/Swiss mice), IC-21 murine macrophages (C57BL/6 mice), RAW 264.7 murine macrophages (BALB/c mice), and Chinese Hamster Ovary (CHO-K1) cells were obtained from the American Type Culture Collection. NIH/3T3, IC-21, RAW 264.7, and CHO cells were maintained in RPMI 1640 medium supplemented with 10% fetal bovine serum (Gibco). NIH/3T3-*cya* cells were maintained in RPMI 1640 medium supplemented with 10% fetal bovine serum, zeocin (300 μg/ml), and hygromcin (100 μg/ml) (Invitrogen). Cells were grown in the presence of 6% CO_2 at 37°C and used between passages 10 and 20. Zebrafish Pac2 embryonic fibroblast cells were kindly provided by W. Chen (Oregon Health and Science University) and maintained in supplemented Leibovitz Medium (Gibco) containing 15% fetal calf serum and grown at 30ºC at 0.5% CO_2 (32).

Expression and isolation of recombinant PA, EF, and LfnTcsL$^{1-556}$. PA-pET15b and EF-pET15b plasmids were generous gifts from Dr. R. John Collier (Harvard Medical School). Each plasmid was transformed into BL21(DE3) *E. coli* cells (Novagen) for protein expression. *E. coli* cultures were incubated at 37°C until an OD_{600} of 1.0 was reached, at which point protein expression was induced with 0.1 mM isopropyl-β-D-thiolgalactopyranoside (Denville Scientific) overnight at 16°C. Following overnight induction, the proteins were purified using nickel affinity chromatography according to the manufacturer's instructions (Novagen). As previously described (60), LFnTcsL$^{1-556}$ was expressed from pMQ1 and also isolated by nickel affinity chromatography.

Construction of the EF mutant, EF-K346R. EF-K346R was previously described by Xia et al. (64) and is a mutant form of EF lacking adenylate cyclase activity due to a base substitution (K to R) in the ATP-binding site. EF-K346R was constructed using the Stratagene Quikchange Kit to introduce a point mutation, according to the manufacturer's protocol, into functional EF using the EF-pET15b plasmid. The primers used were as follows: 5'-GGTGTGGCTACAAGGGGATTGAATGTTCATGG-3' for the forward primer and 5'-CCATGAACATTCAATCCCCTTGTAGCCACACC-3' for the reverse. Following DNA sequencing and transformation of pET15b/EF-K346R into *E. coli*

BL21 (DE3) cells, EF-K346R was expressed and purified as described above for the other proteins used in this study.

Zebrafish maintenance and care. Zebrafish were maintained at 28.5º C on a 14 h light/10 h dark cycle in 10-gallon tanks in a Z-plex stand-alone unit (Aquatic Habitats). Embryos used for toxin treatment were obtained by placing two females and one male (which had been separated the night before) in a 1.0 liter mating chamber for up to one hour. The embryos were subsequently collected, bleached, sorted according to morphology, and maintained in sterile embryo water (10% Hank's solution with full strength calcium and magnesium, pH 7.0) at 28.5º C (61).

Treatment of zebrafish embryos with ET. Within 15 min following fertilization, zebrafish embryos were separated into a 24-well plate containing 10 embryos/well, in a final volume of 1 ml. The stage of development was determined by morphology (25). ET-treated embryos were incubated with a range of concentrations (10 μg PA + 10 μg EF, 20 μg PA + 20 μg EF, or 40 μg PA + 40 μg EF), with each concentration inducing representative defects. Control treatments included 40 μg/ml PA alone, 40 μg/ml EF alone, 40 μg/ml PA + 40 μg/ml EF-K346R, or 20 mM Tris, pH 8.0 alone. Each treatment was performed in replicates of five (for a total of 50 embryos/treatment). The embryos were observed for seven days post-treatment for morphological changes. Whole bisected fish were processed into paraffin, sectioned on a sagittal plane, stained

with hematoxylin and eosin, and histopathology of ET-treated embryos was performed at the University of Oregon Zebrafish International Resource Center.

Cell viability assays. Cell viability was assessed at the indicated time points using the CCK-8 viability assay according to the manufacturer's protocol (Dojindo Laboratories). This colorimetric assay was performed using WST-8 [2-(2-methoxy-4-nitrophenyl)-3-(4-nitrophenyl)-5-(2,4-disulfophenyl)-2H-tetrazolium, monosodium salt], which is reduced to a formazan derivative by cellular dehydrogenases. The level of WST-8 formazan was determined by reading A_{450}, which yields an increased absorbance proportional to the level of cellular dehydrogenases. Briefly, following addition of the WST-8 dye to each well of a 96-well plate, the A_{450} was recorded for each well and percent viability was calculated using the formula $(A_{test}-A_{background})/(A_{control}-A_{background})*100$, where A=absorbance at A_{450}, background = media alone, and control = cells treated with 20 mM Tris, pH 8.0. In the indicated experiments, Caspase Inhibitor VI (ZVAD-FMK) and staurosporine were obtained from Calbiochem, Inc.

Determination of cAMP levels. Cells were plated in a 96-well plate at a density of 2 X 10^5 cells/ml and incubated overnight (14-16 h) at 37°C. Following ET treatment or induction, cells were lysed, supernatants collected, and cAMP levels determined. cAMP levels were determined using the cAMP BioTrak Enzyme-immunoassay (EIA) according to the manufacturer's protocol

(Amersham Pharmacia Biotech). Levels of cAMP are reported in pmol/mg of total cellular protein.

Western blotting. For all western blotting experiments, cells were grown in T-25 flasks until ~ 75% confluency was attained. Following treatment with the indicated reagent, cells were incubated in 2 ml of lysis buffer (1% SDS, 50 mM Tris pH 7.4, 5 mM EDTA) on ice for 15 min. Following incubation on ice, cells were passed through a 22-gauge needle 10 times and subsequently pelleted via centrifugation at 10,000 RPM for 10 min to obtain supernatants containing cellular protein. Samples (10 μg/well) were separated via 10% SDS-PAGE, after which protein was transferred to PVDF for blotting. Western blotting was performed using either anti-Caspase-3 or anti-PARP primary antibodies according to the manufacturer's protocol (Cell Signaling Technology).

Transfection of NIH/3T3 cells with cya. PCR was used to amplify *cya* from pXO1, the toxin-encoding plasmid of *B. anthracis*. For PCR amplification and subsequent cloning, two oligonucleotides were designed. As a forward primer the first oligonucleotide with the sequence 5'-GACTGAGGTACCGCCATGGATGAACATTACACTGAGAGTGAT-3' was designed to hybridize to the 5' region of *cya* starting at the sequence encoding for mature EF. This primer was also designed to encode a Kozak sequence (GCCATGG) and a *Kpn*I restriction site upstream of the homologous region. As a reverse primer a second oligonucleotide with the sequence 5'-

GACTGAGAATTCAGTTTTTCATCAATAATTTTTTGGAA-3', was designed to hybridize to the 3' end of *cya* and included sequences which encoded for a downstream *Eco*RI restriction site. The PCR amplification product was subsequently restricted with *Kpn*I and *Eco*RI and directionally cloned into compatible sites of pGene/V5-His plasmid version B (Invitrogen). The ligation mixture was transformed into *E. coli* XL1-blue and candidate clones were identified by plasmid mini-prep and subsequent restriction analysis.

For transfection, the EF-encoding plasmid was linearized with *Sap*I, and transfected into GeneSwitch-NIH/3T3 fibroblast cells (Invitrogen) via lipofection according to the manufacturer's protocol using the LipofectAMINE PLUS Reagent Kit (Gibco). Cells that were transfected following lipofection were identified by growth on F-12 (HAM) selective medium (Gibco) containing zeocin (300 μg/ml) and hygromycin (100 μg/ml). Cells resistant to both zeocin and hygromycin were selected as transfectants and maintained under drug pressure for the experiments in this study. For EF expression, the cells were exposed to concentrations of mifepristone (Invitrogen) prior to cAMP and cell viability determinations.

TUNEL assay of apoptosis. Cells were grown in T-25 flasks until ~ 75% confluence was attained, at which point cells were harvested and fixed in 1% paraformaldehyde for 30 min. Following fixing, cells were allowed to permeabilize overnight at -20°C in 70% ethanol. Following permeabilization,

cells were incubated with BrdUTP (Molecular Probes) for 2 h at 37°C for labeling of nicked DNA indicative of apoptosis. Cells were subsequently incubated in the presence of anti-BrdU alexa fluor 488-labeled antibody (Molecular Probes) for 30 min at room temperature. Following TUNEL staining, cells were analyzed using a FACSCalibur flow cytometer and data was analyzed using CELLQUEST software (Becton Dickinson).

CYTOTOXIC ACTIVITY OF *BACILLUS ANTHRACIS* PROTECTIVE ANTIGEN OBSERVED IN A MACROPHAGE CELL LINE OVEREXPRESSING ANTXR1

Cytotoxic Activity of *Bacillus anthracis* Protective Antigen Observed in a Macrophage Cell Line Overexpressing ANTXR1. (Isabelle I. Salles*, Daniel E. Voth*, Sabrina C. Ward, Kathleen M. Averette, Rodney K. Tweten, Kenneth A. Bradley, and Jimmy D. Ballard. *Cellular Microbiology. In press*. *I.I.S. and D.E.V. contributed equally to this work.)

Bacillus anthracis, the causative agent of anthrax, produces two major virulence factors, a poly-D-glutamic acid capsule and anthrax toxin (AT). AT is composed of three polypeptides, protective antigen (PA, 83 kDa) and two catalytic moieties, edema factor (EF, 89 kDa) and lethal factor (LF, 90 kDa). Binary combination of PA plus LF yields lethal toxin (LT), while PA plus EF produces edema toxin (ET) (14, 29, 31). There is a notable attenuation in virulence for isogenic strains of *B. anthracis* containing disruptions in genes encoding for PA, LF, or EF, suggesting these toxin subunits play an important part in anthrax disease (44). Thus, delineation of AT's mechanism of action - including defining aspects of cell entry, substrate modification, and protein structure - provides relevant insights into how *B. anthracis* causes disease.

PA, the focus of the current study, has historically been considered to be non-toxic, serving only as a mediator of cell entry for LF and EF. Thus, studies to date have focused on defining the mechanisms by which PA localizes to the cell surface, oligomerizes, and translocates LF and EF into the cytoplasm. Two PA

receptors have been identified and are encoded by the TEM8/ANTXR1 and CMG2/ANTXR2 genes (8, 53), and PA binds directly to integrin-like inserted domains (I domains) on these receptors. The crystal structure of the ANTXR2 I domain has recently been solved in isolation and in complex with both monomeric and heptameric forms of PA (27, 28, 52). While no structure for ANTXR1 has been reported, the interaction of PA with ANTXR1 I domain exhibits characteristics similar to that of CMG2 (7, 8), although PA binds ANTRX1 with a lower affinity (27, 62) (S.C.W. and K.A.B., unpublished observations and (54)) and PA bound to ANTXR1 forms pores at a more neutral pH than PA bound to ANTXR2 (47).

Following receptor binding, PA is cleaved by a furin-like protease at the sequence $RKKR^{167}$, causing the release of the amino-terminal PA20 (20 kDa) peptide and leaving a receptor-bound 63 kDa form of PA (PA_{63}). PA_{63} forms a heptameric prepore structure to which EF and LF bind (39, 40, 49). PA oligomerization and binding of LF and EF accelerates the clearance of heptameric PA_{63} from the cell surface by promoting uptake of the complex via receptor-mediated endocytosis in a lipid-raft-dependent manner (1, 4). Acidic pH triggers conformational changes and membrane insertion of the heptameric PA_{63} β-barrel into the vesicle membrane and the translocation of LF and EF into the cytosol of mammalian cells (5, 36). Within the cytosol, LF functions as a metalloprotease cleaving mitogen-activated protein kinase kinases, and EF, as a calmodulin-

dependent adenylate cyclase, generates high levels of cAMP (14, 29). Thus, the current model of anthrax intoxication indicates that EF and LF are solely responsible for alterations in cell physiology, with PA serving only as a conduit for cell entry via interaction with ANTXR1 and ANTXR2.

Despite these important advances in understanding the activity of PA, little is known about the influence of receptor levels on the activities of this protein within the cell, and it is conceivable that the formation of heptamers could be limited at several steps of cellular intoxication. The amount of furin-like protease, the availability of lipid-rafts, the rate of endocytosis, and levels of available PA receptor could each contribute to the extent of heptamer formation and sensitivity to LT. Thus, in the current study, experiments were performed to determine if expression levels of ANTXRs influence PA-related processes during intoxication. Herein, we show that heightened expression of ANTXR1 results in increased levels of cell-associated heptameric PA and report that under these conditions PA alone induces cytotoxicity. These findings suggest, for the first time, that under certain conditions, exposure to PA can lead to cell death in the absence of LF or EF.

RESULTS

Stability of SDS-resistant PA oligomers in RAW 264.7^{ANTXR1} cells. Using a transduced cell line designed to overexpress ANTXR1, we were able to initially assess the impact of increased receptor levels on PA oligomer formation

and stability during intoxication. In these experiments, normal RAW 264.7 macrophages or RAW 264.7^{ANTXR1} cells were treated with PA, incubated 1 h, and then washed extensively to remove any extracellular PA remaining in the media. Lysates were then collected from these cells over a 10 h time period and characterized for levels of the heptameric pore-form of PA. PA heptamers that have undergone acidic pH-mediated conformational transitions are resistant to dissociation by SDS and, therefore, can be detected by SDS-PAGE (33, 36). To assess oligomer levels, extracts from PA-treated RAW 264.7 and RAW 264.7^{ANTXR1} cells were examined by immunoblot. As shown in Fig. A-10, distinct differences in the stability of the PA oligomer in RAW 264.7^{ANTXR1} cells and RAW 264.7 cells were observed. While oligomer formation was transient in RAW 264.7 macrophages, PA heptamer was detected in RAW 264.7^{ANTXR1} cells over a 10 h period. Additionally, the level of PA heptamer detected was up to 2.5-fold higher in RAW 264.7^{ANTXR1} as compared with RAW 264.7 cells. Densitometry analysis was used to determine the rate of turnover for the PA oligomer. Interestingly, as summarized in Table A-1, in addition to the increased accumulation of PA heptamer in RAW 264.7^{ANTXR1} cells, heptamer levels in these cells appeared to decline at a rate slower than that observed in cells expressing basal levels of receptor. Collectively, these experimental findings suggest PA heptamers accumulate to higher levels and are degraded at a slower rate in RAW 264.7^{ANTXR1} cells compared to RAW 264.7 cells.

Figure A-10. Analysis of PA oligomers in RAW 264.7^{ANTXR1} cells. RAW 264.7 or RAW 264.7^{ANTXR1} cells were treated with PA (1 μg/ml) for 1 h at 4˚C and subsequently washed to remove any unbound protein. Cell lysates were collected at the indicated times (h), and equivalent amounts of cytosolic protein were analyzed by SDS-PAGE and immunoblot using anti-PA or anti-tubulin antiserum and corresponding secondary antibodies conjugated to HRP. Negative control = C represents mock treated cells. Positive controls for PA-heptamer mobility are indicated, **+**.

Figure A-10.

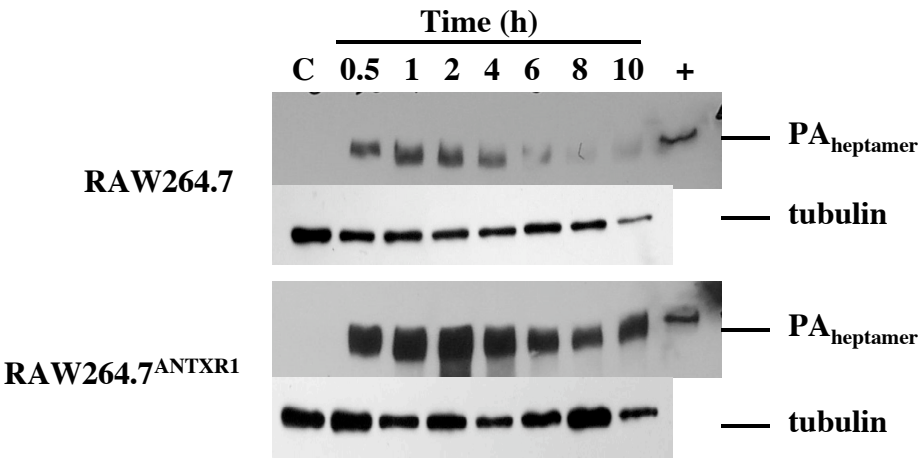
Time (h)
C 0.5 1 2 4 6 8 10 +
RAW264.7
PA heptamer
tubulin
RAW264.7ANTXR1
PA heptamer
tubulin

Table A-1.

Table A-1. Relative PA heptamer levels and rates of degradation in RAW 264.7 and RAW 264.7^{ANTXR1} cells

Time (h)	Band Intensity[a]		Fold Difference	Degradation Rates (Adjusted[b])	
	Normal[c]	ANTXR1[d]		Normal[c]	ANTXR1[d]
0	5,741	6,325	NA	1468 units/h	1164 units/h
0.5	15,567	19,443	1.25		
				P=0.0253	P=0.0208
1	18,975	27,256	1.43		
				R=0.87	R=0.85
2	15,488	23,525	1.51		
4	12,745	27,709	2.17		
6	7,424	19,742	2.65		
8	5,340	10,919	2.04		
10	6,720	13,398	2.0		

a: Band intensity determined by densitometry analysis, arbitrary units
b: Degradation rate adjusted to reflect 1.45 fold overall higher band intensity of PA oligomer in RAW 264.7^{ANTXR1} versus normal RAW 264.7 cells
c: Normal RAW 264.7 cells
d: RAW 264.7^{ANTXr1} normalized to control based on relative tubulin levels

PA-mediated cytotoxicity in RAW 264.7^{ANTXR1} cells. Given the inordinate stability of PA heptamers within RAW 264.7^{ANTXR1} cells, we next sought to determine how sustained formation, and increased levels, of this pore complex might influence cell viability. Previous studies have shown that mixing of lysosomal contents with the cytoplasm can lead to activation of death pathways (57), and we suspected such an event could be plausible if PA exhibited sustained heptamer formation.

For these reasons, RAW 264.7^{ANTXR1} cells were examined for cytotoxicity following exposure to PA. When exposed to PA, RAW 264.7^{ANTXR1} cells exhibited significant rounding and condensation indicative of a cytopathic effect (Fig. A-11). Normal RAW 264.7 macrophages did not exhibit changes in cell morphology following treatment with PA, which is consistent with what has been previously reported for PA (41).

As shown in Fig. A-11A, approximately 70% of RAW 264.7^{ANTXR1} cells were killed by treatment with PA (≥ 1 μg/ml), whereas PA had no effect on RAW 264.7 cells. The loss in cell viability began 6 h after the addition of PA and was more significant at 12 and 24 h. By 72 h, cell numbers began to recover, apparently as a result of outgrowth of the cells that survived treatment with PA (Fig. A-11B). Further analysis of PA-treated RAW 264.7^{ANTXR1} cells using trypan blue exclusion staining indicated that the decrease in cell number was a direct result of cytotoxicity and not a cytostatic effect (Fig. A-11H).

Figure A-11. Cytotoxic effects of PA on RAW 264.7^{ANTXR1} cells. (A) Dose curve demonstrating PA cytotoxicity in RAW 264.7^{ANTXR1} cells. RAW 264.7 cells (closed circles) or RAW 264.7 ^{ANTXR1} cells (open squares) were treated with PA and assayed for viability after 24 h. (B) Time-course of PA cytotoxicity. RAW 264.7^{ANTXR1} cells were treated with either 1 μg (closed circles) or 5 μg (open squares) of PA and monitored over time for viability. (C) RAW 264.7 cells or RAW 264.7^{ANTXR1} cells were incubated with various amounts of PA in combination with a range of concentrations of LF for 24 h and assayed for viability. Solid lines = RAW 264.7 macrophages, dashed lines = RAW 264.7^{ANTXR1} cells, closed circles = 0.1 μg/ml PA, open squares = 1.0 μg/ml PA, open triangles = 5.0 μg/ml PA. (D – H) Photomicrographs of RAW 264.7 or RAW 264.7^{ANTXR1} cells treated with 5 μg/ml PA or corresponding buffer control for 24 h. (D) RAW 264.7 cells plus buffer control, (E) RAW 264.7 cells plus PA, (F) RAW 264.7^{ANTXR1} cells plus buffer control, (G) RAW 264.7^{ANTXR1} cells plus PA. (H) Trypan blue staining of PA-treated RAW 264.7^{ANTXR1} cells at 24 h post-exposure.

Figure A-11.

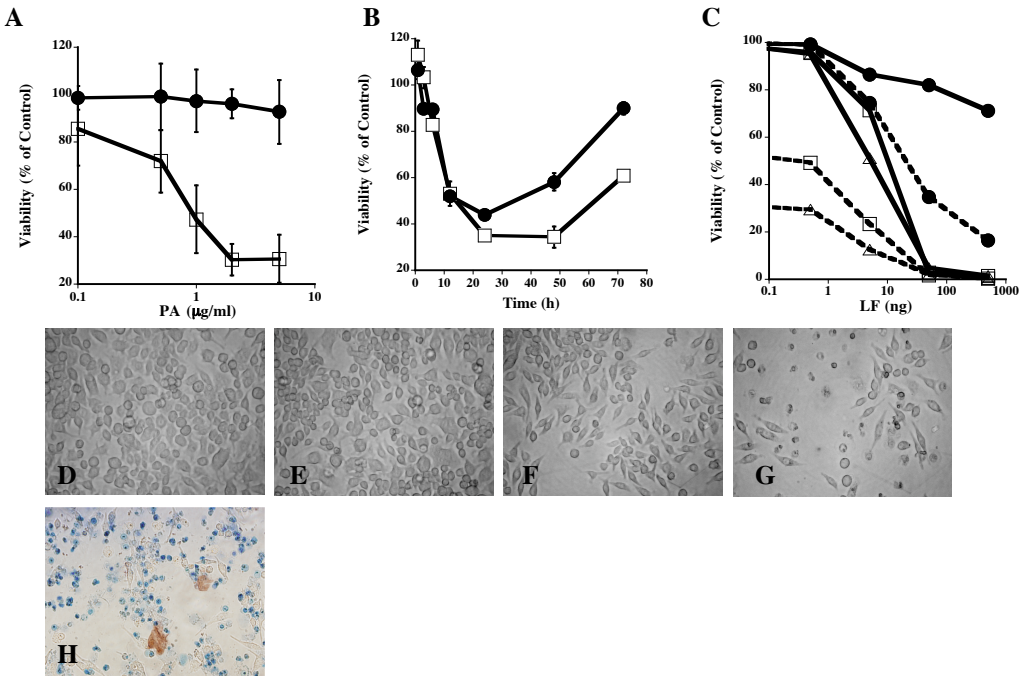
A
Viability (% of Control)
PA (µg/ml)
B
Viability (% of Control)
Time (h)
C
Viability (% of Control)
LF (ng)
D
E
F
G
H

We next examined how the overexpression of ANTXR1 influenced sensitivity to LT. Previous work found that Chinese hamster ovary cells overexpressing ANTXR1 display increased sensitivity to challenge with PA + LF_NDTA (7, 8). Consistent with this finding, RAW 264.7^{ANTXR1} cells display an increased sensitivity to LT compared to wild type RAW 264.7 cells (Fig. A-11C). Thus, higher receptor levels not only correlated with sensitivity to PA, but also reduced the minimal cytotoxic dose of LT.

Analysis of ANTXR1 derivatives in PA-mediated cytotoxicity. Given the finding of PA cytotoxicity, we next sought to determine if cell killing required a fully intact receptor and/or functional PA-ANTXR1 interactions. Cells expressing ANTXR1 that lacks a cytoplasmic tail ($ANTXR1_{1-345}$) or a mutant form of ANTXR1 unable to bind PA ($ANTXR1_{D50A}$) were treated with PA for 24 h (Fig. A-12A). RAW $264.7^{ANTXR1(1-345)}$ cells displayed the same sensitivity to PA as RAW 264.7^{ANTXR1} cells, whereas RAW $264.7^{ANTXR1(D50A)}$ cells were significantly less sensitive to PA. Collectively, these results suggested effective PA-mediated toxicity required ANTXR1 with a functional PA-binding site, but did not depend on the receptor's cytoplasmic tail.

Analysis of PA mutants. Given the results using mutants of ANTXR1, reciprocal experiments were next performed to confirm the necessity of functional PA for cytoxicity. To accomplish this, RAW 264.7^{ANTXR1} cells were challenged with PA mutants defective for important activities. The first mutant, PA(SSSR),

Figure A-12. Influence of ANTXR1 derivatives and PA mutants on PA-induced cytotoxicity. (A) RAW 264.7 cells (open squares) and RAW 264.7 cellls expressing ANTXR1 (closed squares), $ANTXR1_{(D50A)}$ (open circles) or $ANTXR1_{(1-345)}$ (closed diamonds) were treated for 24 h with a range of PA concentrations and subsequently assayed for cell viability. (B) RAW 264.7 or RAW 264.7^{ANTXR1} cells were treated with 1 μg/ml PA (black bars), the furin-insensitive form of PA: PASSSR (white bars), or the pore formation deficient mutant $PA_{K397D, D425K}$ (grey bars) and assayed for cell viability 24 h post treatment.

Figure A-12.

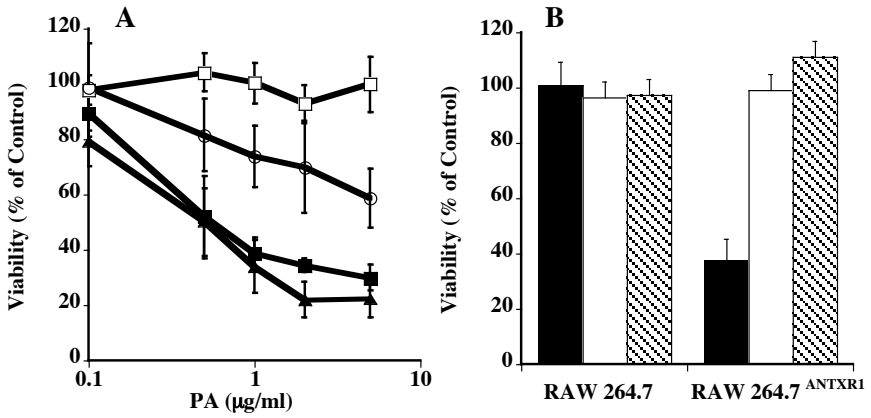
A
120
100
80
60
40
20
0
Viability (% of Control)
0.1
1
10
PA (µg/ml)
B
120
100
80
60
40
20
0
Viability (% of Control)
RAW 264.7
RAW 264.7 ANTXR1

binds receptor but is not proteolytically cleaved at the cell surface (2, 18). A second derivative of PA ($PA_{K397D, D425K}$) binds to the receptor, oligomerizes, and interacts with LF, but is defective in LF translocation (55). As shown in Fig. A-12B, neither PA mutant was cytotoxic to RAW 264.7^{ANTXR1} or RAW $264.7^{ANTXR1(1-345)}$ cells suggesting that PA binding, oligomerization, and effective channel formation are required for cytotoxic effects on RAW 264.7^{ANTXR1} macrophages.

PA-mediated cytotoxicity requires endosomal acidification. Previous results have shown that the acidic pH of the endosome triggers formation of SDS-resistant oligomers and membrane insertion of PA (16, 35, 46). To determine if endosomal acidification is necessary for PA-induced cytotoxicity, RAW 264.7^{ANTXR1} cells were incubated with various concentrations of the vacuolar H+ ATPase inhibitor bafilomycin A1, then treated with PA and assayed for survival. Pretreatment with bafilomycin protected RAW 264.7^{ANTXR1} cells from LT or PA alone (Fig. A-13A), showing that PA cytotoxicity depends on endosomal acidification. These results, along with the PA mutant analysis, demonstrate the necessity for functional channel formation by PA in order to cause cell death. Yet, it was possible that channels might be inordinately formed at the cell surface due to increased levels of PA localizing to the plasma membrane of RAW 264.7^{ANTXR1} cells. We excluded this possibility by using a $^{86}Rb^{+}$ release assay to show that the degree of cell-surface channel formation did not differ in RAW 264.7^{ANTXR1} and normal RAW 264.7 cells (Fig. A-13B). Furthermore, channel

Figure A-13. The role of acid pH during PA-mediated cytotoxicity in RAW 264.7^{ANTXR1} cells. (A) RAW 264.7^{ANTXR1} cells were treated with 5 μg/ml PA or 1μg/ml LT (1 μg/ml of each PA and LF), and with bafilomycin or MeOH when indicated, 30 min prior to PA or LT treatments. Cell viability was assayed by WST-8 reactivity at 24 h following treatment compared to cells treated with 20 mM Tris pH 8.0. (B) Channel formation by PA in cells expressing normal and high levels of ANTXR1. RAW 264.7^{ANTXR1} cells were loaded with $^{86}Rb^{+}$ and incubated for 2 h at 4°C with PA, PA_{SSSR}, $PA_{K397D,\ D425K}$ or with 20 mM Tris pH 8.0. Unbound toxin was removed by washing, fresh medium (20 mM Tris-MES, 145 mM NaCl, pH 5.0) was added, and the incubation was continued for 30 min. Percent of $^{86}Rb^{+}$ released was calculated as described in Experimental Procedures.

Figure A-13.

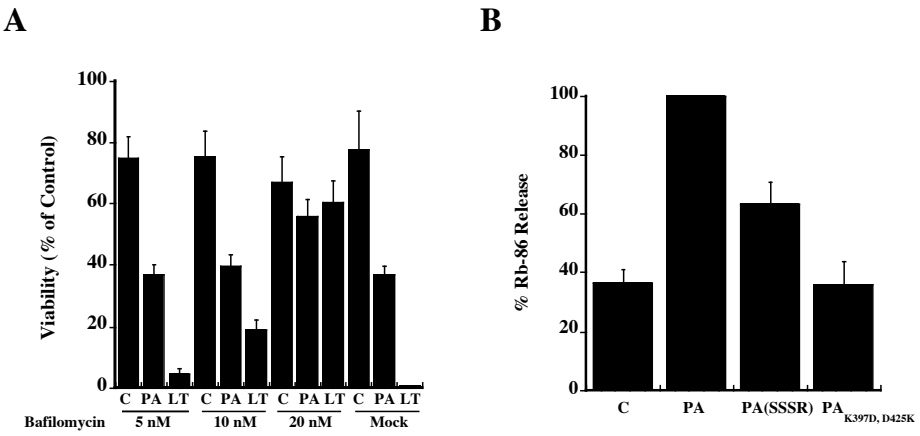
A
B
Viability (% of Control)
100
80
60
40
20
0
C PA LT C PA LT C PA LT C PA LT
Bafilomycin
5 nM
10 nM
20 nM
Mock
% Rb-86 Release
C
PA
PA(SSSR)
PA K397D, D425K

formation strictly required an acidic pH and could not be detected at neutral pH (data not shown).

Mechanism of PA cytotoxicity in RAW 264.7^{ANTXR1} macrophages. The relatively slow time-course of cell death in RAW 264.7^{ANTXR1} macrophages corresponded with a rate expected for apoptosis. Furthermore, this is the expected type of cell death, which would occur following sustained mixing of lysosomal and cytoplasmic contents. Thus, PA-treated cells were assayed for several common hallmarks of apoptosis. As shown in Fig. A-14, treatment of RAW 264.7^{ANTXR1} macrophages resulted in chromosomal fragmentation, activation of caspase-3, and cleavage of PARP, all of which are consistent with a caspase-3-dependent, apoptotic mechanism of cell death. In addition, caspase-3, but not caspase-8, was activated in PA-treated cells, suggesting activation of apoptosis occurred through an intrinsic pathway. Finally, we assessed activation of Bid since this is a known intermediary between caspase-3 activation and release of lysosomal contents (57). Corresponding to caspase-3 activation, cleaved Bid was also detected in PA-treated RAW 264.7^{ANTXR1} cells, further supporting the possibility that sustained formation of PA heptamers could lead to induction of apoptosis by release of vesicular proteins. Finally, analysis of lysates from RAW 264.7^{ANTXR1} cells treated with $PA_{K397D,\ D425K}$ did not reveal activation of caspase-3 or Bid (Fig. A-14D), which is in line with the observations that this mutant of PA is unable to cause cell death

Figure A-14. Induction of apoptosis in PA-treated RAW 264.7^{ANTXR1} macrophages. (A and B) RAW 264.7^{ANTXR1} cells were incubated with 20 mM Tris (A) or PA (B) for 15 h and subsequently analyzed via TUNEL staining and flow cytometry. Brackets indicate area of apoptotic cells. (C) RAW 264.7 or RAW 264.7^{ANTXR1} cells were incubated with 20 mM Tris or PA for 15 h, and cell lysates were isolated and analyzed by immunoblot. Cell lysates were separated using 4-20% SDS-PAGE, and proteins were transferred to a PVDF membrane and analyzed for activation of apoptosis-related proteins, including caspase-3, PARP, Bid and caspase-8, using corresponding primary antibodies and matched HRP conjugated secondary. (D) RAW 264.7 or RAW 264.7^{ANTXR1} cells were incubated with PA(K397D, D425K) for 15 h and subsequently subjected to immunoblot analysis as described above to detect caspase-3 and Bid.

Figure A-14.

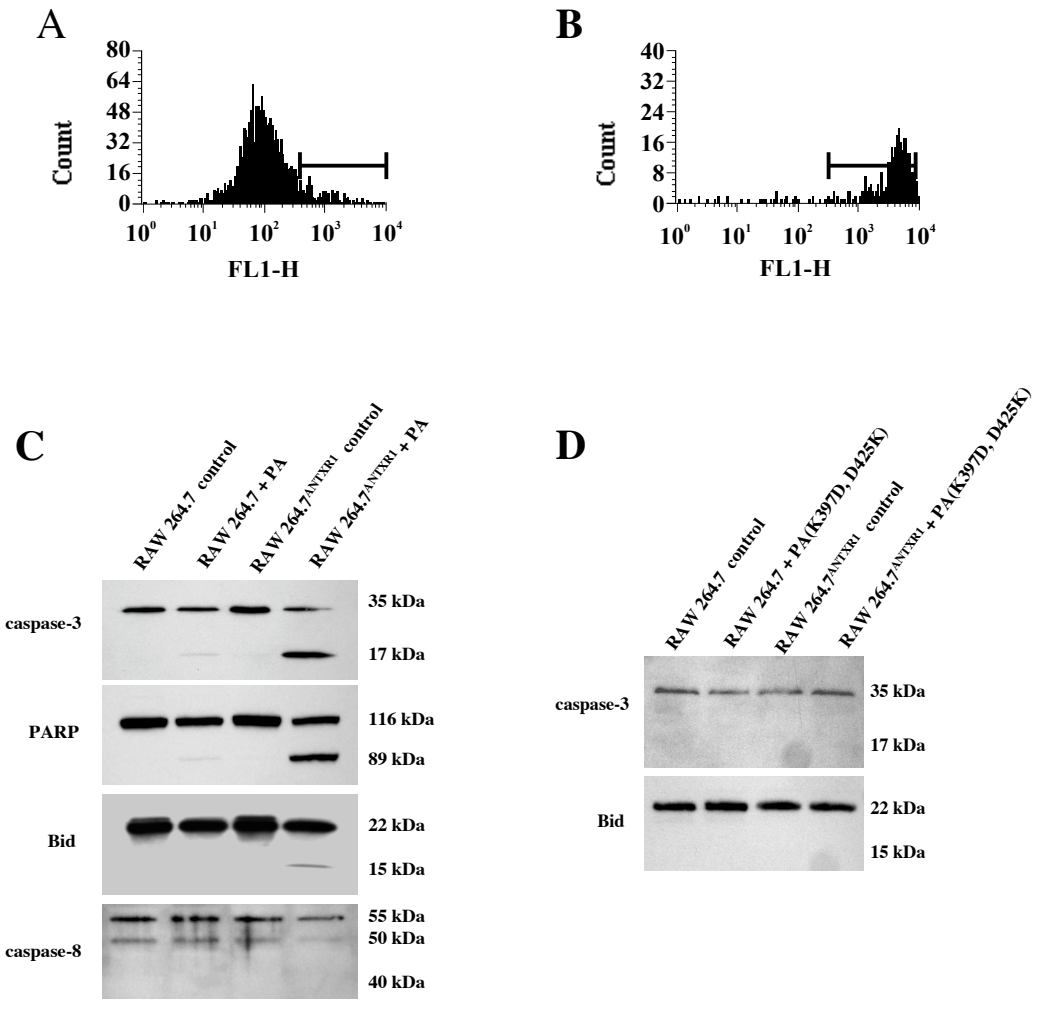
A
Count
80
64
48
32
16
0
10^0 10^1 10^2 10^3 10^4
FL1-H
B
Count
40
32
24
16
8
0
10^0 10^1 10^2 10^3 10^4
FL1-H
C
RAW 264.7 control
RAW 264.7 + PA
RAW 264.7$^{\Delta NTXR1}$ control
RAW 264.7$^{\Delta NTXR1}$ + PA
caspase-3
35 kDa
17 kDa
PARP
116 kDa
89 kDa
Bid
22 kDa
15 kDa
caspase-8
55 kDa
50 kDa
40 kDa
D
RAW 264.7 control
RAW 264.7 + PA(K397D, D425K)
RAW 264.7$^{\Delta NTXR1}$ control
RAW 264.7$^{\Delta NTXR1}$ + PA(K397D, D425K)
caspase-3
35 kDa
17 kDa
Bid
22 kDa
15 kDa

DISCUSSION

PA is essential for AT intoxication of mammalian cells and is known to make at least three defined contributions to the activity of this toxin. First, PA binds to the cell surface, which is critical for localizing the proteins of AT to target cells. Second, following proteolytic processing, PA interacts with EF and LF to form toxic complexes. Third, PA mediates the translocation of EF and LF into the cytoplasm of targeted cells where these enzymes alter cell function. Although there are several points of interaction with the cell, including cell surface receptors and membranes, prior to the current work, PA has not been reported to influence cell physiology on its own. In contrast to this longstanding paradigm, results from the current studies indicate PA, in the absence of EF or LF, is cytotoxic to macrophages that overexpress ANTXR1.

The initial purpose of these experiments was to assess the possible rate-limiting steps in formation of PA heptamers. Based on previous studies, there were several points at which formation of membrane-inserted, SDS-resistant PA heptamers could be limited. Indeed, since AT entry has been found to be limited to lipid-rafts (1, 4), it was conceivable that only marginal amounts of PA could enter the cell despite heightened levels of receptor. Our findings argue against this possibility and suggest that a major limitation in cell entry by PA may be the level of PA receptors. Increasing the levels of PA receptors correlated with heightened amounts of oligomer formation, as well as, an increased sensitivity to

PA. Furthermore, the receptor levels also appear to contribute to the rate at which PA heptamers are degraded within the cell. To date, little is known about the host factors that contribute to toxin stability and function within the cell, but the current data suggest the receptor may be one of the determinants in this process, as higher levels of ANTXR1 correlates with increased heptamer stability. The data also suggest that without appropriate PA degradation, cytotoxicity can occur even in the absence of EF or LF. It is appealing to speculate that degradation of PA represents an important host mechanism of resistance to this protein, and identification of cellular factors involved in this process could add to our understanding of AT intoxication.

Results from experiments examining the effects of ANTXR1 mutants and PA mutants provided insight into the molecular requirements for PA-cytotoxicity. The data suggests functional PA and ANTXR1, with an intact PA binding domain, are necessary for cytotoxicity. Bradley et al. previously showed that CHO cells overexpressing ANTXR1 with a D50A mutation in the MIDAS domain were resistant to treatment with PA and LFnDTA (7). As expected, RAW 264.7$^{ANTXR1(D50A)}$ cells displayed reduced sensitivity to PA, demonstrating the importance of a functional receptor for PA-mediated toxicity. Furthermore, PA mutants resistant to protease cleavage, and thus production of PA_{63} and the heptamer, were not cytotoxic. The double mutant of PA (K397D, D425K), which is defective for translocation of LF, also was not cytotoxic to RAW 264.7^{ANTXR1}

cells, further suggesting PA-mediated cytotoxicity requires a functional PA. RAW 264.7$^{ANTXR1(1-345)}$ cells lacking the cytoplasmic domain of ANTXR1 and RAW 264.7^{ANTXR1} cells were equally sensitive to PA making it unlikely that cytotoxicity was conferred through an intracellular signaling event activated by PA-ANTXR1 interactions. In line with this observation, a previous report by Liu and Leppla found that ANTXR1, lacking a cytoplasmic tail, could mediate binding, uptake, and oligomerization of PA (33), all of which we found to be required for PA-mediated cytotoxicity. Yet, it is worth noting that although the cytoplasmic tail of ANTXR1 was not required for PA-mediated cytotoxicity, this does not dismiss the possibility that other proteins interact with this complex and promote intracellular signaling events, which contribute to cell death. It is unclear how such a process would require functional channel formation by PA, or would need endosomal acidification, but our findings do not completely dismiss this possibility. Overall, the data indicates PA-mediated cytotoxicity requires receptor binding, endosomal acidification, and sustained oligomer formation.

ANTXR1's role in PA cytotoxicity may primarily involve localizing increased amounts of this protein to the cell surface, rather than sustaining oligomer formation. Recent work by Rainey and colleagues described the dissociation of ANTXRs from the PA oligomer at acidic pH, indicating that PA may dissociate from receptor during pore formation (47). Based on these observations, sustained oligomer and pore formation, which we found to be

essential for PA cytotoxicity, do not require ANTXR1 receptor per se. Our findings cannot be completely reconciled with this work, since we are able to correlate oligomer stability with levels of ANTXR1. It is possible that the cellular processes leading to degradation of heptameric PA become saturated when high levels of PA interact with the cell, and this leads to a slower rate of degradation. In this case, ANTXR1 would not have a direct influence on degradation, but could serve only to localize PA to the cell.

Whether increased levels of ANTXR2 also confer sensitivity to PA remains unclear, since we were unable to obtain high expression of this second PA receptor in RAW 264.7 macrophages. Interestingly, Banks and colleagues recently demonstrated that ANTXR2 was the predominant PA receptor in RAW 264.7 macrophages (3). Careful examination of the results shown in Fig. 5 reveals a small amount of caspase-3 and PARP cleavage in wild-type RAW 264.7 macrophages, suggesting ANTXR2 might also trigger apoptosis if present at higher levels. Alternatively, the two ANTXRs may behave differently with respect to PA-mediated toxicity. Indeed, two recent reports identify significant differences in the pH threshold at which PA forms pores depending on the receptor to which it is bound (47, 63). PA bound to ANTXR1 forms pores at a less acidic pH and, therefore, likely forms pores earlier in the endocytic pathway than ANTXR2-bound PA. Differences in the subcellular location at which PA forms pores and uncouples from receptor may lead to differences in pore stability

and cytotoxicity. Clearly, further experimentation will be necessary before any definitive links can be made between ANTXR2 levels and PA-mediated cytotoxicity.

Taken together, the current findings suggest the following preliminary model for PA-mediated cytotoxicity. Due to the increased levels of ANTXR1, PA oligomers are more stable and accumulate to such levels that an inordinate number of pores are generated in acidified vesicles. As a result, apoptosis is triggered in the intoxicated cells, and this leads to caspase-3 cleavage and eventual cell death. While the precise inciting event leading to caspase-3 activation is unclear, there is at least one scenario worth consideration. Due to increased pore formation by PA, proteases, such as cathepsins, may be released from the acidified vesicle, and these proteases trigger the activation of apoptosis. In line with this possibility, cathepsins have been shown in other studies to proteolyze and activate Bid, which leads to caspase-3 activation via modulation of the mitochondria (57). In this case, cleavage of Bid may occur prior to caspase-3 activation and play a more prominent role in activation, rather than amplifying the apoptosis pathway. Alternatively, lysosomal proteases may activate caspase-3, in a system similar to the mechanism described for cytochrome-c-independent apoptosis (22). While still speculative, future studies will closely examine the possibility that release of lysosomal contents initiates apoptosis during PA cytotoxicity.

Studies to date have not determined the relative distribution of ANTXR1 and ANTXR2 on various cell types, but it is now reasonable to suggest that cells with higher ANTXR1 levels could be susceptible to PA treatment and need to be investigated. Interestingly, ANTXR1 was first identified as tumor endothelial marker 8 (TEM8), a gene with increased expression in endothelial cells associated with tumor neovasculature (10, 56). Recently, Bonuccelli et al. reported high levels of TEM8 expression in epithelial cells lining the lungs, as well as, skin and intestines (6). The lungs have been shown to be a primary site of damage during anthrax disease (20), raising the possibility that PA could directly impact this organ due to high levels of ANTXR1.

The current findings also raise concerns about the efficacy of anthrax vaccines consisting of recombinant, functional PA. There is currently no information regarding the variations in receptor levels throughout an outbred population. While further work is needed, the data suggests individuals expressing higher levels of ANTXR1 could suffer side effects from such a vaccine due to PA toxicity. Thus, recombinant, functionally inactive mutants of PA may hold greater promise as vaccine candidates.

MATERIALS AND METHODS

Cell lines. RAW 264.7 cells were purchased from the American Type Culture Collection (TIB-71). Cells were cultured in RPMI 1640 medium

supplemented with 10% fetal calf serum and maintained in a humidified atmosphere of 6% CO_2 at 37°C.

Wild type or mutant forms of ANTXR1 fused to green fluorescent protein (GFP) were stably expressed in RAW 264.7 cells following retroviral transduction as previously described (7). Briefly, pseudotyped murine leukemia virus vectors were generated by transient transfection of ~10^7 HEK 293 cells with 15 μg pMD.gagpol, 5 μg pMD.G (VSV-G envelope protein), and 20 μg of pLEGFP-N1 (Clontech) encoding wild-type or mutant versions of ANTXR1-EGFP fusions. Forty-eight hours after transfection, virus-containing supernatants were harvested, filtered through 0.22 μm syringe filters, and used to infect RAW 264.7 cells. Infections were performed at a multiplicity of infection (MOI) of ~ 5 by adding virus-containing media in the presence of 8 μg/mL polybrene (Sigma) to sub-confluent cultures of RAW 264.7 cells. Forty-eight hours later, 800 μg/mL G418 (Invitrogen) was added to the culture medium of infected cells to select against uninfected cells. For these studies, ANTXR1 splice variant 2 was defined as wild type receptor (8, 53). $ANTXR1_{1\text{-}345}$ represents a C-terminal deletion lacking amino acids 346-368 that results in loss of the cytosolic domain of ANTXR1, and $ANTXR1_{D50A}$ represents an aspartate to alanine mutation at residue 50 that disrupts the MIDAS motif resulting in loss of PA binding.

Purification of recombinant PA, PA mutants, and LF. Recombinant forms of PA and LF expressed in pET15b were purified from *E. coli* BL-21(DE3)

using His-tagged affinity chromatography according to the manufacturer's protocol (Novagen). LPS was removed from the purified protein samples using a polymyxin B column according to manufacturers instructions (Sigma), and endotoxin levels were determined using the limulus amebocyte lysate assay (BioWhittaker) with detection limits at 0.06 endotoxin units per ml. PA_{SSSR}, a furin-insensitive PA, was expressed in pET22b and purified from periplasmic extracts of *E. coli* BL21 and further purified by anion-exchange chromatography. A purified dominant negative (DN) mutant of PA (K397D, D425K) was kindly provided by Dr. R. John Collier and has been previously described (55).

Detection of PA_{63} SDS-resistant oligomers by immunoblotting. RAW 264.7 or RAW 264.7^{ANTXR1} cells were treated for 1 h at 4°C with 1 μg/ml PA, washed with PBS, and then pre-warmed growth media was added to the cells. After different incubation times at 37°C, cells were washed three times in PBS and lysed in NP40 buffer (50 mM Tris-Cl pH 8.0, 1 % Nonidet P-40, 150 mM NaCl) supplemented with protease inhibitors (Complete Mini, Roche). Cell lysates (150 μg total protein/sample) were subjected to SDS-PAGE using 4-15% gradient gels (Biorad). Alternatively, 15 μg total protein/sample of the same cell lysates were separated by 10% SDS-PAGE for analysis of tubulin. Samples were transferred to PVDF membranes, which were then blocked overnight with 5% powdered milk proteins (BioRad) in TBST (50mM Tris, 150 mM NaCl, 0.1% Tween-20, pH 8.0). Western blotting was then performed as previously described

(50) using affinity purified anti-PA polyclonal sera (provided by Dr. G. Jonah Rainey, Salk Institute).

Analysis of PA heptamer stability in RAW 264.7 and RAW 264.7^{ANTXR1} cells. Following detection by immunoblot, band intensities were determined by densitometry using a Fluorchem 8900 imager (Alpha Innotech) and corresponding AlphaEase FC software. Arbitrary units generated from the densitometry analysis were then used to graph the changes in heptamer levels over time using Prism 4 software (GraphPad). Degradation rates were determined using the linear regression function of Prism 4 software. Since PA heptamers accumulated to higher levels in RAW 264.7^{ANTXR1} cells compared to RAW 264.7 cells, the rates of degradation were adjusted accordingly in order to directly compare the two conditions. Adjustments were made by extrapolating to the Y intersect of the lines generated from the results of each treatment, and a ratio (1.6) was determined based on this analysis.

Cell viability and lysosomotropic inhibitor assays. Cells were harvested by scraping and plated at a density of $2x10^4$ cells/well, unless otherwise indicated, in 96-well culture plates. Cells were then treated with PA (5μg/ml to 10 ng/ml), or PA (SSSR) and DN mutants, for 24 h or other indicated times, at which point, they were assayed for cell viability using WST-8 (2-(2-methoxy-4-nitrophenyl)-3-(4-nitrophenyl)-5-(2,4-disulfophenyl)-2H-tetrazolium, monosodium salt (Dojindo Molecular Technologies), which detects levels of

soluble formazan dye reduced from WST-8. Data is presented relative to the proliferation of control samples incubated with 20 mM Tris pH 8.0 and represent an average of at least four measurements from two separate experiments (±SD). For determining the requirement of endosomal acidification for PA-mediated cytotoxicity, bafilomycin (Sigma) was added to cells at different concentrations (5 nM to 20 nM) 30 min prior to PA addition, and cell viability was assayed as described above.

$^{86}Rb^{+}$ efflux measurements. To determine the level of membrane permeabilization during PA-induced cytotoxity, cells were plated at a density of 2 x 10^5 in 24-well culture plates. Approximately 8-10 h after plating, fresh medium containing 10 μCi $^{86}Rb^{+}$ (1Ci=37.0Gbq/g) was added, and cells were incubated overnight under normal growth conditions. Cells were washed with medium, and were then incubated for 2 h at 4°C with fresh medium containing 5 μg/ml PA or PA mutants. Cells were washed twice to remove unbound PA, and isotonic buffer (20 mM MES-Tris, 145 mM NaCl, pH 5.0) was added for 30 min at 4°C. At the end of the incubation period, an aliquot of medium was removed, and released $^{86}Rb^{+}$ was measured using a scintillation counter. Cells were lysed with 1.0 % SDS to determine the amount of retained $^{86}Rb^{+}$. The percentage of released $^{86}Rb^{+}$ was calculated by dividing the $^{86}Rb^{+}$ released by the total amount of $^{86}Rb^{+}$ (retained + released) * 100.

Detection of caspase and Bid activation, PARP cleavage, and TUNEL assays. Lysates from treated RAW 264.7 and RAW 264.7^{ANTXR1} cells were collected 15 h following treatment with 5 μg/ml PA. Lysates were examined by standard immunoblotting using primary antibody (Cell Signaling Technologies) to caspase-3, Bid, poly-ADP-ribose polymerase (PARP), and caspase-8 (BD Pharmingen), followed by the appropriate secondary antibody conjugated to horseradish peroxidase. Bands recognized by the antibody were visualized by addition of the ECL Plus chemilumenescent substrate and autoradiography of the blots (Amersham Pharmacia). For terminal-uridyl nicked end labeling (TUNEL) staining, fragmented DNA was labeled with BrdUTP and detected using an Alexa Fluor 488-labeled anti-BrdU antibody (Molecular Probes). Samples were subsequently analyzed using a FACSscan flow cytometer (Becton Dickinson).

REFERENCES

1. **Abrami, L., S. Liu, P. Cosson, S.H. Leppla, and F.G. van der Goot.** 2003. Anthrax toxin triggers endocytosis of its receptor via a lipid raft-mediated clathrin-dependent process. *J Cell Biol*. **160:**321-328.

2. **Ballard, J.D., R.J. Collier, and M.N. Starnbach.** 1998. Anthrax toxin as a molecular tool for stimulation of cytotoxic T lymphocytes: disulfide-linked epitopes, multiple injections, and role of $CD4^+$ cells. *Infect Immun*. **66:**4696-4699.

3. **Banks, D.J., M. Barnajian, F.J. Maldonado-Arocho, A.M. Sanchez, and K.A. Bradley.** 2005. Anthrax toxin receptor 2 mediates *Bacillus anthracis* killing of macrophages following spore challenge. *Cell Microbiol*. **7:**1173-1185.

4. **Beauregard, K.E., R.J. Collier, and J.A. Swanson.** 2000. Proteolytic activation of receptor-bound anthrax protective antigen on macrophages promotes its internalization. *Cell Microbiol*. **2:**251-258.

5. **Benson, E.L., P.D. Huynh, A. Finkelstein, and R.J. Collier.** 1998. Identification of residues lining the anthrax protective antigen channel. *Biochemistry*. **37:**3941-3948.

6. **Bonuccelli, G., F. Sotgia, P.G. Frank, T.M. Williams, C.J. de Almeida, H.B. Tanowitz, P.E. Scherer, K.A. Hotchkiss, B.I. Terman, B. Rollman, A. Alileche, J. Brojatsch, and M.P. Lisanti.** 2005. ATR/TEM8 is highly expressed in epithelial cells lining *Bacillus anthracis*' three sites of entry: implications for the pathogenesis of anthrax infection. *Am J Physiol Cell Physiol*. **288:**C1402-1410.

7. **Bradley, K.A., J. Mogridge, G. Jonah, A. Rainey, S. Batty, and J.A. Young.** 2003. Binding of anthrax toxin to its receptor is similar to alpha integrin-ligand interactions. *J Biol Chem*. **278:**49342-49347.

8. **Bradley, K.A., J. Mogridge, M. Mourez, R.J. Collier, and J.A. Young.** 2001. Identification of the cellular receptor for anthrax toxin. *Nature*. **414:**225-229.

9. **Brennan, M.A. and B.T. Cookson.** 2000. *Salmonella* induces macrophage death by caspase-1-dependent necrosis. *Mol Microbiol.* **38:**31-40.

10. **Carson-Walter, E.B., D.N. Watkins, A. Nanda, B. Vogelstein, K.W. Kinzler, and B. St Croix.** 2001. Cell surface tumor endothelial markers are conserved in mice and humans. *Cancer Res.* **61:**6649-6655.

11. **Chae, H.J., S.W. Chae, and H.R. Kim.** 2004. Cyclic adenosine monophosphate inhibits nitric oxide-induced apoptosis of cardiac muscle cells in a c-Jun N-terminal kinase-dependent manner. *Immunopharmacol Immunotoxicol.* **26:**249-263.

12. **Chakrabarti, G., X. Zhou, and B.A. McClane.** 2003. Death pathways activated in CaCo-2 cells by *Clostridium perfringens* enterotoxin. *Infect Immun.* **71:**4260-4270.

13. **Duesbery, N.S. and G.F. Vande Woude.** 1999. Anthrax lethal factor causes proteolytic inactivation of mitogen-activated protein kinase kinase. *J Appl Microbiol.* **87:**289-293.

14. **Duesbery, N.S., C.P. Webb, S.H. Leppla, V.M. Gordon, K.R. Klimpel, T.D. Copeland, N.G. Ahn, M.K. Oskarsson, K. Fukasawa, K.D. Paull, and G.F. Vande Woude.** 1998. Proteolytic inactivation of MAP kinase kinase by anthrax lethal factor. *Science*. **280:**734-737.

15. **Escuyer, V., E. Duflot, O. Sezer, A. Danchin, and M. Mock.** 1988. Structural homology between virulence-associated bacterial adenylate cyclases. *Gene*. **71:**293-298.

16. **Friedlander, A.M.** 1986. Macrophages are sensitive to anthrax lethal toxin through an acid- dependent process. *J Biol Chem.* **261:**7123-7126.

17. **Friedlander, A.M., R. Bhatnagar, S.H. Leppla, L. Johnson, and Y. Singh.** 1993. Characterization of macrophage sensitivity and resistance to anthrax lethal toxin. *Infect Immun.* **61:**245-252.

18. **Gordon, V.M. and S.H. Leppla.** 1994. Proteolytic activation of bacterial toxins: role of bacterial and host cell proteases. *Infect Immun.* **62:**333-340.

19. **Grbovic, O., V. Jovic, S. Ruzdijic, V. Pejanovic, L. Rakic, and S. Kanazir.** 2002. 8-Cl-cAMP affects glioma cell-cycle kinetics and selectively induces apoptosis. *Cancer Invest.* **20:**972-982.

20. **Grinberg, L.M., F.A. Abramova, O.V. Yampolskaya, D.H. Walker, and J.H. Smith.** 2001. Quantitative pathology of inhalational anthrax I: quantitative microscopic findings. *Mod Pathol.* **14:**482-495.

21. **Gueirard, P., A. Druilhe, M. Pretolani, and N. Guiso.** 1998. Role of adenylate cyclase-hemolysin in alveolar macrophage apoptosis during *Bordetella pertussis* infection in vivo. *Infect Immun.* **66:**1718-1725.

22. **Hishita, T., S. Tada-Oikawa, K. Tohyama, Y. Miura, T. Nishihara, Y. Tohyama, Y. Yoshida, T. Uchiyama, and S. Kawanishi.** 2001. Caspase-3 activation by lysosomal enzymes in cytochrome c-independent apoptosis in myelodysplastic syndrome-derived cell line P39. *Cancer Res.* **61:**2878-2884.

23. **Hoover, D.L., A.M. Friedlander, L.C. Rogers, I.K. Yoon, R.L. Warren, and A.S. Cross.** 1994. Anthrax edema toxin differentially regulates lipopolysaccharide-induced monocyte production of tumor necrosis factor alpha and interleukin-6 by increasing intracellular cyclic AMP. *Infect Immun.* **62:**4432-4439.

24. **Kim, S., M. Bakre, H. Yin, and J.A. Varner.** 2002. Inhibition of endothelial cell survival and angiogenesis by protein kinase A. *J Clin Invest.* **110:**933-941.

25. **Kimmel, C.B., W.W. Ballard, S.R. Kimmel, B. Ullmann, and T.F. Schilling.** 1995. Stages of embryonic development of the zebrafish. *Dev Dyn.* **203:**253-310.

26. **Krakstad, C., A.E. Christensen, and S.O. Doskeland.** 2004. cAMP protects neutrophils against TNF-{alpha}-induced apoptosis by activation of cAMP-dependent protein kinase, independently of exchange protein directly activated by cAMP (Epac). *J Leukoc Biol.* **76:** 641-647.

27. **Lacy, D.B., D.J. Wigelsworth, R.A. Melnyk, S.C. Harrison, and R.J. Collier.** 2004. Structure of heptameric protective antigen bound to an anthrax toxin receptor: a role for receptor in pH-dependent pore formation. *Proc Natl Acad Sci U S A.* **101:**13147-13151.

28. **Lacy, D.B., D.J. Wigelsworth, H.M. Scobie, J.A. Young, and R.J. Collier.** 2004. Crystal structure of the von Willebrand factor A domain of human capillary morphogenesis protein 2: an anthrax toxin receptor. *Proc Natl Acad Sci U S A*. **101:**6367-6372.

29. **Leppla, S.H.** 1982. Anthrax toxin edema factor: a bacterial adenylate cyclase that increases cyclic AMP concentrations of eukaryotic cells. *Proc Natl Acad Sci U S A*. **79:**3162-3166.

30. **Leppla, S.H.** 1984. *Bacillus anthracis* calmodulin-dependent adenylate cyclase: chemical and enzymatic properties and interactions with eucaryotic cells. *Advances in Cyclic Nucleotide & Protein Phosphorylation Research*. **17:**189-198.

31. **Leppla, S.H.** *The anthrax toxin complex*, in *Sourcebook of Bacterial Protein Toxins*, J. Alouf, Editor. 1991, Academic Press: New York. p. 277-302.

32. **Lin, S., N. Gaiano, P. Culp, J.C. Burns, T. Friedmann, J.K. Yee, and N. Hopkins.** 1994. Integration and germ-line transmission of a pseudotyped retroviral vector in zebrafish. *Science*. **265:**666-669.

33. **Liu, S. and S.H. Leppla.** 2003. Cell surface tumor endothelium marker 8 cytoplasmic tail-independent anthrax toxin binding, proteolytic processing, oligomer formation, and internalization. *J Biol Chem*. **278:**5227-5234.

34. **Michankin, B.N., L.A. Chevchenko, and L.E. Asseeva.** 1992. Adenylate cyclase. A possible factor in the pathogenicity of *Yersinia pestis*. *Bull Soc Pathol Exot*. **85:**17-21.

35. **Milne, J.C. and R.J. Collier.** 1993. pH-dependent permeabilization of the plasma membrane of mammalian cells by anthrax protective antigen. *Mol Microbiol*. **10:**647-653.

36. **Milne, J.C., D. Furlong, P.C. Hanna, J.S. Wall, and R.J. Collier.** 1994. Anthrax protective antigen forms oligomers during intoxication of mammalian cells. *J Biol Chem*. **269:**20607-20612.

37. **Moayeri, M., D. Haines, H.A. Young, and S.H. Leppla.** 2003. *Bacillus anthracis* lethal toxin induces TNF-alpha-independent hypoxia-mediated toxicity in mice. *J Clin Invest*. **112:**670-682.

38. **Moayeri, M., N.W. Martinez, J. Wiggins, H.A. Young, and S.H. Leppla.** 2004. Mouse susceptibility to anthrax lethal toxin is influenced by genetic factors in addition to those controlling macrophage sensitivity. *Infect Immun*. **72:**4439-4447.

39. **Mogridge, J., K. Cunningham, and R.J. Collier.** 2002. Stoichiometry of anthrax toxin complexes. *Biochemistry*. **41:**1079-1082.

40. **Mogridge, J., K. Cunningham, D.B. Lacy, M. Mourez, and R.J. Collier.** 2002. The lethal and edema factors of anthrax toxin bind only to oligomeric forms of the protective antigen. *Proc Natl Acad Sci U S A*. **99:**7045-7048.

41. **Molnar, D.M. and R.A. Altenbern.** 1963. Alterations in the biological activity of protective antigen of *Bacillus anthracis*. *Proc. Soc. Exp. Biol. Med*. **114:**294-297.

42. **Nishihara, H., M. Hwang, S. Kizaka-Kondoh, L. Eckmann, and P.A. Insel.** 2004. Cyclic AMP promotes cAMP-responsive element-binding protein-dependent induction of cellular inhibitor of apoptosis protein-2 and suppresses apoptosis of colon cancer cells through ERK1/2 and p38 MAPK. *J Biol Chem*. **279:**26176-26183.

43. **O'Brien, J., A. Friedlander, T. Dreier, J. Ezzell, and S. Leppla.** 1985. Effects of anthrax toxin components on human neutrophils. *Infect Immun*. **47:**306-310.

44. **Pezard, C., P. Berche, and M. Mock.** 1991. Contribution of individual toxin components to virulence of *Bacillus anthracis*. *Infect Immun*. **59:**3472-3477.

45. **Pezard, C., M. Weber, J.C. Sirard, P. Berche, and M. Mock.** 1995. Protective immunity induced by *Bacillus anthracis* toxin-deficient strains. *Infect Immun*. **63:**1369-1372.

46. **Qa'dan, M., K.A. Christensen, L. Zhang, T.M. Roberts, and R.J. Collier.** 2005. Membrane insertion by anthrax protective antigen in cultured cells. *Mol Cell Biol*. **25:**5492-5498.

47. **Rainey, G.J., D.J. Wigelsworth, P.L. Ryan, H.M. Scobie, R.J. Collier, and J.A. Young.** 2005. Receptor-specific requirements for anthrax toxin delivery into cells. *Proc Natl Acad Sci U S A*. **102:**13278-13283.

48. **Reinehr, R. and D. Haussinger.** 2004. Inhibition of bile salt-induced apoptosis by cyclic AMP involves serine/threonine phosphorylation of CD95. *Gastroenterology*. **126:**249-262.

49. **Ren, G., J. Quispe, S.H. Leppla, and A.K. Mitra.** 2004. Large-scale structural changes accompany binding of lethal factor to anthrax protective antigen: a cryo-electron microscopic study. *Structure*. **12:**2059-2066.

50. **Salles, II, A.E. Tucker, D.E. Voth, and J.D. Ballard.** 2003. Toxin-induced resistance in *Bacillus anthracis* lethal toxin-treated macrophages. *Proc Natl Acad Sci U S A*. **100:**12426-12431.

51. **Sandal, T., C. Stapnes, H. Kleivdal, L. Hedin, and S.O. Doskeland.** 2002. A novel, extraneuronal role for cyclin-dependent protein kinase 5 (CDK5): modulation of cAMP-induced apoptosis in rat leukemia cells. *J Biol Chem*. **277:**20783-20793.

52. **Santelli, E., L.A. Bankston, S.H. Leppla, and R.C. Liddington.** 2004. Crystal structure of a complex between anthrax toxin and its host cell receptor. *Nature*. **430:**905-908.

53. **Scobie, H.M., G.J. Rainey, K.A. Bradley, and J.A. Young.** 2003. Human capillary morphogenesis protein 2 functions as an anthrax toxin receptor. *Proc Natl Acad Sci U S A*. **100:**5170-5174.

54. **Scobie, H.M., D. Thomas, J.M. Marlett, G. Destito, D.J. Wigelsworth, R.J. Collier, J.A. Young, and M. Manchester.** 2005. A soluble receptor decoy protects rats against anthrax lethal toxin challenge. *J Infect Dis*. **192:**1047-1051.

55. **Sellman, B.R., M. Mourez, and R.J. Collier.** 2001. Dominant-negative mutants of a toxin subunit: an approach to therapy of anthrax. *Science*. **292:**695-697.

56. **St Croix, B., C. Rago, V. Velculescu, G. Traverso, K.E. Romans, E. Montgomery, A. Lal, G.J. Riggins, C. Lengauer, B. Vogelstein, and K.W. Kinzler.** 2000. Genes expressed in human tumor endothelium. *Science*. **289:**1197-1202.

57. **Stoka, V., B. Turk, S.L. Schendel, T.H. Kim, T. Cirman, S.J. Snipas, L.M. Ellerby, D. Bredesen, H. Freeze, M. Abrahamson, D. Bromme, S. Krajewski, J.C. Reed, X.M. Yin, V. Turk, and G.S. Salvesen.** 2001. Lysosomal protease pathways to apoptosis. Cleavage of bid, not pro-caspases, is the most likely route. *J Biol Chem.* **276:**3149-3157.

58. **Traver, D., P. Herbomel, E.E. Patton, R.D. Murphey, J.A. Yoder, G.W. Litman, A. Catic, C.T. Amemiya, L.I. Zon, and N.S. Trede.** 2003. The zebrafish as a model organism to study development of the immune system. *Adv Immunol*. **81:**253-330.

59. **Tucker, A.E., Salles, II, D.E. Voth, W. Ortiz-Leduc, H. Wang, I. Dozmorov, M. Centola, and J.D. Ballard.** 2003. Decreased glycogen synthase kinase 3-beta levels and related physiological changes in *Bacillus anthracis* lethal toxin-treated macrophages. *Cell Microbiol*. **5:**523-532.

60. **Voth, D.E., M. Qa'Dan, E.E. Hamm, J.M. Pelfrey, and J.D. Ballard.** 2004. *Clostridium sordellii* lethal toxin is maintained in a multimeric protein complex. *Infect Immun*. **72:**3366-3372.

61. **Westerfield, M.** *The zebrafish book: A guide for the laboratory use of zebrafish (Brachydanio rerio)*. 1993: University of Oregon Press.

62. **Wigelsworth, D.J., B.A. Krantz, K.A. Christensen, D.B. Lacy, S.J. Juris, and R.J. Collier.** 2004. Binding stoichiometry and kinetics of the interaction of a human anthrax toxin receptor, CMG2, with protective antigen. *J Biol Chem*. **279:**23349-23356.

63. **Wolfe, J.T., B.A. Krantz, G.J. Rainey, J.A. Young, and R.J. Collier.** 2005. Whole-cell voltage clamp measurements of anthrax toxin pore current. *J Biol Chem*. **280:**39417-39422.

64. **Xia, Z.G. and D.R. Storm.** 1990. A-type ATP binding consensus sequences are critical for the catalytic activity of the calmodulin-sensitive adenylyl cyclase from *Bacillus anthracis*. *J Biol Chem*. **265:**6517-6520.

65. **Yahr, T.L., A.J. Vallis, M.K. Hancock, J.T. Barbieri, and D.W. Frank.** 1998. ExoY, an adenylate cyclase secreted by the *Pseudomonas aeruginosa* type III system. *Proc Natl Acad Sci U S A*. **95:**13899-13904.

66. **Zhang, L. and P.A. Insel.** 2001. Bcl-2 protects lymphoma cells from apoptosis but not growth arrest promoted by cAMP and dexamethasone. *Am J Physiol Cell Physiol*. **281:**C1642-1647.